An update to this article is included at the end

Heliyon 9 (2023) e14404

Contents lists available at ScienceDirect

Heliyon

journal homepage: www.cell.com/heliyon

Review article

Past and current components-based detailing of particle image velocimetry: A comprehensive review

Daniel Rohacs [a], Onur Yasar [b], Utku Kale [a,c,*], Selcuk Ekici [d], Enver Yalcin [b], Adnan Midilli [e], T. Hikmet Karakoc [f,g]

[a] *Department of Aeronautics and Naval Architecture, Faculty of Transportation Engineering and Vehicle Engineering, Budapest University of Technology and Economics, HU-1111, Budapest, Hungary*
[b] *Department of Mechanical Engineering, Balıkesir University, TR-10145, Balıkesir, Turkey*
[c] *Aviation Academy, Amsterdam University of Applied Sciences, Amsterdam, Netherlands*
[d] *Department of Aviation, Iğdır University, TR-76000, Iğdır, Turkey*
[e] *Faculty of Mechanical Engineering, Department of Mechanical Engineering, Yıldız Technical University, TR-34349, İstanbul, Turkey*
[f] *Faculty of Aeronautics and Astronautics, Eskişehir Technical University, TR-26000, Eskişehir, Turkey*
[g] *Information Technology Research and Application Center, Istanbul Ticaret University, Istanbul, Turkey*

A R T I C L E I N F O

Keywords:
Particle image velocimetry (PIV)
Flow measurement
Component
Non-intrusive
Review
Aviation

A B S T R A C T

Particle image velocimetry has been widely used in various sectors from the automotive to aviation, research, and development, energy, medical, turbines, reactors, electronics, education, refrigeration for flow characterization and investigation. In this study, articles examined in open literature containing the particle image velocimetry techniques are reviewed in terms of components, lasers, cameras, lenses, tracers, computers, synchronizers, and seeders. The results of the evaluation are categorized and explained within the tables and figures. It is anticipated that this paper will be a starting point for researchers willing to study in this area and industrial companies willing to include PIV experimenting in their portfolios. In addition, the study shows in detail the advantages and disadvantages of past and current technologies, which technologies in existing PIV laboratories can be renewed, and which components are used in the PIV laboratories to be installed.

1. Introduction

1.1. Background information

The quantitative flow velocity measurements started with the Pitot tubes. In the 1920s hot wire anemometers were introduced [1]. Hotwire anemometers were important for probe miniaturization, and frequency response [1]. In the 1960s lasers and Laser Doppler Anemometer (LDA) were introduced [1]. In the 1990s the concept of a micro-total analysis system was first introduced [2]. The technology allowed a new wave of microchip electrophoresis. In the early 2000s, a contactless conductivity test was presented [3,4].

With the rapid steps forward in flow measurement systems and electronics sectors, the global velocity measurements became inevitable [1,4]. Therefore, the requirement of making global velocity measurements using the Particle Image Velocimetry (PIV)

* Corresponding author.
E-mail address: kale.utku@kjk.bme.hu (U. Kale).

https://doi.org/10.1016/j.heliyon.2023.e14404
Received 25 October 2022; Received in revised form 25 December 2022; Accepted 3 March 2023
Available online 11 March 2023

technique for advanced fluid flow measurements became a trend research area [1].

PIV can perform instantaneous velocity measurements in two or three-dimensional domains with high accuracy [1]. The measuring technique also enables sufficient spatial resolution and instantaneous vorticity field [5,6] PIV consists of several subsystems but fundamentally composes of four basic components [1]. Components of a PIV setup consists of an optically transparent test-section, a laser, recording hardware, and a computer [1,7].

PIV has a wide range of application areas and is utilized to analyze various flows such as turbulent flow, micron-scale systems, spray atomization, and combustion processes [8]. The technique is also utilized for various sectors like education [9], mining [10], hydrology [11], heat exchangers [12], nuclear reactors [13], aviation [14], chemical engineering [15], air conditioning, and ventilation [16] directly or indirectly from subsonic flows to supersonic flows, the technique finds an application area [8].

A typical PIV application follows a chain of events that starts with the seeding. Flow is seeded with tracer particles [1]. Particles can be also added in measurement [17]. Tracer particles should not disrupt the flow structure. Seeding or added particles must be good enough to follow flow and reflection laser light. Size of the particles is another parameter should be evaluated. Particle size should be inside a range according to the application [17]. Fluorescent dyed particles and silver-coated particles are used in applications [7]. The laser illuminates the tracer particles. Especially, pulsed lasers are used because of various advantages like short duration time or delivering power [7,17]. Due to technological innovations, pulsed lasers offer short duration time and delivering all power at the desired time. Tracer particles scatter laser lights [17]. The camera records movement of particles [11]. The recording may be carried out with a single frame or double frame [7]. The displacement of the particles is visualized through an assessment of the PIV recordings. In order to acquire and assess data amount adequate for detailed investigations, post-processing is also needed [17].

Among all flow measurement techniques, PIV is a feasible and adequate technique for flow measurement. The general advantages of the PIV are given as below [7,17]:

- PIV is a non-intrusive flow measurement technique. Flow isn't affected by particles and other things [18].
- PIV enables indirect velocity measurement. Also, the whole field measurement can be conducted [18].
- Large quantities of image pairs can be obtained. Also, high accuracy is easily possible [19].
- PIV offers three components and three-dimensional measurements with advanced techniques [7,20].
- Laminar or turbulent flow can be investigated via PIV [18].
- PIV can be utilized for channel flow [21].
- PIV is feasible for investigation of inflow and outflow applications [7,17].

This paper aims to review the component-based particle image velocimetry studies from the past to the present. From this point of view, a great number of PIV studies existing in open literature of the most used flow measurement technique of particle image velocimetry are examined and presented in detail concerning components.

1.2. Previous studies of particle image velocimetry

In this section, studies that contain particle image velocimetry technique in open literature are examined from past to present by years.

Prasad [1] reviewed particle image velocimetry and particle tracking velocimetry. PIV, PTV, correlations, components of PIV, and errors are explained. In the study, general information about PIV is provided to the reader.

Sayeed-Bin-Asad et al. [8] examined fish migration along with fish ladders. In the study, particle image velocimetry appliance on fish migration is explained. Quantitative and detailed turbulent flows from previous studies are also examined. According to the results, a large amount of investment in particle image velocimetry is needed in the fishery industry for effectiveness. Also, particle image velocimetry is needed to be improved to overcome the disadvantages.

Grant [9] reviewed the evolution of particle image velocimetry. In the study, the history of PIV, correlations, and particle dynamics are explained. Particle image velocimetry is characterized in detail. According to Grant, PIV is found feasible and expanding method. General suggestions are also explained.

Liu et al. [10] examined the effect of dispersed phase on turbulence characteristics. In the study, different dilute liquid-liquid dispersion is used. PIV and CFD are also utilized in the study. According to the CFD results, with an increase of dispersed volume fraction, turbulent kinetic energy got smaller. On the other hand, viscosity influences the energy dissipation rate under some conditions.

Daigle et al. [11] employed large-scale particle image velocimetry for the measurement of river ice velocity. Two orthorectification techniques are presented. The study is performed on St. Lawrence and Montmorency rivers. According to the results, two orthorectification techniques provide an estimation of pixel physical dimensions. Strong consistency between the numerical model and measurements is found in velocity values in the case of moderate ice coverage.

Liu et al. [12] employed stereoscopic particle image velocimetry to shell and tube heat exchangers. With the use of SPIV, flow field is measured. Furthermore, numerical simulation is also, and different helical baffles are considered. The results reveal that maximum relative errors are found as almost 3%, 6%, and 1.5%. The values have belonged to x, y, and z-direction, respectively. In the case of 480, 1000, and 1500 of Reynolds number, the values of deviations for the maximum transverse velocity components between simulation and experiments do not exceed 9%. In higher Reynolds Number, vortex strength increases. Moreover, the values of deviations for vorticity and z velocity distribution between experimental and numerical results are restricted to 8% and 5%.

Wang et al. [13] investigated the converging region of two submerged parallel jets. With the use of particle image velocimetry, various flow parameters are analyzed. According to the results, in PIV M1 the standard deviation of measurements does not exceed 3%. As the ratio of the y-axis to jet width changed from 3.5 to 8.5, strong momentum transfer occurred. Namely, the momentum transfer occurred noticeably after MP. At the inner edges, lateral motions of the jets could be observed under some conditions.

Chen et al. [14] examined the tracking characteristics of tracer particles in the study, and supersonic flow conditions are taken into account. Particle image velocimetry is utilized for the motion of tracer particles. According to the results, 30 nm TiO_2 particles are found as the better choice in terms of tracking characteristics with insignificant agglomeration. Additionally, measurement of the shock thickness is affected by tracking deviation slightly. The seeding system is found feasible for mitigating the agglomeration of tracer particles.

Pan et al. [15] examined the macroscopic characteristics of the turbulent flow. In the study, PIV and LES coupled with a sliding mesh approach are used. Also, a vessel equipped with an agitator is utilized. According to the results, a long-short blade agitator shows considerably different turbulent characteristics from conventional agitators. Furthermore, the direction of the flow in the vortex above the short blades is found to be entirely different from the classical Rushton turbine. Consequently, long-short blades agitator could show good results in terms of some parameters. The mass exchange could be observed in the almost entire tank.

Li et al. [16] investigated the air distribution performance of a swirl diffuser. By using two-dimensional particle image velocimetry, flow field measurement is performed. The results indicate that strong rotation and vortex near the swirl diffuser outlet could be seen in the center region. Moreover, the dimensionless velocity had an inverse relationship with the dimensionless vertical height and dimensionless horizontal distance. The situation is valid in the case of dimensionless horizontal distance and dimensionless vertical height being greater than 1 and 4, respectively. At any flow rate, the swirl diffuser could generate more induced air and decline the draught effect efficiently.

Adrian [22] reviewed Particle Image Velocimetry, milestones, current status, future advances, and goals. Information about PIV, components, state of art, and desirable developments are explained. Also, Stereo PIV and previous and future works are discussed.

Song et al. [23] employed particle image velocimetry to twisted tape. In the study, measurements of the flow field are carried out via PIV. According to the results, increasing the radius caused linear velocity direction made stronger. Higher Reynolds number made the friction loss smaller at the wall. Additionally, the higher Reynolds numbers result in convergence in profiles of velocity.

Tang et al. [24] proposed a methodology called wavelength division multiplexing depending on PIV. In the study, the viability of WDM-PIV is discussed. Therefore, a triple-pulsed PIV system is utilized. According to the results, SPEC is not found as the best choice for WDM-PIV. Velocity differences are not considered in the two regions. Consequently, the WDM technique is found feasible method to realize multiple pulsed PIV.

Wen et al. [25] employed particle image velocimetry to plate-fin heat exchangers. In the study, flow parameters such as streamlines and velocity contour graphs are revealed. The results show that flow maldistribution is found to be a crucial factor in the conventional header. Furthermore, the uniformity of fluid distribution could be improved in the y and z directions. The improvement could be possible via the improved header configuration with the punched baffle. Thanks to the punched baffle, the flow maldistribution parameter and the ratio of the maximum velocity to the minimum decrease.

Prasad et al. [26] carried out a study for the effects of resolving the spot. By using arrays of various resolutions, the effects of resolving spots are investigated. According to the results, as the pixel size became bigger than the particle image, the mean bias error became important owing to the finite numerical resolution of the correlation function. Contrary to the situation, with the particle image became larger, random error in the electronic images dominated owing to irregularities.

Rockwell et al. [27] carried out a critical evaluation of the PIV technique using laser scanning techniques. In the study, the characterization of unsteady flows utilizing laser scanning methods is also evaluated. According to the results, high-resolution PIV supplied effective illumination for small particles in case of diameters are below the diffraction limit. Optimization of scanning method needed some concepts such as illumination time, exposure, and the retrace time of laser scan.

Brandt and Merzkirch [28] performed particle image measurements for a spray jet. Particle image velocimetry is used for the velocity measurement of droplets. According to Brandt and Merzkirch, PIV is feasible for the measurement of velocity distribution in the spray jet. Compared to PDA, the accuracy of PIV is lower in terms of the size range.

Bryanston-Cross et al. [29] employed digital particle image velocimetry to wind tunnel working at transonic speeds. In the study, quantitative visualization is realized. According to the results, the shock and separation bubbles are not far from each other at the rear of the fan casing. The position of the separation bubble is found with the Mach number of 0.82. Also, the shock is found to extend almost 75 mm from the wing.

Jambunathan et al. [30] conducted a study for an improved cross-correlation method. The improved cross-correlation algorithm is used for particle image velocimetry. The results show that improvement inaccuracy could be seen clearly. Relative errors got smaller and correlation coefficients increased. Consequently, the improved cross-correlation algorithm had a better result for simulated uniform, re-circulating, and bi-axial shearing flows, respectively.

Gray and Greated [31] conducted a study about the evolution of particle image velocimetry. Flow illumination methods and recording methods are compared. Also, image analysis, post-processing, stereoscopic systems, and new developments are explained. According to the results, PIV could not reach its full potential, so further developments are required.

Adrian [32] investigated digital particle image velocimetry. Spatial resolution and dynamic ranges are also examined. According to Adrian, matching the resolution of medium and particle image diameter is found as significant in terms of resolution. Obtaining 100–500 μm of spatial resolution is possible under some conditions.

Melling [33] investigated the suitable tracer particles for the PIV technique. Flow tracking capabilities, light scattering characteristics, and aerodynamic tracking capabilities of tracer particles are examined. According to Melling, having about 1 μm or smaller diameters are better choices in the case of typical turbulent or high-speed gas flows. Furthermore, a larger maximum particle size is found feasible via hollow or porous particles with a lower density ratio. LDA and PIV showed similar difficulties in terms of seeding. To acquire a high-quality particle image velocimetry record, scattering is significant.

Ettema et al. [34] applied particle image velocimetry to ice and water velocities. According to the results, PIV is found feasible for determining ice velocities. Moreover, using ice velocity via PIV resulted in a difference of 5% in ice discharge.

Santiago et al. [35] carried out a study for micron-scale particle image velocimetry. Micro PIV was used for measuring flow fields. According to the results, instantaneous velocities are affected by Brownian motion. The stochastic effect of Brownian motion had an influence on instantaneous velocities. Also, the accuracy of the fluid velocity measurements is affected by some parameters such as the diffraction limit of the recording optics and the interaction of the fluid with the finite-sized seed particles. Moreover, noise in the particle image field is characterized as other limitation parameters. On the other hand, approaching a velocity is observed as 35 μm/s. The situation is seen at the midplane.

Quenot et al. [36] employed dynamic programming to particle image velocimetry. In the study, a considerable increase in spatial resolution and accuracy is achieved. According to the results, by means of ODP-PIV, the accuracy is acquired as better than 0.5 pixel/frame for two-image sequences. Furthermore, the accuracy is lower than 0.2 pixel/frame for four-image sequences. The latter situation occurred even with a 10% noise level and a 10% rate of appearance and disappearance of particles.

Meinhart et al. [37] carried out a study about micron scale particle image velocimetry. The accuracy of the PIV system is evaluated in a microchannel. According to the results, PIV measurements had an agreement within 2%. The situation is valid for the analytical solution for flow in a rectangular channel.

Rosengarten et al. [38] employed particle image velocimetry to heat transfer process in a rectangular cavity. In the study, mantle heat exchangers utilized in solar water heaters are evaluated. Also, a CFD package was used. The results showed that the effect of turbulence decreased with the decrease of the Reynolds number. In the bottom of the tank, heat transfer wasn't found suitable for solar water heaters.

Hopkins et al. [39] presented a technique for complex geometries. The technique is also demonstrated. PIV was used for flow visualization. The results showed that an eddy owing to an adverse pressure gradient was observed. PIV had a limitation for complex geometries. PIV could be used for measurements in any cross-section as an index of refraction matching the working fluid to the model.

Scarano and Riethmuller [40] presented a method based on cross-correlation for PIV. The performance of the method is investigated and also compared with the conventional cross-correlation method. According to the results, using cross-correlation interrogation steps is found important for the window refinement method. Also, the window offset with sub-pixel precision influenced the pixelation. Finally, choosing a proper correlation peak fit function got less important.

Forliti et al. [41] quantified the bias and precise errors for DPIV. In the study, uniform displacement is utilized. According to the results, interrogation region size had a bit effect on the bias error. The Gaussian and the corrected Whittaker results showed good consistency with each other for the potential core portion of the jet.

Sharp and Adrian [42] conducted a study about flow structures around the Rushton turbine. In the study, particle image velocimetry is used for small-scale flow structures. The results showed that discrepancies belong to mean and RMS velocities between 50 frame and 100 frame ensembles did not exceed 3%. Also, local dissipation is broken up with the getting far from the blade in r and z directions, respectively. Finally, the ratios of mean squared velocity gradients are in the range of 0.2 and 1.8.

Kim et al. [43] carried out a study with micro-particle image velocimetry. In the study, two microchannel configurations are used. Experimental measurements and numerical simulation results of channels are compared to each other. According to the results, near the sharp corners, strong electric fields could be seen. The electric fields near sharp corners caused an increase in the streamwise velocity. Moreover, adverse pressure gradient couldn't be seen in pure electro-osmotic flow for a grooved-channel.

Dierkshiede et al. [44] employed endoscopic particle image velocimetry to internal combustion engines and turbomachinery. E-PIV measurements are carried out in the internal combustion engine. The results are compared with the measurements of standard optical access through a window. The results showed that only the upper part of the tumble flow vortex could be seen. The situation came from the limited size of the field of view. Also, in the cylinder, strong air motion had velocities greater than 10 m/s from right to left. Consequently, E-PIV was found advantageous.

Deen et al. [45] examined the recent developments of particle image velocimetry. In the study, especially two-phase bubbly flows are focused. Two-phase PIV, correlation methods are explained. The results showed that the dispersed phase could cause various problems in particularly at high gas fractions. The shadows of bubbles and bubbles are accepted as the main problems. The shadows measured continuous phase harder.

Cho et al. [46] carried out two-dimensional particle image velocimetry measurements for the refrigeration compartment. Duct systems were analyzed via FLUENT. The results showed that the new duct system is feasible for cooling the door basket region efficiently. Also, the new system improved the uniformity of the temperature distribution in the refrigeration compartment owing to its effectiveness.

Sugii et al. [47] applied a high-resolution particle image velocimetry method to arteriole in the rat mesentery. High-resolution PIV is utilized to measure velocity in arteriole and determine mesentery motion. The results indicated that the arteriole velocity profiles are acquired as blunt at the center region. Near the wall, the structures are sharper. Also, the maximum velocity is measured at approximately 3.0 mm/s at the center of the arteriole. Finally, the method is found effective for measuring blood flow in microvessels.

Richard et al. [48] investigated the interaction between a water mist and a diffusion flame via PIV. The flow pattern was also examined. According to the results, the momentum of water spray reduced the soot. And cyclic expansion of the flames caused an increase in the radial component of the velocity.

Deen et al. [49] performed a study about aerated Rushton turbine impeller. Two camera particle image velocimetry is utilized to acquire angle-resolved velocities and turbulence data. In the study, single-phase flow and a gas-liquid flow are taken into account.

Moreover, CFX 4.3 is utilized for simulations. According to the results, trailing vortices nearly vanished completely as the tank is aerated in the situation of single-phase flow. Moreover, the flow field transformed to be less periodic than without gas. Finally, the presence of gas does not affect the absolute liquid velocity fluctuations.

Choi et al. [50] investigated the relationship between a bubble and fluid. The relationship is analyzed via a moving object flow image analyzer (MOFIA) including PIV. According to the results, the spatial relationship between the three-dimensional bubble and the velocity field could be seen obviously. In addition, the minor axis of an oblate spheroidal bubble and the direction of motion of the bubble are the same as each other. The situation came from the deformation of the bubble and the drag force by the fluid. Finally, the movements of small and large bubbles are observed spirally.

Hu et al. [51] performed a study about the simultaneous measurement of velocity and passive scalar concentration fields. Combined particle image velocimetry and planar laser-induced fluorescence techniques are used for measurements. The results reveal that instability gets bigger downstream. Also, jet flow transformed into turbulence as the large vortex rings decayed. In the shear layers between the jet flow and ambient flows, high turbulence intensity and high concentration fluctuation regions could be seen.

Bömmels and Rösgen [52] evaluated the components for the combined PIV and DGV system via pulsed laser. According to the main results, the laser linewidth was 11.6 MHz as the velocity is about 6.3 m/s. The strongest absorption pattern has belonged to the line at GHz.

White et al. [53] carried out a study on deformation measurements in geotechnical models and element tests. Particle image velocimetry and close-range photogrammetry are used for tests. According to the results, the system had some advantages such as better accuracy, precision than previous image-based methods of displacement measurement. Also, the achievement is obtained had a relationship with an order of magnitude.

Fei et al. [54] investigated the flow field around ring packing via PIV measurements and CFD simulations. A new Plum Flower Mini Ring is developed and compared with the Pall Ring and Intalox Saddle. The results indicated that with the decrease in the height/diameter ratio of the ring packing, the separation process was improved, and the pressure drop decreased. Furthermore, the PFMR had a lower pressure drop. Also, the PFMR showed better mass transfer efficiency.

Bröder and Sommerfeld [55] investigated bubble interactions in turbulent flow via a combined PIV/PTV system. In the study, some parameters such as the spatial changes of the bubble size distribution, coalescence rates are observed. According to Bröder and Sommerfeld, the combined system is found feasible for analyzing the behavior of bubble swarms. Moreover, other effects are not as dominant as the collision rate. The overall coalescence rate was around 3%.

Cao et al. [56] carried out a study about a centerline injector. In the study, the viscosity-stratified flow is carried out via PIV and LIF techniques. Also, circular geometry is used. The results indicate that a sharp increase in RMS axial velocity and instantaneous PIV realization has a good agreement with each other. The unstable region shows different modes because of parameters such as viscosity ratio, volume flux ratio, and Reynolds number. Also, two modes are seen in the study.

Khan et al. [57] investigated complex turbulent flows via two-dimensional PIV. Complex turbulent flows are revealed utilizing 2D PIV. According to the results, the flow was almost axial below the impeller. The flow was composed of axial and radial flow in the remainder of the vessel. In LDA, RMS axial velocity was slightly lower.

Kilander and Rasmuson [58] conducted a study about hydrodynamics and turbulence in a square tank. In the study, the tank is stirred with Lightnin A310. Also, LES-PIV is utilized. According to Kilander and Rasmuson, the LES-PIV method and direct approach reveal a good consistency about dissipation. Furthermore, LES-PIV and direct calculation show differences in mean value owing to the filter width. Moreover, LES-PIV method is found to be insufficient to explain turbulence in the bulk accurately.

Bown et al. [59] employed micro-particle image velocimetry to two microchannel flows. The effect of out-of-plane resolution is investigated. PIV results and CFD simulations are compared. According to the results, a small deviation is observed in the case of the isotropically etched, straight channel in terms of velocities. Close to the top and bottom of the channel, results of the measurement plane and measured velocity have 1% and 10% errors respectively. Interrogation volume depth is one of the reasons for systematic errors near walls.

Dezhong et al. [60] revealed a drag reduction of turbulent water flow. In the study, surface additives are utilized. PIV and PDA are used for measurements. According to the results, in the region of complete drag reduction, friction factor and Reynolds number have an inverse relationship with each other. However, in the region of post drag reduction, the friction factor and Reynolds number have a direct relationship with each other till the Dean's line. Near the wall region of the solution, the velocity gradient of turbulent water flow is higher. In the center, the situation became reversed.

Westerweel and Scarano [61] presented an adaptation of the original median test. The test is revealed for discovering the spurious PIV data. According to Westerweel and Scarano, a small adaptation of the original algorithm causes a universal distribution of the normalized residual. Moreover, a single detection threshold could be possible in a variety of flow conditions without information on flow conditions. The universal character enables to use a single detection threshold especially in transient flows.

Yoon et al. [62] employed gas phase particle image velocimetry to reactant flow channels. Particle Image Velocimetry is also used for measurements of gas-phase velocity fields. According to the results, particles larger than 1 μm diameter are found to be insufficient for deceleration. Seeding with water droplets is offered.

Yamamoto et al. [63] carried out a study on turbulent combustion. In the study, PIV and LDV are used utilized, respectively. The results reveal that smaller interrogation areas supplied higher spatial resolution. In LDV measurements, low-velocity data is not found. Furthermore, PIV and LDV give similar results in terms of the integral length scale. Furthermore, both techniques propose similar results in cold flow and combustion.

Al-Hajeri et al. [64] investigated single ceramic candle filters by using PIV and CFD. PIV and FLUENT software are utilized in the study. The results show that the direct measurement of the radius is found as an appropriate method. PIV and CFD have a good agreement for face velocity of 4 cm/s, particularly low-velocity ratios. Furthermore, in the case of Stokes number lower than 250, a little variation of radius convergence is seen.

Thet et al. [65] investigated hydrodynamics and regime transition in bubble columns. In the study, experiments are carried out with and without an internal draught tube. Also, PIV is used for flow visualization. The results indicate that Reynolds stress got smaller with the use of a draught tube. On the other hand, an earlier transition to a heterogeneous regime could be performed by increasing the viscosity of the liquid. Aspect ratio in glucose aqueous solution influences the transition gas velocity.

Xu et al. [66] performed a study about near-surface turbulence via PIV. In the study, mass transfer across the gas-water interface and flow parameters are revealed. The results show that wind speed and the mass transfer velocity generally have a direct relationship with each other. Also, using bulk turbulence is not so effective in terms of some parameters. On the other hand, a possible general relationship could be extracted in the study.

Triep et al. [67] investigated the micro axial blood pump. In the study, three different impeller designs are used. Digital particle image velocimetry and computational fluid dynamics are used for investigation. The results reveal that DPIV and CFD show a difference in very high-velocity gradient regions. Some drawbacks could be overcome via micro DPIV. Generally, CFD and DPIV have a good agreement in results.

Bach et al. [68] investigated the thermal spraying process. In the study, atmospheric plasma spraying (APS) and high-velocity oxygen fuel plasma spraying (HVOF) are used. PIV is also utilized. According to the results, particle velocities are affected by combustion chamber pressure significantly. Contrary to combustion chamber pressure, particle velocities are not dependent on oxygen/fuel mixture. Oxygen/fuel mixture affects the temperature of spray particles. Consequently, PIV is found to be a proper method for thermal spraying.

Güler et al. [69] investigated drift reduction potential and spray characteristics of three different drift retardants. In the study, particle image velocimetry software is utilized for the measurement of droplet velocity. For this purpose, wind tunnels and hollow cone nozzle spraying are also used. The results indicate that slightly higher velocities are related to drift retardants. In terms of ground drift potential and the airborne deposit, polyvinyl polymer and nonionic colloidal are not reasonable respectively.

Dijkhuizen et al. [70] applied particle image velocimetry to granular temperature fields. In the study, velocity and temperature fields are measured. According to the results increasing, particle image density has a nearly decreasing effect on the error and granular temperature. Compared to a standard three-point Gaussian fit, the least-square fit peaked more accurately.

Wieneke [71] investigated the volumetric self-calibration technique. In the study, analyzes of tomographic particle image velocimetry and three-dimensional particle tracking velocimetry are also based. According to Wieneke, the method has some advantages in terms of decreasing ghost particles and seeding densities. Moreover, the mentioned technique is also found feasible for stereoscopic particle image velocimetry via thicker light sheets. Moreover, the method is found as a good choice for the quality of the volumetric vector field.

Santos et al. [72] employed particle image velocimetry to reaction injection molding. Several flow parameters are acquired via PIV. The results show that the spatial distribution of the flow dynamics is matched in the x-z plane. The situation occurs for the first time. Due to the opposition of two forces, the instability and mixing in RIM occur.

Dietrich et al. [73] employed particle image velocimetry to examine bubble passage at a liquid-liquid interface. In the study, a high-speed camera and Newtonian liquids are utilized. According to the results, interfacial, elastic, and viscous forces together have a deformation effect over the bubble and interface considerably. Intermolecular forces show a crucial role before the rupture as the film gets thinner. On the other hand, as the bubble approaches the interface, the liquid-liquid interface is deformed. The situation comes from upward flow at the front of the bubble.

Andersen et al. [74] applied PIV, LIF, and CFD to thermal stratification devices. In the study energy efficiency is focused. Two stratification pipes are used. According to the results, horizontal heat transfer could be decreased by employing a smaller inner and outer diameter of fabric pipes. The calculated thermo-syphonical flow rate shows lower values in fabric pipes for 1 L/min. CFD is found a reliable tool but further validations are required.

Pascual et al. [75] examined turbulent flow in typical cooling crystallizer geometry. SPIV and LES are utilized in the study. According to the results, the local heat flux shows higher values in the middle region of the heat exchanger surface between the shaft and outer wall. Instantaneous fluctuations in the flow have no effects on the temperature profile at the heat exchanger surface due to the fastness. Furthermore, large eddy simulation with the Lattice-Boltzmann scheme is found as suitable for the study.

Deshpande et al. [76] performed a study about jet loop reactors. In the study PIV, LDV and HFA are used for measurements. PIV, LDV, and HFA are utilized for several parameters. CFD predictions are also utilized. According to the main results, PIV and LDV have a good agreement in terms of mean axial velocity under some conditions. Three techniques have advantages and disadvantages. For the axial location of 0.1 and 0.2 m, LES predictions have a great consistency with experimental results. On the other hand, a strong agreement is observed in the measured and predicted ε profiles like mean velocity.

Müller et al. [77] employed stereoscopic particle image velocimetry and acetone planar laser-induced fluorescence to freeboard of a fluidized bed. In the study, the parameters of bubbles such as eruption and stream of bubbles are examined. According to the results, the bubble eruption profile of a stream of bubbles and the eruption of a single bubble show nearly the same trends. Furthermore, bubble-induced turbulence diminishes quickly. The time-averaged flow profiles show different motions at the center of the fluidized bed and walls separately.

Olayiwola et al. [78] conducted a study on laminar flow systems. In the study, the systems with periodic finned surfaces are investigated. PIV software and CFD are also utilized. The results indicate that the periodic recirculation eddies are observed near the fins. Eddies are strongly affected by employed oscillation. Compared to other geometries, triangular finned geometry shows the best performance by taking into account enhanced average crossflow velocity.

Körbahti [79] investigated flexible delta wings. In the study, a low-speed wind tunnel in subsonic flows is used. Particle image velocimetry is utilized for visualization of the wake behind the delta wing. According to Körbahti, a delta wing with a thickness of 1 mm has an interaction with limit cycle vibrations under some conditions. Moreover, air velocity has a relationship with gravity. PIV is found as feasible for revealing wake behind delta wing in the study.

Yayla et al. [80] examined the non-slender diamond wing. In the study, particle image velocimetry is used for visualization of flow structure. According to the results, the angle of deviation affects flow structures. Free flow affects the breakdown of vortexes. Moreover, wing surface is related to non-continuum flow after vortex breakdown.

Guo et al. [81] applied particle image velocimetry to the vertical water channel. Using particle image velocimetry, several flow parameters are revealed. The results show that large coherent vortexes could be seen around the centerline of the mixing layer. The negative value of instantaneous fluctuations could be seen everywhere near the vortexes. On the other hand, the peak values of Reynolds number are seen centerline of the mixing layer.

Ragnarsson et al. [82] focused on the physical modeling of argon shroud. PIV is used for gas inlet designs. The highest oxygen contents are observed in vertical injection. Also, the modest flow rate of argon gas is a good choice. Furthermore, argon production could be better employing dual inlets.

Cooper and Tait [83] investigated water worked gravel deposits. PIV measurements are performed for flow velocities. Detailed data and flow parameters are revealed. According to Cooper and Tait, drag-generated forces show higher values at lower submergences over both deposits. Decomposing the total fluid force into substantial physical components could be achieved. Furthermore, the form of induced forces gives smaller values. However, the pattern shows a considerable difference over the two deposits, particularly in the bed roughness layer.

Nordlund and Lundtröm [84] carried out a study about dual-scale porous media. In the study, flow behavior is revealed using micron-scale particle image velocimetry. The results show that the flow rate has a strong effect on the shape of the flow front in the dual-scale region. The slit velocity vectors near the flow front are observed as almost perpendicular to the front. Higher flow rates show lagging at the front in the micro-scale silt region.

Oner et al. [85] performed a study about flow around a horizontal circular cylinder. Flow velocities are measured via particle image velocimetry. Also, multiple linear regression and artificial neural networks are utilized for the study. According to Oner et al., artificial neural networks are found a better choice in terms of results. The values of maximum tangential velocities, which are acquired at out of boundary layer, are influenced by Reynolds number, gap ratio, and α angle respectively. Moreover, the tangential velocity with different angles decreases after just out of the boundary layer. The situation occurs in the region affected by the curved surface of the cylinder.

Mgharaz et al. [86] developed a fiber laser model in different designs. In the study, two specific cavities are described and Q-switched Yb-doped double-clad fiber lasers are chosen. According to the results, designing two cavities could be achieved. Furthermore, the rise time of the electro-optic modulator is found as an important parameter. Consequently, Yb-doped DC fiber lasers are found feasible.

Ragni et al. [87] carried out a study about particle response time. Particle image velocimetry is used in the study. According to the results, the shortest time response has belonged to dehydrated solid particles of 100 nm smaller. The other sets of solid seeding materials give a relaxation time of 2 μs. The time response, which is calculated by employing ensemble-averaged correlation is a bit greater than the time response related to the maximum occurrence.

Satake et al. [88] performed a study about circuits for particle image velocimetry. In the study, the performance of the circuit is evaluated. The comparison is performed via C++ code. According to the results, FPGA conducts the calculation 8.93 times faster than PC. The system is found feasible in terms of reading artificial PIV standard images and real experimental images. Finally, both results and FORTRAN codes have consistency with each other in terms of velocity vectors.

Umeyama and Matsuki [89] performed a study about the kinetics of internal waves. Particle image velocimetry is used for measurements. Some parameters such as the experimental vector field of velocity and vertical distributions and components are revealed in the study. According to Umeyama and Matsuki, the accuracy of particle image velocimetry is proven. A vortex pair existed as the thickness ratio was large enough in two density layers.

Green et al. [90] employed PIV as an attraction channel for fishways. In the study, the flow field is revealed. PIV is used for visualization. According to the results, depth over the ramp does not have a strong influence over the maximum velocity. However, the depth influenced downstream traceability, water attraction, and characteristics of the obstruction at the inlet are located in upstream and flow patterns, respectively.

Kähler et al. [91] investigated the spatial resolution in digital particle image velocimetry. In the study, the resolution limit of digital particle image velocimetry is focused mainly. Spatial resolution is examined in terms of tracer particles and the imaging and recording system. According to the results, the resolution is based upon particle image diameter in the case of single-pixel ensemble correlation. In particle tracking velocimetry, spatial resolution is not restricted by particle image diameter. The resolution is influenced by image size and density directly in the case of window correlation methods.

Kürekci and Ozcan [92] employed particle image velocimetry in a cubical cavity. In the study, PIV and CFD are used for velocity measurements and the numerical solution, respectively. Natural convection is focused on the study. According to Kürekci and Ozcan, PIV and CFD results have consistency with each other in the case of the midplane of the enclosure. However, some differences between them are also observed. Furthermore, near the hot and cold walls, the temperature field shows high gradients. Moreover, Nusselt Numbers in the study do not show a significant deviation from previous works of literature.

Figueredo-Cardero et al. [93] employed particle image velocimetry to animal cell perfusion processes. PIV is utilized for the main fluid flow. According to the results, at the filter-fluid boundary, the discrepancy in the fluid tangential velocity and filter tip speed is not seen. Additionally, the tangential velocity slip is found almost 10% of the filter tip speed under the conditions explained in the study. Reynolds stress components in TC systems are smaller than those in RCF systems in the case of the bulk of the annular region.

El-gendy et al. [94] applied particle image velocimetry to a gelled waxy oil pipeline. In the study, pressure profile and PIV are utilized. According to the results, increasing upstream pressure after gelation rapidly is not enough to restart the flow. The delayed restart could be the pusher fluid pressure is slightly lower than the critical value. Delay time could be reduced using pusher fluid pressure. On the other hand, gel shear modulus could reach a steady state lately under some conditions.

Ryerson and Schwenk [95] investigated a simple digital particle image velocimetry, which had some properties, such as being widely available, cheap, and having high accuracy. According to Ryerson and Schwenk, more affordable, high-speed video cameras could be possible. Furthermore, the same situation is possible for laser light sources too.

Simo Tala et al. [96] employed particle image velocimetry to a model of the heat exchanger. PIV is used for revealing flow characteristics. In the study, two components particle image velocimetry and multirow finned tube exchanger are utilized. According to the results, the angular evolution of the flow structure results in a rise of secondary vortical structures. Additionally, noticeable vorticity generation is seen in the vicinity of fin tube junctions. The main horseshoe vortex strength has the smallest value at the first junction.

Atibeni et al. [97] performed a study about the flow field in a stirred tank. In the study, particle image velocimetry is used for the flow field. Also, floating particles are taken into account. According to the results, down triangular baffles are found as the best configuration. As the down triangular baffle is used, the reduction of specific power consumption is approximately 58%. Moreover, reduction in some parameters is greater than standard baffles by using down triangular baffles.

Jung et al. [98] carried out a study about high-speed blood flows. With the use of time-resolved X-ray PIV, the velocity field is acquired. High-speed blood flow is investigated. The performance of the system is assessed in terms of minimum exposure time. According to the results, time-resolved X-ray PIV and theoretical results show consistency with each other. Furthermore, a higher frame rate and lower spatial resolution result in higher maximum velocity. Consequently, time-resolved X-ray PIV is feasible for the measurement of blood flows.

Hayasaka et al. [99] investigated the flow field generated by vorticella. Particle image velocimetry is used in the study. The stability and mixing performance of vorticella are focused. According to the results, Vorticella influences the maximum of 56% of the chamber area. Moreover, a single-cell of Vorticella causes two vortical flows in front of the cell body. The position of a single cell in a single chamber is found mas feasible.

Weheliye et al. [100] employed phase-resolved particle image velocimetry to cylindrical shaken bioreactors. In the study, fluid mechanics of shaken bioreactors are analyzed via phase-resolved particle image velocimetry. According to the results, the flow shows generally two counter-rotating vortices near the free surface under some situations. Changes in the movement of two counter-rotating vortices could be achieved by increasing rotational speed. Increasing Froude number causes an increasing effect on the extent of out of phase flow increased.

Fujimura and Hotta [101] carried out a study about wrinkles on women's faces. In the study relationship between the movement of the face and wrinkles is explained via particle image velocimetry. According to Fujimura and Hotta, the parameters such as angle show no noticeable difference between both groups. However, on the forehead, velocity shows a noticeable difference at the top site between both groups. The older group has more deformation on the forehead.

Hoque et al. [102] applied particle image velocimetry to oscillating grid apparatus. In the study, the energy spectrum and velocity field are analyzed. According to the results, the spectral slope of $-5/3$ is revealed. Furthermore, the peak value of Duuu/rε is acquired nearly 4/5. The peak value has consistency with the Kolmogorov similarity hypothesis. The longitudinal and transverse energy spectra show a similar trend in the inertial subrange. The overlap reveals the almost homogeneous and isotropic turbulence velocity field in the experimental system.

Muste et al. [103] employed large-scale particle image velocimetry to shallow free-surface flows. In the study, the capabilities of the mentioned technique are examined. The results point out that large-scale particle image velocimetry is found feasible for the measurement of velocities in shallow and low-velocity flows. The mentioned method allows the assessment of velocity-derived quantities.

Keller et al. [104] carried out a study about a large-scale hydraulic model. Particle image velocimetry is used for the acquisition of a horizontal velocity field. According to the results, the air core in the water vortex hinders the resolution of the whole field. Furthermore, the rotation of measured horizontal velocity around the vortex influences a wide area. The situation shows the feasibility of two-dimensional Navier Stokes equations. The deviation of circulation values from the median circulation number does not exceed 10%.

Akar and Kücük [105] carried out a study about the unsteady flow structure downstream of the inner cylinder. In the study, controlling the unsteady flow structure is the main target. Particle image velocimetry is used for revealing flow characteristics. Also, seven different diameters are used in the study. According to Akar and Kücük, vortex shedding is affected by the perforated outer cylinder downstream. The ratio of inner diameter to outer diameter influences controlling of the flow.

Soydan et al. [106] investigated the turbulent flow around a horizontal cylinder laid on a channel bed. In the study, particle image velocimetry is utilized for measurements. Also, FLUENT software is used for numerical solution. According to the results, Reynolds stress models do not always present correct results exactly in the study. In terms of separation zones, the Reynolds stress model shows some deviations from experiments.

Liu et al. [107] performed a study about flow structures around continuous cryogenic Taylor bubbles. PIV is used for revealing flow structures. In the study, a concentric glass tube with different diameters and inclination angles is utilized. The results point out that the minimum stable distance between Taylor bubbles has the smallest value in the case of inclination angle from vertical was 60°. The distance increases from 60° to 30°. Furthermore, the maximum error and the maximum error of the curve in the study are found as

7.9% and 4.7%, respectively.

Decker et al. [108] conducted a study about gas-solid flow in ducts. PIV and CFD are used for experiments and numerical analysis respectively. For numerical analysis, CFD code in FLUENT 13 is used. According to the main results, the kinetic theory of the granular materials equilibrium model shows satisfactory results for the representation of the solid turbulence in the dilute gas-solid flow. The effects of the curve in the development of the flow are found significant. The effects also could be seen in the second horizontal duct.

Pawar et al. [109] carried out a study of dynamic jet behavior. Dynamic jet behavior and turbulent flow properties are examined using particle image velocimetry. The results point out that with the increase of axial position, the RMS values became smaller. The situation occurs at the center of the jet. Compared to the center of the jet, the RMS values are greater in the shear layer. The velocity profiles, decay, and spreading rate have consistency with previous studies in the literature.

Salem et al. [110] performed a study about the two-dimensional rough wall with narrow apertures. In the study, PIV is used for the measurement of the streamwise velocity and aperture velocities respectively. According to the results, higher aperture velocities make the vortex decline. The higher exit layer height declines the vortex. Moreover, rotor speeds and mean slot velocities influence over the reversal flow in the slot.

Del Campo et al. [111] employed stereoscopic particle image velocimetry to a wind tunnel. In the study, several parameters such as three-dimensional velocity field, the pressure distribution, aerodynamic loads are acquired. Also, the rotating blade of a HAWT is utilized. According to the results, viscous stresses could be ignored anywhere. The Coriolis force is significant for the acquisition of tangential loading correctly. Furthermore, normal forces obtained with the use of SPIV are lower than those of panel code. Also, SPIV has more uncertainties owing to spatial resolution.

Karakas et al. [112] carried out a study about three-dimensional models with four different airfoil profiles. Digital particle image velocimetry is used for flow visualization. According to the results, examinations are not influenced by the cross-section shape of the wing. On the other hand, oscillation parameters are stronger. Particularly, in terms of thrust and general flow pattern, oscillation parameters are more important.

Hongwei et al. [113] carried out a study about optical flow measurement technology. In the study, a comparison of optical flow algorithm and particle image velocimetry is also performed. The results point out that a smoother velocity field could be acquired via the optical flow algorithm. Therefore, the optical flow algorithm is feasible for complex flows. Additionally, the weighted value affects the error.

Sergis et al. [114] employed particle image velocimetry to two replicas of HyperVapotron geometries. In the study, the flow field in HyperVapotron geometries is also revealed. According to the results, the MAST geometry has smaller groove speeds. The geometry is also more sensitive to hydrodynamic end effects. The locational stabilities of both geometries are not influenced considerably by means of free stream velocity changes.

Vali et al. [115] carried out a study about small pool fires. In the study, the velocity field is measured via two-dimensional particle image velocimetry. According to the results, a pair of vortices is seen under the liquid surface that high mass transfer occurred. In that situation, noticeable fluid motions are not seen in the depth of the pool. Additionally, the boundary condition at the bottom of the pool affects the size of vortices.

Keramaris [116] employed hot film anemometry and particle image velocimetry to open channel flows. In the study, two flow measurements are performed and compared. Also, impermeable and permeable beds are utilized. According to Keramaris, HFA and PIV have consistency with each other in terms of the results considering velocity distribution. Between HFA and PIV, small differences are found concerning turbulent intensities. However, PIV has more accuracy in Reynolds stresses.

Fu et al. [117] employed three-dimensional particle tracking velocimetry and two-dimensional particle image velocimetry to indoor airflow. Two measurement techniques are used and compared in terms of low turbulence airflow in actual experimental conditions. The results indicate that three-dimensional particle tracking velocimetry could not give acceptable results in the case of smaller tracking densities than 2. However, in the case of greater tracking densities such as 4, three-dimensional particle tracking velocimetry is more efficient than typical particle image velocimetry.

Mühlich et al. [118] employed particle image velocimetry to vacuum–steam–vacuum treatment. Solid motions are revealed via particle image velocimetry and digital image analysis. According to the results, PIV and DIA are found feasible for the VSV process. Moreover, the accessibility of powder particles is influenced by transient hydrodynamics.

Ozturk et al. [119] studied the flow characteristics of multiple circular cylinders in a heat exchanger model. In the study, the cylinders are in a rectangular duct. By using laser particle image velocimetry, flow characteristics are revealed. The results show that arrangements of cylinders cause unsteady flow. Moreover, horseshoe vortices could be observed near the cylinder bases.

Tuncer et al. [120] carried out a study about flow past a swirl pane. Flow field visualization is performed via particle image velocimetry. According to the results, a stable recirculation zone and secondary weak recirculation zones have detected in the study. Consequently, the acquisition of the flame in the case of reacting flow could be possible.

Oner [121] examined two-dimensional turbulent flow around a smooth pipeline. In the study, particle image velocimetry is utilized for revealing flow velocities. Also, ANSYS is used for the numerical model. k-ω, k-ε and SST turbulence models are used. According to Oner, a large separation area is observed in the study. Furthermore, k-ε turbulence model is found as the worst choice in terms of geometries of pair of vortices and velocity field.

Ruonan et al. [122] employed acoustic doppler velocimetry and particle image velocimetry to open channel flow. In terms of several parameters, the performances of the two techniques are compared with each other. The feasibility of acoustic doppler velocimetry is also examined. According to the results, acoustic doppler velocimetry and particle image velocimetry show nearly the same results for a sweet point in the case of the sampling rate of more than 40 Hz. Moreover, the sampling rate has a considerable effect on the turbulent intensity and Reynolds stresses. However, the effect of sampling rate on time-averaged velocity could be ignored.

Consequently, assessment of the results of acoustic doppler velocimetry is significant in open-channel flows.

Im et al. [123] employed particle image velocimetry to 1/4 scaled-down model of the CANDU reactor. With the use of PIV, the flow field is revealed. Also, the Archimedes number is used for scaling analysis. According to the results, inertial momentum influences the biased position in the inlet jet. But the effects of inertia momentum could be ignored at higher values of Archimedes number. Higher values of Archimedes number cause the bias magnitude of impingement position to increase. Also, buoyancy effects affect the biased magnitude.

Oguma and Fujisawa [124] studied aerodynamic sound sources for a semi-circular in a uniform flow. By using particle image velocimetry, the sound source distribution is investigated. According to Oguma and Fujisawa, the aerodynamic sound of the circular cylinder is found greater than those of the semi-circular cylinder. However, the semi-circular cylinder offers better acoustic performance than the circular cylinder. The accelerated mean velocity region is longer in the circular cylinder.

Oguz et al. [125] investigated the cylinders located in deep water. In the study, the effect and intensity loads are examined. Particle image velocimetry is used for measurements. According to the results, wire thickness influences turbulent kinetic energy and Reynolds shear stress. To acquire an effective flow control, choosing porosity ratio and wire thickness as 0.6 and 4 mm are reasonable.

Ziegenhein and Lucas [126] employed particle image velocimetry to bubble columns. With the use of particle image velocimetry, measurements of liquid velocity and turbulence are performed. The results indicate that subareas generally have nearly no influence over the results. The sampling bias causes a flat velocity profile. The situation is valid for all volume flows. On the other hand, the sampling bias influences the normal component of the Reynolds stress tensor. In addition, the sampling bias has no influence near the wall in the case of all volume flows.

Fleischhauer et al. [127] employed particle image velocimetry to vibrational finishing. By using PIV, measurements of surface media velocity fields are carried out. According to the results, the motion of the bowl influences the fixed peaks. Furthermore, the media size, vibration amplitude, and moisture of media affect the indicators of the intensity of the random media motion.

Cristofano et al. [128] carried out a study about bathtub vortices. With the use of particle image velocimetry, experiments are performed. According to the results, a higher distance from the exit made the radius of the orbital motion around the hole bigger. Flow rate also influences the radius. Moreover, the flow rate has a reverse effect on the maximum dimensionless circulation. The maximum normalized circulation increases with the rise of distance from the hole.

Dogan ve Igcı [129] applied particle image velocimetry to a rectangular channel. In the study, test section surfaces are painted, and special filters are utilized. According to Dogan ve Igcı, reflection to the camera with laser light is found undesirable. Proper fog intensity and laser light are two important parameters for the quality of results. On the other hand, a signal to noise ratio is characterized as an affecting parameter of vectors.

Boutin et al. [130] carried out a systematic study on the multi-channel fluidic network. By using two dimensional and two components particle image velocimetry, velocity vectors, and flow distribution properties are acquired. CFD is also utilized for comparison in the study. The results indicate that the maximum possible uncertainty is found at approximately 13%. Furthermore, the PIV technique and CFD give similar results in the case of high flow rate conditions. Flow distribution could be affected by the locations and sizes of vortices.

Kirmse and Chaves [131] employed particle image velocimetry to melt the atomization process. In the study, particle image velocimetry is used for measurements. According to Kirmse and Chaves, small discrepancies between X5CrNi18-10 and X3CrNiMo13-4 are found. Namely, the metals give similar results. The breakup of the melt is observed approximately 60 mm from the nozzle in both cases. Moreover, the velocity change ranges from 120 m/s to 210 m/s.

Akar et al. [132], examined perforation and its effect on the cylinder body. With the use of particle image velocimetry, flow structures are investigated. According to the results, a porosity ratio of 0.6 is found as a significant value for Reynolds stresses and jet flow. Hence, the most useful flow control is acquired at 0.6 of the porosity ratio in the study.

Gong et al. [133] investigated the velocity distribution of a waterjet ship model. In the study, particle image velocimetry is used for velocity distribution. According to the results, the transverse vector is caused by the existence of the pumping action of the waterjet in cross-sectional speed. The cross-sectional speed increases inflow non-uniformity. Furthermore, the molded lines from the midship to the ship stern vary considerably.

Hu et al. [134] examined flow around an inclined square cylinder. With the use of particle image velocimetry, the flow field is observed. In the study, two types of inclinations and angles are used. The results indicate that the forward inclination improved the downwash. The downwash becomes a downward axial flow as the forward inclination angle increases enough. However, the backward inclination angle improves upwash. Moreover, the angle is large enough, the upwash becomes upward axial flow.

Kurec et al. [135] investigated the pressure wave, exchanger demonstrator. In the study, PIV and CFD are used for experiments and simulation respectively. For CFD simulations, standard k-ω, SST k-ω, and SST-SAS are used. CFD simulations are performed via ANSYS Fluent v.15. The results reveal that SST-SAS is a better choice in terms of mixing gases in the channel. Namely, the SST-SAS model has more consistency with the PIV result. In terms of penetration, SST k-ω shows good results and Standard k-ω has more differences with results.

Shokri et al. [136] examined a dilute liquid-solid mixture via planar PIV/PTV. With the use of planar PIV/PTV, the turbulent motion is revealed. High Reynolds numbers are considered. The results indicate that the influence of the coarse particles could be ignored for the liquid phase turbulence. Turbulent particle fluctuations of the liquid phase are not as large as those of streamwise and radial directions. 2 mm particles show an almost linear concentration gradient from the center to the pipe wall and greater radial transport.

Wen et al. [137] employed particle image velocimetry to shell and tube heat exchanger. In the study, a shell and tube heat exchanger with helical baffles is analyzed. PIV is used for revealing the flow field. According to the results, fold baffles influence both axial and radial velocities in the case of the external of the tube bundle. On the other hand, cross-sections A and B have smaller flushing angles. The situation is observed in the improved heat exchanger. Flow pattern is found periodic in shell side and the integrative performance of the improved heat exchanger is increased about 2–8%

Mitchell Ferguson et al. [138] proposed a methodology for regular, polychromatic, and irregular waves. Velocity fields around an oscillating water column are acquired using particle image velocimetry. In the case of an irregular wave, total kinetic energy and energy that are included in vortices had a linear relationship with each other. Additionally, polychromatic wave and the irregular wave give similar results via energy balance in terms of total kinetic energy. However, the two waves give very different results in terms of the amount of energy included by vortices.

Ismail et al. [139] employed particle image velocimetry to extra-cardiac tricuspid valves. In the study, flow patterns are revealed via two and three-dimensional particle image velocimetry. According to the results, three-dimensional flows could be observed in the immediate upstream and downstream of the valve. The situation could come from the complex anatomy of the right atrium. On the other hand, three-dimensional particle image velocimetry could be used in terms of the evaluation of the performance of the heart valves. Moreover, two-dimensional particle image velocimetry could be used in regions such as the middle of the atrium.

Patalano et al. [140] focused on a toolbox for LSPIV and LSPTV. In the study, RIVeR is developed for processing in Matlab. According to the results, RIVeR does not need an appreciable amount of computational time. The RIVeR is found as a useful method in the study.

Gürlek [141] investigated the flow field in a rectangular channel. In the study, the channel that included cylindrical ribs inside it is investigated. With the use of particle image velocimetry, several flow parameters are acquired. According to Gürlek; separation region over left obstacle could be seen under some conditions. Different from the left side, flow separation could not be seen on the surfaces of right obstacles in the study. The situation is valid for Reynolds numbers of 2900, 8400, and 15 000. In addition, the characteristics of the flow field are dependent on time under some conditions particularly in 15 000 of Reynolds number.

Jiang et al. [142] investigated intermediate pressure jets. In the study, different nozzle parameters are used. Also, both methods are examined via particle image velocimetry and the volume of fluid level set method. The results reveal that PIV and simulation have consistency with each other at different distances from the nozzle. On the other hand, the maximum velocities of jets become smaller by getting far away from the nozzles. Contrary to the maximum velocities of jets, distribution widths of the velocity field show reversal results under the same condition. Simulation results are found lower than PIV results in terms of maximum velocity.

Thomas et al. [143] employed particle image to an orbiting dish. In the study, PIV, CFD, and solution of Stokes' second problem are used. Validation of CFD is also performed. According to the results, in the case of z-direction of 0.5 mm and average normalized velocity magnitudes, particle image velocimetry and model show an average difference of 8.1%. In the same situation, the model and the analytical solution show an average difference of 20.8%. Consequently, validation increases the reliability of CFD solutions.

Zhang et al. [144] employed particle image velocimetry to the reactor coolant pump model. Flow characteristics are also revealed via PIV. According to the results, velocity values become greater step by step in the circumferential direction with the rotation of the impeller in the case of the spherical casing. Near each blade trailing edge, vortex shedding could be observed. In the diffuser channel, non-uniform velocity distributions exist in circumferential and axial directions.

Goyal et al. [145] investigated hydraulic turbines especially Francis turbines. In the study, steady and transient measurements are conducted. PIV is used for measurements. The results indicate that the maximum deviation is seen at the steady-state condition with a value of 2.4%. Furthermore, the deviation of both axial and radial velocities is found approximately 3–4% in the case of load variation. Test rig and PIV reveal repeatability well.

Xie et al. [146] employed particle image velocimetry to Dynamic Filtration module. With the use of PIV and CFD, measurements and comparisons are performed. The results reveal that complex physical configuration influences velocity fields and profiles considerably. Different feeding flow rates do not affect velocity magnitude noticeably. Moreover, the angular velocity has more contribution than the radial velocity regarding velocity magnitude. PIV and CFD have significant consistency with each other in terms of velocity.

Zhang et al. [147] investigated the flow structures in a low specific speed centrifugal pump. With the use of two-dimensional two components particle image velocimetry, flow structures are revealed. According to the results, several vorticity sheets occur at different flow rates. The cutting effect could be ignored particularly at low flow rates in the above analysis. At high flow rates, velocities increase noticeably near the blade suction side. However, the typical jet-wake flow pattern is not seen.

Espinoza et al. [148] employed angle-resolved two-dimensional particle image velocimetry to a high shear mixer. In the study, particle image velocimetry is used for the flow field. The results indicate that the highest radial velocities could be observed close to the outer stator hole. Furthermore, the additional flow rate from the pump caused the flow numbers made increased, which were calculated for steady operating conditions. Moreover, better transfer of the tangential momentum could be performed with narrower holes.

Haidari et al. [149] investigated the performances of six commercial feed spacers. In the study, pressure drops and actual velocities of six commercial feed spacers are compared with each other. Particle image velocimetry is used for velocity profiles. The results indicate that the higher Reynolds number results in an increase of pressure drop in the case of constant geometry of spacer and feed channel. Furthermore, pressure drop has an inverse relationship with channel height in zigzag spacers. The situation could be carried out via thickness of transverse filaments in cavity spacers got greater. Also, the flow rate with each spacer affects the pressure drop. Geometric characteristics of transverse filaments influence hydraulic conditions in channels with cavity spacers.

Cortada-Garcia et al. [150] investigated the flow characteristics of the lab-scale mixer. CFD is used for the agitation of non-Newtonian fluids. PIV is also utilized. According to the results, the impeller causes strong transverse motion than axial and radial components. Also, the impeller could be able to minimize stagnant zones. On the other hand, Metzner and Otto's constant from CFD is found comparable with other industrial impellers utilized for viscous liquids.

Yayla and Teksin [151] examined flow structures and downstream wake around a cylindrical body. In the study, 2500, 5000, and 7500 Reynolds numbers are considered. Stereoscopic particle image velocimetry is used for the investigation of the flow field. According to Yayla and Teskin, vortex shedding is influenced significantly via a flexible splitter plate. Also, fluctuations are diminished noticeably via control material. Several flow parameters show symmetrical patterns concerning the centerline of the circular cylinder for the bare cylinder case.

Alekseenko et al. [152] applied high-speed tomographic particle image velocimetry to swirling turbulent jets. In the study, three flow cases are considered. Tomographic particle image velocimetry is used for measurements. According to the results, in the mixing layer of the non-swirling and low-swirl jets, toroidal vortices exist. Moreover, the flow dynamics have a relationship with a strong flow precession around the central recirculation region. The amplitude of the axisymmetric mode gets greater along with downstream of the non-swirling and low swirl jets owing to the development of ring-like vortices.

Chen and Liu [153] studied the particle image velocimetry for combustion measurements. In the study, the process of PIV, types of PIV, combustion studies are examined. According to results, PIV is found feasible for the acquisition of instantaneous combustion processes, such as local extinction and ignition. Using other optical diagnostics with particle image velocimetry could be beneficial for combustion processes. Furthermore, particle image velocimetry data could be utilized for numerical modeling of combustion mechanisms with a wide range of conditions.

Durhasan et al. [154] investigated flow structures of perforated cylinders. With the use of particle image velocimetry, flow structures are revealed. The results show that flow fluctuations in the wake region could be decreased using increasing the porosity parameter. Perforated cylinders also could prevent Karman Vortex. Moreover, perforated cylinders are found as a feasible method in the present and future studies.

Riccomi et al. [155] employed ghost particle velocimetry to T-shaped branched junction. Several experiments are carried out to utilize the feasibility of ghost particle velocimetry for conducting flow field measurements. Micro PIV is used for validation. According to the results, the Reynolds number influences the performance of ghost particle velocimetry. Moreover, ghost particle velocimetry could not give adequate results in the case of the 400 Reynolds number. Consequently, both methods show the same performance in the case of low Reynolds numbers regarding some conditions.

Sun and Huang [156] investigated the motion of aeolian sand. In the study, measurements were performed via particle image velocimetry. The results indicat that higher incoming wind speeds cause an increase in the mean velocity of aeolian sand particles in the case of leeward slop area. Furthermore, increasing height results in the increase of mean horizontal velocity and vertical velocity of aeolian sand particles in the case of different heights. Moreover, several relationships and functions are found.

Liu et al. [157] employed two-dimensional particle image velocimetry to rotary type energy recovery device (REDR). By using two-dimensional particle image velocimetry, flow structures are revealed. Phase-locking and time-averaged processing methods are also used. According to the results, the entrance effect could be seen in the duct. The effect results in vortexes. Moreover, the effect also increases turbulence intensity level. RERD performance is influenced by the repeating sequences of vortexes.

You et al. [158] carried out a study about the smooth rotating channel. In the study, particle image velocimetry is used for the acquisition of flow fields. The results show that Coriolis and buoyancy forces affect the secondary flow. The situation occurs in the cross-section plane. By increasing rotation number and streamwise directions, the secondary flow could be improved. Moreover, increasing buoyancy force results in separated flow occurrence near the leading side.

Hu et al. [159] examined high solid anaerobic digestion. Particle image velocimetry is used for the measurement of the flow field. According to the results, rotation speed shows no considerable influence over HSAD's flow field. Furthermore, 3% laponite suspension is found useful for the flow field.

Akıllı et al. [160] investigated the effects of the splitter plates on flow characteristics. In the study, the plates are located in shallow water. By using particle image velocimetry, flow changes and structures are seen. The results indicate that turbulent kinetic energy is related to plate height. Turbulent kinetic energy is declined considerably after the plate height of 6 mm. Also, the best flow control is acquired plate height of 10 mm.

Park et al. [161] investigated the measurement accuracies of X-ray particle image velocimetry and micro-particle image velocimetry. In the study, a circular pipe and concentric stenosis are utilized. According to the results, X-ray particle image velocimetry is found generally feasible for stenoses. Besides, X-ray particle image velocimetry is adequate for the measurement of wall shear stress in the near-wall region. However, the technique has some drawbacks in two-dimensional velocity extraction.

Wang et al. [162] examined the square tank with double and single 45° up-pumping pitched blade turbines. Time-averaged flow fields are revealed via particle image velocimetry. The results indicate that a single impeller generated a high-velocity region, which is approximately 0.4 times the length of the cross-section of the tank in the z-direction. Compared to the upper impeller, the lower impeller has a smaller flow number. Three numerical methods could be regarded as feasible for stirred square tanks.

Miyashita et al. [163] investigated the particle behavior of electric precipitators. In the study, particle image velocimetry is utilized for revealing particle behaviors. The results indicate that increasing discharge current made particle velocity greater. The situation is observed as higher in positive discharge than negative discharge. Furthermore, increasing the discharge current causes particle angle just below the wire electrode to tend toward -90°. Considerable discrepancies between fluid drag due to ionic wind and Coulomb force are not observed under the experimental conditions.

Yalcin et al. [164] examined effusion film cooling. In the study, effusion plates are used, and particle image velocimetry is utilized. The results indicate that film formation is related to flow rates. Furthermore, film formation could be seen more clearly via lower effusion cooling hole angle. Using 30° of effusion cooling hole angle is better for film formation.

Dogan et al. [165] carried out a study about the interaction between a sphere wake and a free water surface. Particle image velocimetry and visualization techniques are used for flow parameters. In the study, Reynolds numbers vary from 2.5 × 103 to 1 × 104. According to the results, shedding from vortices near the sphere is observed. Furthermore, the vortices have a motion in the direction downstream. In the direction of downstream, vortices change. Consequently, submerge location of the sphere has an influence overflow separated from the sphere.

Loboda et al. [166] investigated turbulent eddy scales in diffusion flames. In the study, infrared thermography and particle image velocimetry are also used. According to the results, the two techniques have consistency with each other. Also, the sizes of large eddy-like structures and temperature inhomogeneities have a strong relationship with each other.

Banaei et al. [167] examined bubbling gas-solid fluidized bed. In the study, borescopes particle image velocimetry is used. Also, published positron emission particle tracking is also utilized for comparison. The results reveal that BPIV and PEPT have consistency with each other. However, some substantial disagreements are determined. Consequently, the borescope is found feasible for the measurement of the local solids volume fraction.

Vaagsaether et al. [168] investigated propagating flames in hydrogen-air explosions. With the use of particle image velocimetry, measurements are carried out. In the study, hydrogen and air explosions are focused. The results show that the flow velocity and strain rates around the obstacle become greater with the decrease of cross-section area from the obstacle. Vortices could be noticed in the wake of the obstacle. On the other hand, the maximum flow velocities are found as 13 m/s and 23 m/s for 14% and 17% hydrogen respectively.

González-Acuña et al. [169] examined three main optical flow algorithms used in particle image velocimetry. In the study, the fractional calculus of algorithms is examined. According to the results, the three methods could collapse under some conditions. Furthermore, the methods show lower performances at smaller values of α. The fractional Lucas–Kanade method shows the best performance.

Head et al. [170] examined the usefulness of planar particle image velocimetry for vapor flows. In the study, low-speed unconventional vapor flows are selected. According to the results, the D4 vapor is found transparent enough for planar particle image velocimetry. Particles are found capable of following the flow adequately owing to the Stokes number is 6.5 × 10–5. The relative uncertainty does not exceed 1%.

Wu et al. [171] investigated thermal image velocimetry and particle image velocimetry. In the study, natural convection near indoor heated surfaces is considered. The results indicat that thermal image velocimetry is found feasible for visualization of the airflow field. Besides, the linear correlation could be used between TIV and PIV6. Namely, a linear correlation could be presented between PIV and TIV.

Kluska et al. [172] analyzed the pyrolysis of a single cylindrical wood. In the study, ATR 01/600 pyrolysis reactor is used. Particle image velocimetry is utilized for visualization of the two-dimensional velocity field. The results reveal that the first slowdown gas velocity at the temperature of 100 °C has a relationship with inherent moisture. The increasing heating rate of the wood sample made the intensity of degassing of pyrolytic gases become greater. Besides, the thickness of the gas cushion becomes more improved with the increasing heating rate. Also, evaporation of moisture and devolatilization influence the gas cushion.

Ahmadi et al. [173] examined the turbulence statistics of the solid and liquid phases. In the study, horizontal turbulent channel flow is examined. Combined particle image velocimetry and particle tracking velocimetry are utilized for the acquisition of the instantaneous velocity of glass beads. According to the results, the liquid phase has lower velocities than those of the solid phase. The situation is valid for the near-wall region for the larger particles and higher flow Reynolds numbers. The influence of solid-phase volumetric concentration over the solid phase could be ignored.

Bardera et al. [174] investigated flow structures around the ski jump ramp of an aircraft carrier. In the study, decreasing adverse aerodynamic effects are also examined. PIV is used for the visualization of flow structures. The results reveal that a turbulent region could be seen over the ski jump ramp too. Besides, the columnar vortex generator is found advantageous in the case of decreasing the disadvantages of conical vortex systems.

2. Methodology

Particle image velocimetry is a flow velocity measurement technique. PIV is non-intrusive visualization and flow velocity measurement procedure that presents velocity fields and flow characteristics [23]. Main components of PIV can be classified as camera, lens, laser, computer and synchronizer [7,175]. In this section, PIV studies in open literature are analyzed from the point of its main components.

Camera is one of the significant components of PIV. In recording, cameras become inevitable [176]. Especially, highly sensitive cameras and high energy lasers are notable for acquisition of proper images [153]. Cameras are examined in terms of brands, sensor types, pixels, angles, bit and resolutions.

Lenses can be accepted as component of PIV. Lenses are advantageous for focusing [37]. In particular, focusing can be done with lenses easily [37]. Lenses can be divided into groups in terms of shape [7] Lenses are investigated via brand, aperture and focal length.

Lasers are fundamental components of PIV. Laser materials show changes. Atomic or molecular gas can be regarded as materials for lasers [7]. On the other hand, solid materials or semiconductor materials can be utilized. Pump source and mirror configuration are worthy factors in lasers [7]. Lasers are used for illumination of particles in PIV [153]. In lasers; wavelength, energy, sheet thickness, brand and type are distinctive parameters [143]. Lasers are explained with brands, energy, laser sheet thickness and wavelength.

Seeding and tracers are two distinctive factors in PIV measurements [87]. One should notice that seeded particles must be in optimal diameter [33]. However, tracer response and signal to noise ratio should not be ignored [33]. In tracers; density, phase, material, diameter and chemical properties are worthy [8]. Tracers are analyzed from the point of material, diameter and seeder brands.

Computers are generally used for correlation or storage in PIV applications [17]. Performance of computers depends on processor speed. Moreover, larger memory influences performance in computers [7]. Thus, computers are examined in sense of brands, essential features.

Synchronizers are required for PIV operation in sense of components working adaptable, For the synchronization of camera and laser, pulse delay generators are utilized [130]. In coordinate operation of components are unimaginable in PIV [130]. In the studies, synchronizers are investigated with brands.

2.1. Historical developments and recent advances of PIV

The first appearance of PIV in the literature dates back to 1984. Since its emergence, PIV has been an area of interest. The success of PIV in the study of turbulent flows allows it to be a frequently used flow measurement technique in the literature [22,177]. With the use of two dimensional PIV with a single camera, two dimensional measurements can be conducted. However, the deficiency of a single camera led to the need for three-dimensional measurements, bringing the multi-camera system in the past. Multi-camera systems brought tomographic and stereoscopic PIV approaches [177].

Measurement of flow and velocity in three dimensional is an important topic. Three dimensional PIV techniques gained importance in the early 1990s [178]. In this regard, tomographic PIV has a special place. Tomographic PIV, known as volumetric PIV, enables to visualization of flow structures in three dimensional [179]. Tomographic PIV is based on tomographic reconstruction with four cameras. In the tomographic PIV system, four cameras are placed around the experimental setup [180]. Due to the multi camera arrangement, flow structures and particle distribution can be obtained in three dimensional easily. However, high laser pulse energy is needed for volumetric PIV. Moreover, small lens apertures are significant parameters for the tomographic PIV system to visualize measurement volume [179,181]. Researchers have recently focused on reactor coolant pumps and jet noise prediction via tomographic PIV [182,183].

Three dimensional flow visualization isn't limited to tomographic PIV. Three dimensional particle tracking velocimetry (3D PTV) can also be involved in flow and velocity measurement techniques. Concordantly, three dimensional particle tracking velocimetry depends on a stereoscopic PTV system, which is used for velocity measurement. 3D PTV is also utilized for visualization of flow structures in three dimensional [184]. The system includes four cameras, like a tomographic PIV system. Multi camera system is useful for high speed flows [185]. One of the main advantages of volumetric PTV system is to enable real time and three dimensional flow measurements [184,186]. Recent investigations about volumetric PTV are related to Ahmed body wake and robotic PTV [187,188].

Defocusing PIV shouldn't be neglected in respect to volumetric flow and velocity measurement. Therefore, defocusing PIV system is a type of volumetric PIV technique. Like tomographic PIV and tomographic PTV systems, defocusing PIV allows three dimensional flow and velocity measurement [179]. In defocusing PIV system, camera and focused plane exist. Furthermore, pinhole aperture can be involved in the system [189]. In comparison to other PIV techniques, defocusing PIV method is regarded as simple. Only one camera is used in defocusing PIV. Compared to tomographic PIV and tomographic PTV systems, pinhole apertures are required due to the one camera arrangement [178,190]. Hindrances of defocusing PIV system are using with low particle densities and giving poor spatial resolution. The hindrances are caused from one camera arrangement [178]. One of the latest works considers nano scale defocusing particle image velocimetry. With the use of nano scale defocusing particle image velocimetry, motion of submicrometer particles are studied [191].

Digital Image Correlation (DIC) is expressed as a non-contact optical technique for full field measurement [192,193]. Digital image processing and numerical computation are essential methods for digital image correlation. Image based deformation is also accepted as a basis of the technique [194]. In comparison to PIV methods, digital image correlation is generally utilized for surface cracks and strain evolution [195,196]. Recent investigations about digital image correlation reveal the significance of damage evolution with layered hard sandstone [196].

Neural networks can be combined with PIV or PTV. Thus, neural networks are a promising tool for engineering systems. Neural networks were employed for fluid mechanics in the 1990s. Neural networks are also applied to PIV and PTV systems to obtain fluid velocity [197]. Neural networks can be used for volumetric particle tracking velocimetry to decrease computation time [198]. Furthermore, a combination of PIV/PTV techniques with neural networks can be useful [199]. Recently, neural networks have been used with liquid phase extraction in two-phase flow [200]. Furthermore, physics-informed neural networks are applied to stereoscopic PIV to enhance flow visualization [201].

Low power illumination sources are still used with flow visualization techniques. In this regard, particle shadow velocimetry (PSV) is one of the types of particle image velocimetry, which uses low power illumination sources. LEDs are one of the sources for PSV setups. LEDs are more economical and have high repetition rates [202]. In particle shadow velocimetry, direct in-line volume illumination is important for measurements. Direct in-line volume illumination results in narrow depth-of-field (DOF) [203]. One of the latest studies about particle shadow geometry examines tomographic arrangement. Volumetric particle shadow velocimetry can be utilized with smartphones [204].

Light field imaging (LFI) is another visual information technique. In light field imaging, higher dimensions are used for images [205,206]. On the other hand, light field imaging technique can be utilized for computer vision. The technique is significant for computational photography [206]. Multiview imaging in a single shot is one of the desired features for the cameras [206,207]. In recent years, light field imaging has been taken into account with transformers [208].

Holography is used for illumination like PIV or PTV. Concordantly, holography is related to three dimensional illusion for engineers [209,210]. Holography is related to recording the interference pattern from the superposition pattern. The superposition pattern is determined by considering the beam [211,212]. With the use of holography, three dimensional visual information can be acquired [213]. The techniques are also crucial for particle image velocimetry. Holographic particle image velocimetry (HPIV) can be used for optical visualization. In HPIV, holographic recordings of flow and reference waves with different angles are regarded [214]. One of the recent studies focuses on a combination of PIV and PTV. Digital inline holographic microscopy PIV/PTV is studied [215].

The motion of an object or flow is also significant. Hence, the optical flow technique is based on the motion parameters of moving objects or flows. The method can be carried out via motion detection between two frames [216,217]. In the optical flow method, moving objects from the static background objects are taken into consideration. With the use of the optical flow technique, vector fields in two dimensional can be obtained. Acquisition of motion field is also possible. Optical flow technique can be employed in vehicle navigation [218]. Moreover, object tracking and Traffic Surveillance are other application areas of optical flow [219,220]. Recent investigations regard optical flow techniques for real-time motion estimation [221].

3. Results

Particle image velocimetry and its components are one of the most comprehensive research subjects in open literature. Therefore, number of 163 particle image velocimetry studies and components are examined. Various results are found about lasers, seeding, cameras. However, less data is found in synchronizers and computers.

3.1. Camera

One of the components of particle image velocimetry is the camera. In PIV applications, two types of camera sensors are used. Charged Coupled Device (CCD) and Complementary Metal Oxide Semiconductor (CMOS) are main camera sensors. In CCD sensors, a semiconducting substrate made of silicon, n-layer, and p-layer exist. In CMOS sensors, MOS-FET transistors are also important. CMOS sensors have some advantages such as high sensitivity and relatively low noise level [7]. In Table 1, camera and video recorder brands, image capture systems, types of cameras, bit values, pixel counts and arrays, pixel sequences, resolutions/pixel values, and spatial resolutions are summarized. When Table 1 is examined in detail, it is seen that many different studies use various cameras, video recorders, image capture systems, and types of cameras. Apart from the brands, cameras have various features such as bit values, pixel counts, pixel arrays, pixel sequences, resolutions. Also, bit values, pixel counts, pixel arrays, pixel sequences, resolutions, pixel values, image sizes, sensors sizes, spatial resolutions values are categorized by year and given by the year. With resolution values, sensor sizes, pixel sizes, input resolutions, image resolutions, resolution ratios, intensity resolutions, recording resolutions, gray value images, gray level resolutions, digital frame store resolutions are also taken into account together. When Tables 1 and 2 are examined in detail; bit values, spatial resolutions, resolution values vary at various intervals. In Table 2, sensors, pixel spacing values, and the angle between cameras can be seen. In figures, two decimal places are considered. Due to the two decimal places, negligible deviations may be seen.

Particle image velocimetry is regarded as admired flow measurement technique [1,7]. Planar particle image velocimetry is carried out via camera and correlation techniques. With the became widespread of digital processing, particle image velocmetry types improved [222]. Time resolved particle image velocimetry, stereoscopic particle image velocimetry, scanning particle image velocimetry, holographic particle image velocimetry and tomographic particle image velocimetry become available [222]. In particle image velocimetry applications, 2D2C particle image velocimetry is preferred. However, sometimes time resolved particle image velocimetry, tomographic particle image velocimetry and stereoscopic particle image velocimetry are used [222].

Three-dimensional particle image velocimetry techniques need further efforts. Cheap and reliable three-dimensional particle image velocimetry continues to be developed. On the other hand, three dimensional micro scale particle image velocimetry especially for unsteady flows must come a long way [223]. In particle image velocimetry applications, multiphase flows can be improved. Namely, clouds moving in sky, cars running in a road can be visualized and recorded [223]. Consequently, particle image velocimetry is capable of anything that moves in universe. The mentioned capability always requires endless improvement [223].

Apart from the mentioned topics, peak locking is regarded as one of the undesired situation and drawback in particle image velocimetry [224]. For preventing peak locking, 2 pixels of particle image diameter can be a good choice. The value can be taken as the minimum value [225,226]. More than 3 pixels is not well too much [222].

As illustrated in Fig. 1, camera brands are not available in nearly 44–45% of PIV studies. The most used brands are TSI and LaVision. TSI and LaVision cameras are used in almost 9–10% of PIV studies. In some studies, more than one brand is used. Except for TSI and LaVision brands; Fujifilm, Canon, Adimec, Dalsa, Panasonic, Pulnix, COHU, EG & G Petricon, AOS Technologies, Memrecam, Duncantech, Vision Systems Technology, Optronis brands have lowest percent and are used in almost 1% of PIV studies.

According to Fig. 1, there are various camera brands. The most known brands are Kodak, Sony, TSI, Dantec, Nikon, Canon, Fujifilm, TSI, and LaVision have the most significant percentage, while Dantec and Photron have considerable usage in PIV studies. Dantec and Photron are used in almost 4–5% of PIV studies. Cameras should record images with good quality. Namely, missing data or unclear images should not be existed [7]. Moreover, camera should record the images in time accurately [17]. Recording can be performed on a single frame or sequences of frames. Recording with high quality is another factor [17]. Poor recording makes no sense. After recording, image assessment and post-processing are done [7].

According to Fig. 2, in some PIV studies cameras have more than one feature. In nearly 59–60% of PIV studies, types of cameras are not mentioned. The highest percentage has belonged to high-speed cameras. High-speed cameras are used in almost 15–16% of PIV studies. High speed cameras are capable of recording images in short time. High speed cameras can be used with high speed lasers for acquisition of good quality [17]. Therefore, high-speed camera is widely preferred in PIV applications. In other types of camera, infrared, pixelfly, color, single frame, low noise, high quantum efficiency and non-intensified cameras have the same percentage of

Table 1
Cameras, video recorders, image capture systems, types of cameras, bit values, resolution values, pixel counts, pixel arrays, pixel sequences, resolutions and spatial resolutions.

Ref.	Camera brands	Video recorder brands	Image capture system brands	Camera types	Bit values mentioned in the study	Pixel count	Pixel array	Pixel sequence	Resolutions/pixel values mentioned in the study	Spatial resolutions
[1]	N/A	N/A	N/A	N/A	N/A	N/A	N/A	N/A	N/A	N/A
[8]	N/A	N/A	N/A	N/A	N/A	N/A	N/A	N/A	N/A	N/A
[9]	N/A	N/A	N/A	N/A	N/A	N/A	N/A	N/A	N/A	N/A
[10]	Flow Sense EO 40	N/A	N/A	N/A	N/A	N/A	N/A	N/A	N/A	N/A
[11]	Canon Rebel T2İ DSLR	N/A	N/A	N/A	N/A	N/A	N/A	N/A	18 Mpix	N/A
[12]	N/A	N/A	N/A	N/A	12 bit	N/A	N/A	N/A	2048 × 2048 pixel	N/A
[13]	GX3 V-190-B/W	N/A	N/A	N/A	N/A	N/A	N/A	N/A	1280 × 1214 pixel (Maximum Resolution)	N/A
[14]	IPX-11M	N/A	N/A	N/A	12 bit	N/A	N/A	N/A	4000 × 2672 pixels, 11 M	N/A
[15]	N/A	N/A	N/A	N/A	N/A	N/A	N/A	N/A	4000 × 2672 pixel	N/A
[16]	Nikon Camera, Type: 630157 Powerview plus 2 MP	N/A	N/A	High quantum efficiency and low noise digital camera	N/A	N/A	N/A	N/A	1.6 k x 1.2 k pixel (pixel resolution), 2 MP	N/A
[22]	N/A	N/A	N/A	N/A	N/A	N/A	N/A	N/A	N/A	N/A
[23]	N/A	N/A	N/A	N/A	14 bit (Dynamic range)	N/A	N/A	N/A	1600 × 1200 piksel (2 Mpx)	N/A
[24]	DuncanTech MS3100 CIR	N/A	N/A	Multispectral camera	N/A	N/A	N/A	N/A	1276 × 875 (Image Resolution)	N/A
[25]	N/A	N/A	N/A	N/A	N/A	N/A	N/A	N/A	1018 × 1018 pixels (Image)	N/A
[26]	EG & G Reticon photodiode camera	N/A	N/A	Photodiode camera	N/A	256 × 256	N/A	N/A	N/A	N/A
[27]	N/A	N/A	N/A	Video camera	N/A	N/A	N/A	N/A	N/A	N/A
[28]	N/A	N/A	N/A	Open shutter camera	N/A	N/A	N/A	N/A	N/A	N/A
[29]	COHU 4910 series	N/A	N/A	N/A	N/A	N/A	N/A	N/A	512 × 512 pixel (Digital frame store resolution)	N/A
[30]	Pulnix TLC-X CCD camera	Sony U-Matic VO-58OOPS video recorder	N/A	N/A	8 bit (resolution frame)	N/A	N/A	512 × 512 pixel	8 bit (resolution frame)	N/A
[31]	N/A	N/A	N/A	N/A	N/A	N/A	N/A	N/A	N/A	N/A
[32]	N/A	N/A	N/A	N/A	N/A	N/A	N/A	N/A	N/A	N/A
[33]	N/A	N/A	N/A	N/A	N/A	N/A	N/A	N/A	N/A	N/A
[34]	Sony SSC-C374	Sony EVO-9650 video recorder	N/A	Color camera	8 Bit (Mentioned In Study)	N/A	N/A	N/A	640 by 480 pixels of 8 bit (Gray level resolution)	N/A
[35]	Princeton Instruments Pentamax 512 EFT	N/A	N/A	N/A	12 bit (resolution)	N/A	512 × 512 pixel (Array)	N/A	12 bit (resolution)	N/A
[36]	N/A	N/A	N/A	Color camera	24 bit frame grabber	N/A	N/A	N/A	N/A	N/A
[37]	Princeton Instruments	N/A	N/A	Cooled interline-transfer camera	12 bit	N/A	N/A	N/A	1300 × 1030 pixel	Order 1 μm & 13.6 μm × 4.4 μm & 13.6 μm × 0.9 μm

(*continued on next page*)

Table 1 (*continued*)

Ref.	Camera brands	Video recorder brands	Image capture system brands	Camera types	Bit values mentioned in the study	Pixel count	Pixel array	Pixel sequence	Resolutions/pixel values mentioned in the study	Spatial resolutions
[38]	Panasonic EZ1	N/A	N/A	Digital video camera	N/A	N/A	N/A	N/A	N/A	N/A
[39]	Kodak ES1.0	N/A	N/A	N/A	N/A	N/A	N/A	N/A	1 K × 1 K (pixel resolution)	N/A
[40]	N/A	N/A	N/A	N/A	8 bit (Video sensor)	N/A	N/A	N/A	640 × 480 pixel (Video sensor)	N/A
[41]	N/A	N/A	KODAK MEGAPLUS Image Capture System "TSI Model 630042"	N/A	8 bit (images)	N/A	N/A	N/A	N/A	N/A
[42]	TSI PIV 10-30	N/A	N/A	Standard Camera	N/A	N/A	N/A	N/A	1 K × 1 K	0.5 mm
[43]	Sony XC-73, Edmund Industrial Optics, NJ	N/A	N/A	Interline transfer monochrome camera	N/A	N/A	N/A	N/A	640 × 480 pixel (Image)	16 × 16 pixels
[44]	FlowMaster3S, LaVision, Gottingen, Germany	N/A	N/A	High resolution double frame camera	12 bit dynamics	N/A	N/A	N/A	1024 × 1280 pixel (Images)	N/A
[45]	N/A	N/A	N/A	N/A	N/A	N/A	N/A	N/A	N/A	N/A
[46]	N/A	N/A	N/A	N/A	8 bit	N/A	N/A	N/A	1 K × 1 K	N/A
[47]	N/A	N/A	N/A	High speed camera	8 bit (for images)	N/A	N/A	N/A	512 × 512 pixels (for images)	0.8 μm × 0.8 μm
[48]	N/A	N/A	N/A	High resolution video camera	N/A	N/A	N/A	N/A	1300 × 1030 pixel	N/A
[49]	Kodak Megaplus ES 1.0	N/A	N/A	N/A	N/A	N/A	N/A	N/A	1008 × 1018 pixel (Image)	N/A
[50]	N/A	N/A	N/A	High speed camera	N/A	N/A	N/A	N/A	N/A	N/A
[51]	TSI PIVCAM10-30	N/A	N/A	High resolution camera	N/A	N/A	N/A	N/A	1 K × 1 K	N/A
[52]	N/A	N/A	N/A	N/A	N/A	N/A	N/A	N/A	N/A	N/A
[53]	Kodak DC280	N/A	N/A	Digital still camera	N/A	N/A	N/A	N/A	2 Megapixel	N/A
[54]	AF Micro Nikkor	N/A	N/A	Video camera	N/A	N/A	N/A	N/A	N/A	N/A
[55]	PCO SensiCam	N/A	N/A	Double shutter camera & High speed camera	12 bit, 8 bit (transformation images)	N/A	N/A	N/A	1280 × 1024 pixel	N/A
[56]	Kodak 1.0 ES (for PIV and LIF)	N/A	N/A	High resolution camera (for LIF) & Digital camera (for PIV)	N/A	N/A	N/A	N/A	1 K × 1 K pixel	N/A
[57]	TSI PIV 10-30	N/A	N/A	N/A	N/A	N/A	N/A	N/A	1 K × 1 K	N/A
[58]	N/A	N/A	N/A	N/A	N/A	N/A	N/A	N/A	1008 × 1008 pixel	N/A
[59]	PCO Sensicam	N/A	N/A	N/A	N/A	N/A	N/A	N/A	N/A	N/A
[60]	N/A	N/A	N/A	N/A	N/A	N/A	N/A	N/A	N/A	N/A
[61]	N/A	N/A	N/A	N/A	N/A	N/A	N/A	N/A	N/A	N/A
[62]	N/A	N/A	N/A	N/A	12 bit	N/A	N/A	N/A	2 K × 2 K pixel	42 μm (for X), 42 μm (for Y) & 42 μm (for X), 63 μm (for Y) & 40–60 μm

(*continued on next page*)

Table 1 (*continued*)

Ref.	Camera brands	Video recorder brands	Image capture system brands	Camera types	Bit values mentioned in the study	Pixel count	Pixel array	Pixel sequence	Resolutions/pixel values mentioned in the study	Spatial resolutions
[63]	TSI PIVCAM13-8	N/A	N/A	N/A	N/A	N/A	1024 × 1280 pixel	N/A	N/A	0.85 mm
[64]	N/A	N/A	N/A	N/A	N/A	N/A	N/A	N/A	N/A	N/A
[65]	PowerView	N/A	N/A	N/A	N/A	N/A	N/A	N/A	2 K × 2 K pixel	N/A
[66]	PixelFly HiRes® model	N/A	N/A	N/A	N/A	N/A	N/A	N/A	N/A	N/A
[67]	SensiCam PCO AG, Kelheim, Germany	N/A	N/A	Double shutter camera	N/A	N/A	N/A	N/A	1280 × 1024 pixel	N/A
[68]	N/A	N/A	N/A	N/A	N/A	N/A	N/A	N/A	N/A	N/A
[69]	N/A	N/A	N/A	N/A	N/A	N/A	N/A	N/A	N/A	N/A
[70]	N/A	N/A	N/A	N/A	N/A	N/A	N/A	N/A	N/A	N/A
[71]	N/A	N/A	N/A	N/A	N/A	N/A	N/A	N/A	N/A	N/A
[72]	PIVCAM 10–30 from TSI	N/A	N/A	N/A	N/A	N/A	N/A	N/A	1016 × 1024 pixel	N/A
[73]	VNR 950, SYSMA INDUSTRIE	N/A	N/A	High speed digital video camera	N/A	N/A	N/A	N/A	256 × 256 pixel (Gray value image)	N/A
[74]	N/A	N/A	N/A	N/A	N/A	N/A	N/A	N/A	N/A	N/A
[75]	N/A	N/A	N/A	N/A	N/A	N/A	N/A	N/A	N/A	N/A
[76]	Powerview 4 MP, TSI (for PIV)	N/A	N/A	High resolution camera	N/A	N/A	N/A	N/A	4 M (Camera resolution) & 2048 × 2048 pixel (Recording Resolution) for PIV	N/A
[77]	Sensicam, PCO imaging, Germany (fo SPIV) & Lavision Nanostar, Germany (for acetone PLIF)	N/A	N/A	Intensified camera (ICCD-Acetone PLIF)	16-bit precision and 12 bit dynamic range (PLIF)	N/A	N/A	N/A	1280 × 1024 pixel (for PIV) & 1280 × 1024 pixel (for acetone PLIF)	N/A
[78]	N/A	N/A	N/A	Pixelfly camera	N/A	N/A	N/A	N/A	640 × 512 pixel (Reduced Image Resolution)	N/A
[79]	N/A	N/A	N/A	N/A	N/A	N/A	N/A	N/A	N/A	N/A
[80]	N/A	N/A	N/A	High resolution camera	N/A	N/A	N/A	N/A	1186 × 1600 pixel	N/A
[81]	ImagerPro4M	N/A	N/A	N/A	8 bit	N/A	N/A	N/A	2048 × 2048 pixel	N/A
[82]	N/A	N/A	N/A	N/A	N/A	N/A	N/A	N/A	N/A	N/A
[83]	N/A	N/A	N/A	N/A	N/A	N/A	N/A	N/A	N/A	N/A
[84]	LaVision FlowMaster Imager Pro (for micro PIV) & Color View (for macroscopic experiments)	N/A	N/A	N/A	N/A	N/A	N/A	N/A	N/A	1280 × 1024 pixels per frame
[85]	N/A	N/A	N/A	N/A	N/A	N/A	N/A	N/A	N/A	N/A
[86]	N/A	N/A	N/A	N/A	N/A	N/A	N/A	N/A	N/A	N/A
[87]	LaVision Imager Intense	N/A	N/A	N/A	12 bit	N/A	N/A	N/A	1376 × 1040 pixel	N/A
[88]	N/A	N/A	N/A	High resolution digital camera	N/A	N/A	N/A	N/A	1280 × 1024 pixel	N/A
[89]	N/A	N/A	N/A	High definition digital video camera	N/A	N/A	N/A	N/A	2016 × 1134 pixel (Maximum resolution)	N/A
[90]	LaVision FlowMaster Imager Pro	N/A	N/A	N/A	N/A	N/A	N/A	N/A	N/A	1280 × 1024 pixels per frame (Spatial Resolution)

(*continued on next page*)

Table 1 (*continued*)

Ref.	Camera brands	Video recorder brands	Image capture system brands	Camera types	Bit values mentioned in the study	Pixel count	Pixel array	Pixel sequence	Resolutions/pixel values mentioned in the study	Spatial resolutions
[91]	PCO.4000 & PCO Sensicam QE	N/A	N/A	N/A	N/A	N/A	N/A	N/A	256 × 256 pixel (Image size)	N/A
[92]	Dantec Dynamics Hi Sense MK II	N/A	N/A	N/A	N/A	N/A	N/A	N/A	N/A	N/A
[93]	N/A	N/A	N/A	N/A	N/A	N/A	N/A	N/A	1600 × 1186 pixel	Slightly lower than 0.1 mm
[94]	Imager ProX4M Lavision	N/A	N/A	N/A	N/A	N/A	N/A	N/A	2048 × 2048 pixel	N/A
[95]	Casio EX-FH100s & Fujifilm FinePixs HS10 digital camera	N/A	N/A	Digital camera (Both cameras)	N/A	N/A	N/A	N/A	1280 720 pixels; 3648 2736; 640 × 480 pixels; 448 × 336; 640 × 480 pixels; 448 × 336; 224 × 168 pixels and 224 × 64 pixels	N/A
[96]	Dantec	N/A	N/A	N/A	N/A	N/A	N/A	N/A	2048 × 2048 pixel	N/A
[97]	Powerview,TSI	N/A	N/A	Black and white camera	N/A	N/A	N/A	N/A	4008 × 2672 pixel	N/A
[98]	Photron, FASTCAM ultima APX	N/A	N/A	High speed camera	N/A	N/A	N/A	N/A	1024 × 1024 pixel	Less than 5 μm
[99]	Digital Sight DS-2Mv, Nikon	N/A	N/A	N/A	N/A	N/A	N/A	N/A	N/A	N/A
[100]	Dantec	N/A	N/A	Intensified camera	N/A	N/A	N/A	N/A	N/A	N/A
[101]	Adimec 1000 M, 1000 9 1000 pixels, Adimec Co. Ltd.,Boston	N/A	N/A	Infrared camera	N/A	N/A	N/A	N/A	1000 × 1000 pixel	N/A
[102]	Phantom v640	N/A	N/A	N/A	N/A	N/A	N/A	N/A	1600 × 1600 pixel	N/A
[103]	Casio EX-F1 and AOS MOTIONeer	N/A	N/A	Digital camera & High speed digital camera	N/A	N/A	N/A	N/A	512 × 384 pixel (Image Size for Casio EX-F1) & 1280 × 1024 pixel (for AOS MOTIONeer)	N/A
[104]	N/A	N/A	N/A	N/A	12 bit (Intensity resolution)	N/A	N/A	N/A	12 bit (Intensity resolution)	4 Mpx (2048 pixel × 2048 pixel)
[105]	Sony DRC-TR355E	N/A	N/A	Digital camera	N/A	N/A	N/A	N/A	N/A	N/A
[106]	N/A	N/A	N/A	N/A	N/A	N/A	N/A	N/A	N/A	N/A
[107]	N/A	N/A	N/A	High speed digital camera	N/A	N/A	N/A	N/A	1280 × 800 pixel (Maximum Resolution)	0.025–0.075 mm/pixel
[108]	N/A	N/A	N/A	N/A	N/A	N/A	N/A	N/A	N/A	N/A
[109]	LaVision Imager Pro	N/A	N/A	High speed camera	N/A	N/A	N/A	N/A	N/A	N/A
[110]	Phantom	N/A	N/A	High speed video camera	N/A	N/A	N/A	N/A	N/A	N/A
[111]	Imager Pro LX	N/A	N/A	N/A	N/A	N/A	N/A	N/A	4830 × 3230 pixel (16 Mpx) & 18 pixel/mm (Image Resolution)	1.78 mm
[112]	N/A	N/A	N/A	N/A	10 bit	N/A	N/A	N/A	1600 × 1200 pixel	N/A
[113]	N/A	N/A	N/A	High speed camera	N/A	N/A	N/A	N/A	N/A	N/A
[114]	LaVision Imager Intense	N/A	N/A	Non-intensified camera	N/A	N/A	N/A	N/A	1376 × 1040 pixel	30 μm
[115]	MV-D1024E-160, Photon Focus	N/A	N/A	High speed camera	N/A	N/A	N/A	N/A	1024 × 1024 pixel (for 100 fps collection)	N/A
[116]	Kodak MEGAPLUS ES 1.0	N/A	N/A	N/A	8 bit	N/A	1600 × 1192 pixel	N/A	1 K × 1 K	N/A

(*continued on next page*)

Table 1 (*continued*)

Ref.	Camera brands	Video recorder brands	Image capture system brands	Camera types	Bit values mentioned in the study	Pixel count	Pixel array	Pixel sequence	Resolutions/pixel values mentioned in the study	Spatial resolutions
[117]	Dalsa 4M60 (for PTV)	N/A	N/A	Digital camera (PTV)	N/A	N/A	N/A	N/A	1024 × 1024 pixel (for PTV) & 1370 × 1040 pixel (for PIV)	N/A
[118]	Memrecam fx RX6 (NAC ImageTechnology, D)	N/A	N/A	High speed camera	N/A	N/A	N/A	N/A	512 × 512 pixel (Maximum Possible Resolution)	N/A
[119]	N/A	N/A	N/A	Digital camera	N/A	N/A	N/A	N/A	N/A	1024 × 1024 pixels
[120]	N/A	N/A	N/A	N/A	N/A	N/A	N/A	N/A	1600 × 1200 pixel	N/A
[121]	N/A	N/A	N/A	N/A	N/A	N/A	N/A	N/A	N/A	N/A
[122]	N/A	N/A	N/A	N/A	N/A	N/A	N/A	N/A	2560 × 1920 pixel (capable for 1300 Hz). 72 × 840 pixel (size of images for 400 Hz)	N/A
[123]	PowerViewTM Plus, TSI Inc	N/A	N/A	High speed camera	12-bit quantization levels	N/A	N/A	N/A	1600 × 1200 pixel	N/A
[124]	N/A	N/A	N/A	N/A	12 bit	N/A	N/A	N/A	1280 × 1024 pixel	N/A
[125]	N/A	N/A	N/A	N/A	N/A	N/A	N/A	N/A	N/A	N/A
[126]	N/A	N/A	N/A	High speed camera	N/A	N/A	N/A	N/A	1376 × 1040 pixel (Images)	N/A
[127]	Motionxtra HG-XR	N/A	N/A	N/A	N/A	N/A	N/A	N/A	1128 × 1504 pixel (Images)	N/A
[128]	BW Photron Ultima APX	N/A	N/A	High speed camera	10 bit	N/A	N/A	N/A	1024 × 1024 pixel (for 50 fps)	N/A
[129]	NA	N/A	N/A	N/A	N/A	N/A	N/A	N/A	N/A	N/A
[130]	DANTEC, FlowSense	N/A	N/A	N/A	N/A	N/A	N/A	N/A	2048 × 2048 pixel	0.17 mm for double-channel device and 0.19 mm for 15-channel device
[131]	PCO 1600	N/A	N/A	High dynamic double shutter cooled camera	14 bit (Dynamic)	N/A	N/A	N/A	1600 × 1200 pixel (Image Sensor Resolution)	N/A
[132]	Sony DRC-TR355E	N/A	N/A	Digital camera	N/A	N/A	N/A	N/A	N/A	N/A
[133]	N/A	N/A	N/A	N/A	N/A	N/A	N/A	N/A	2048 × 2048 pixel (Resolution ratio)	N/A
[134]	Flowsense EO, Dantec Dynamics	N/A	N/A	High speed camera	N/A	N/A	N/A	N/A	640 × 480 pixel	N/A
[135]	N/A	N/A	N/A	N/A	N/A	N/A	N/A	N/A	N/A	0.74 mm × 0.74 mm
[136]	Imager Intense, LaVision GmbH	N/A	N/A	N/A	N/A	N/A	N/A	N/A	1376 × 1040 pixel (Pixel resolution)	0.27 pixel/mm and 42.6 pixel/mm
[137]	N/A	N/A	N/A	N/A	N/A	N/A	N/A	N/A	N/A	N/A
[138]	N/A	N/A	N/A	N/A	N/A	N/A	N/A	N/A	2560 × 2150 pixel	N/A
[139]	Imager pro X, LaVision, Germany (2D and 3D PIV)	N/A	N/A	N/A	N/A	N/A	N/A	N/A	N/A	1600 × 1200 pixel2 (for 2D PIV)
[140]	N/A	N/A	N/A	N/A	N/A	N/A	N/A	N/A	1920 × 1080 pixels (Image)	N/A
[141]	Nikon AF Micro 60f/2.8D	N/A	N/A	Digital camera	N/A	N/A	N/A	N/A	1600 × 1200 pixel	N/A
[142]	630059POWERVIEW Plus 4 MP	N/A	N/A	Frame straddling camera	N/A	N/A	N/A	N/A	4 MP	N/A

(*continued on next page*)

Table 1 (*continued*)

Ref.	Camera brands	Video recorder brands	Image capture system brands	Camera types	Bit values mentioned in the study	Pixel count	Pixel array	Pixel sequence	Resolutions/pixel values mentioned in the study	Spatial resolutions
[143]	TSI PowerviewPlus 4 MP	N/A	N/A	High resolution digital camera	N/A	N/A	N/A	N/A	2048 × 2048 pixel (Image pixel)	0.35 mm
[144]	FlowSense EO 2 M DANTEC DYNAMICS A/S	N/A	N/A	N/A	N/A	N/A	N/A	N/A	N/A	1600 × 1200 pixel
[145]	VC-4MC-M180	N/A	N/A	N/A	N/A	N/A	N/A	N/A	2400 × 2400 pixel & 2032 × 2048 pixel for 276.0 mm × 278.0 mm	N/A
[146]	DANTEC Dynamic, Flow sense EO'	N/A	N/A	N/A	N/A	N/A	N/A	N/A	2048 × 2048 pixel	N/A
[147]	PowerViewTM Plus, TSI Inc	N/A	N/A	N/A	N/A	N/A	N/A	N/A	N/A	1600 pixel × 1200 pixel
[148]	630 091, TSI Inc., USA	N/A	N/A	Single frame-straddling camera	12 bit	N/A	N/A	N/A	2048 2048 pixel (4 Megapixel)	38.58 μm/pixel
[149]	N/A	N/A	N/A	High speed camera	N/A	N/A	N/A	N/A	N/A	N/A
[150]	TSI PowerViewTM Plus	N/A	N/A	Straddling camera	N/A	N/A	N/A	N/A	2048 × 2048 pixel	N/A
[151]	N/A	N/A	N/A	N/A	8 bit	N/A	N/A	N/A	1600 × 1186 pixel	N/A
[152]	Photron FASTCAM SAS	N/A	N/A	High speed camera	N/A	N/A	N/A	N/A	1024 × 1024 pixel (Sensor Size)	N/A
[153]	N/A	N/A	N/A	N/A	N/A	N/A	N/A	N/A	N/A	N/A
[154]	Dantec Dynamics A/S, FlowSense 2 M	N/A	N/A	N/A	N/A	N/A	N/A	N/A	1600 × 1200 pixel	N/A
[155]	Powerview plus (Micro PIV) and Photron SA5 (GPV)	N/A	N/A	High resolution camera (μPIV) & High speed camera (GPV)	N/A	N/A	N/A	N/A	4 MP (Micro PIV) & 1 MP (GPV)	N/A
[156]	Nikon's PowerView plus	N/A	N/A	High speed camera	N/A	N/A	N/A	N/A	2 MP- 200 MP	N/A
[157]	N/A	N/A	N/A	N/A	N/A	N/A	N/A	N/A	1632 × 1200 pixel	N/A
[158]	N/A	N/A	N/A	Digital camera	14 bit	N/A	N/A	N/A	2048 × 2048 pixel	N/A
[159]	N/A	N/A	N/A	N/A	N/A	N/A	N/A	N/A	N/A	N/A
[160]	N/A	N/A	N/A	N/A	N/A	N/A	N/A	N/A	N/A	N/A
[161]	SA 1.1, Photron, Japan	N/A	N/A	High speed camera	N/A	N/A	N/A	N/A	NA	N/A
[162]	PIVCAM13-8	N/A	N/A	Frame straddling camera	N/A	N/A	N/A	N/A	2048 × 2048 pixel	N/A
[163]	Photron FASTCAM SA 4	N/A	N/A	High speed camera	N/A	N/A	N/A	N/A	832 × 576 pixel	N/A
[164]	N/A	N/A	N/A	High speed camera	N/A	N/A	N/A	N/A	N/A	N/A
[165]	N/A	N/A	N/A	N/A	N/A	N/A	N/A	N/A	1600 × 1186 pixel	N/A
[166]	Videoscan 4021	N/A	N/A	N/A	N/A	N/A	N/A	N/A	N/A	2048 × 2048 pixel
[167]	OPTRO-NIS CP80-4-M-500	N/A	N/A	N/A	N/A	N/A	N/A	N/A	N/A	N/A
[168]	Photron SA-Z	N/A	N/A	High speed camera	N/A	N/A	N/A	N/A	N/A	N/A
[169]	N/A	N/A	N/A	N/A	N/A	N/A	N/A	N/A	N/A	N/A
[170]	Imager Pro 4 M	N/A	N/A	High speed camera	N/A	N/A	N/A	N/A	11 × 11 μm (Pixel size)	N/A
[171]	PIVCAM13-8 and FLIR-T1040	N/A	N/A	Double frame high sensitivity camera & Infrared camera	N/A	N/A	N/A	N/A	2048 × 2048 pixel (PIV) & 1024 × 768 pixel (TIV)	N/A
[172]	Sense EO 4 M	N/A	N/A	N/A	N/A	N/A	N/A	N/A	2048 × 2048 pixel (Picture)	N/A
[173]	Imager Intense, LaVision, GmbH	N/A	N/A	N/A	12 bit (Digital resolution)	N/A	N/A	N/A	1040 × 1376 pixel (Sensor size) and 12 bit (Digital resolution)	N/A
[174]	N/A	N/A	N/A	N/A	N/A	N/A	N/A	N/A	2048 × 2048 pixel	N/A

Table 2
Sensors, pixel spacing values and angle between cameras.

Ref.	Sensors	Pixel spacing and pixel pitch	Angle between cameras
[1]	N/A	N/A	N/A
[8]	N/A	N/A	N/A
[9]	N/A	N/A	N/A
[10]	CCD	N/A	N/A
[11]	N/A	N/A	N/A
[12]	CCD	N/A	90°
[13]	N/A	N/A	N/A
[14]	CCD	N/A	N/A
[15]	CCD	N/A	N/A
[16]	CCD	N/A	N/A
[22]	N/A	N/A	N/A
[23]	CCD	N/A	N/A
[24]	CCD (Multispectral Camera)	N/A	N/A
[25]	CCD	N/A	N/A
[26]	N/A	N/A	N/A
[27]	N/A	N/A	N/A
[28]	N/A	N/A	N/A
[29]	CCD	N/A	N/A
[30]	CCD	N/A	N/A
[31]	N/A	N/A	N/A
[32]	N/A	N/A	N/A
[33]	N/A	N/A	N/A
[34]	CCD	N/A	N/A
[35]	CCD	N/A	N/A
[36]	CCD	N/A	N/A
[37]	CCD	6.8 μm (Pixel spacing)	N/A
[38]	N/A	N/A	N/A
[39]	CCD	N/A	N/A
[40]	CCD (Video Sensor)	N/A	N/A
[41]	CCD (Array)	N/A	N/A
[42]	CCD	N/A	N/A
[43]	CCD	N/A	N/A
[44]	CCD	N/A	N/A
[45]	N/A	N/A	N/A
[46]	CCD	N/A	N/A
[47]	CCD	N/A	N/A
[48]	CCD	N/A	N/A
[49]	N/A	N/A	N/A
[50]	CCD	N/A	N/A
[51]	CCD	N/A	N/A
[52]	CCD	N/A	N/A
[53]	CCD	N/A	N/A
[54]	N/A	N/A	N/A
[55]	CCD (Other camera)	N/A	N/A
[56]	CCD	N/A	N/A
[57]	CCD	N/A	N/A
[58]	CCD	N/A	N/A
[59]	CCD	N/A	N/A
[60]	N/A	N/A	N/A
[61]	N/A	N/A	N/A
[62]	CCD	N/A	N/A
[63]	CCD	N/A	N/A
[64]	N/A	N/A	N/A
[65]	CCD	N/A	N/A
[66]	N/A	N/A	150
[67]	CCD	N/A	N/A
[68]	CCD	N/A	N/A
[69]	N/A	N/A	N/A
[70]	CCD	N/A	N/A
[71]	N/A	N/A	N/A
[72]	CCD	N/A	N/A
[73]	N/A	N/A	N/A
[74]	CCD	N/A	N/A
[75]	N/A	N/A	N/A
[76]	CCD	N/A	N/A
[77]	CCD (for PIV) & ICCD (for acetone PLIF)	N/A	45° (SPIV)
[78]	CCD	N/A	N/A
[79]	N/A	N/A	N/A

(*continued on next page*)

Table 2 (*continued*)

Ref.	Sensors	Pixel spacing and pixel pitch	Angle between cameras
[80]	N/A	N/A	N/A
[81]	CCD	N/A	N/A
[82]	N/A	N/A	N/A
[83]	N/A	N/A	N/A
[84]	CCD	N/A	N/A
[85]	CCD	N/A	N/A
[86]	N/A	N/A	N/A
[87]	CCD	6.45 μm (Pixel pitch)	N/A
[88]	CCD	N/A	N/A
[89]	N/A	N/A	N/A
[90]	CCD	N/A	N/A
[91]	N/A	N/A	N/A
[92]	CCD	N/A	N/A
[93]	CCD	N/A	N/A
[94]	CCD	N/A	N/A
[95]	CMOS	N/A	N/A
[96]	CCD	N/A	N/A
[97]	CCD	N/A	N/A
[98]	CMOS	N/A	N/A
[99]	CCD	N/A	N/A
[100]	N/A	N/A	N/A
[101]	N/A	N/A	N/A
[102]	N/A	N/A	N/A
[103]	N/A	N/A	N/A
[104]	CCD	N/A	N/A
[105]	N/A	N/A	N/A
[106]	N/A	N/A	N/A
[107]	CCD	N/A	N/A
[108]	N/A	N/A	N/A
[109]	N/A	N/A	N/A
[110]	N/A	N/A	N/A
[111]	N/A	N/A	N/A
[112]	CCD	N/A	N/A
[113]	CCD	N/A	N/A
[114]	CCD	N/A	N/A
[115]	CMOS	N/A	N/A
[116]	CCD	N/A	N/A
[117]	CMOS (for PTV)	N/A	N/A
[118]	N/A	N/A	N/A
[119]	CCD	N/A	N/A
[120]	CCD	N/A	N/A
[121]	CCD	N/A	N/A
[122]	CMOS	N/A	N/A
[123]	CCD	N/A	N/A
[124]	CCD	N/A	N/A
[125]	N/A	N/A	N/A
[126]	N/A	N/A	N/A
[127]	N/A	N/A	N/A
[128]	CMOS	N/A	N/A
[129]	CCD	N/A	N/A
[130]	CCD	N/A	N/A
[131]	CCD	N/A	N/A
[132]	N/A	N/A	N/A
[133]	CCD	N/A	N/A
[134]	CCD	N/A	N/A
[135]	CMOS	N/A	N/A
[136]	CCD	N/A	N/A
[137]	CCD	N/A	N/A
[138]	CMOS	N/A	N/A
[139]	CCD	N/A	30°
[140]	N/A	N/A	N/A
[141]	N/A	N/A	N/A
[142]	CCD	N/A	N/A
[143]	N/A	N/A	N/A
[144]	CCD	N/A	N/A
[145]	CCD	N/A	N/A
[146]	CCD	N/A	N/A
[147]	CCD	N/A	N/A
[148]	CCD	N/A	N/A

(*continued on next page*)

Table 2 (*continued*)

Ref.	Sensors	Pixel spacing and pixel pitch	Angle between cameras
[149]	N/A	N/A	N/A
[150]	CCD	N/A	N/A
[151]	CCD	N/A	N/A
[152]	CMOS	N/A	N/A
[153]	N/A	N/A	N/A
[154]	CCD	N/A	N/A
[155]	CCD (Micro PIV)	N/A	N/A
[156]	CCD	N/A	N/A
[157]	CCD	N/A	N/A
[158]	CCD	N/A	N/A
[159]	CMOS	N/A	N/A
[160]	CCD	N/A	N/A
[161]	N/A	N/A	N/A
[162]	CCD	N/A	N/A
[163]	N/A	N/A	N/A
[164]	N/A	N/A	N/A
[165]	CCD	N/A	N/A
[166]	CCD	N/A	N/A
[167]	N/A	N/A	N/A
[168]	N/A	N/A	N/A
[169]	N/A	N/A	N/A
[170]	N/A	N/A	N/A
[171]	CCD	N/A	N/A
[172]	N/A	N/A	N/A
[173]	CCD	N/A	N/A
[174]	CCD	N/A	N/A

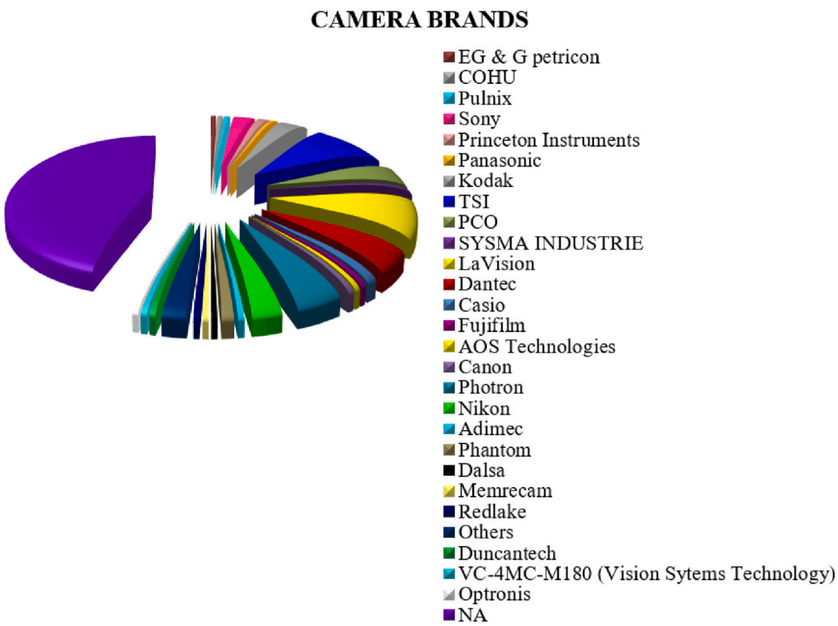

Fig. 1. Camera brands.

nearly 1%. In complex flows, multi frame recording is a good choice owing to increase the accuracy level [222,227].

After the high speed cameras, digital cameras and high resolution cameras are utilized in 10–11% and 5–6% of PIV studies respectively. With the rapid developments in imaging sector, high speed cameras become important in PIV applications. Due to the rapid developments of cameras, video recorders and image capture systems fell into disuse [7].

Figs. 3 and 4 clearly indicate that video recorders and image capture systems are not available in most of the PIV studies. As mentioned above, in the 1990s, recording technology was not as good as to present's. So, video recorders and image capture systems were common in the 1990s. Now high-speed cameras are used owing to technological developments [7]. High-speed cameras are able to record images in less time [228]. Consequently, high speed camera is widely preferred in PIV applications [17,228].

According to Figs. 5–9; bit values and pixel count values are not available in nearly 82–83% and 99% of the number of various PIV

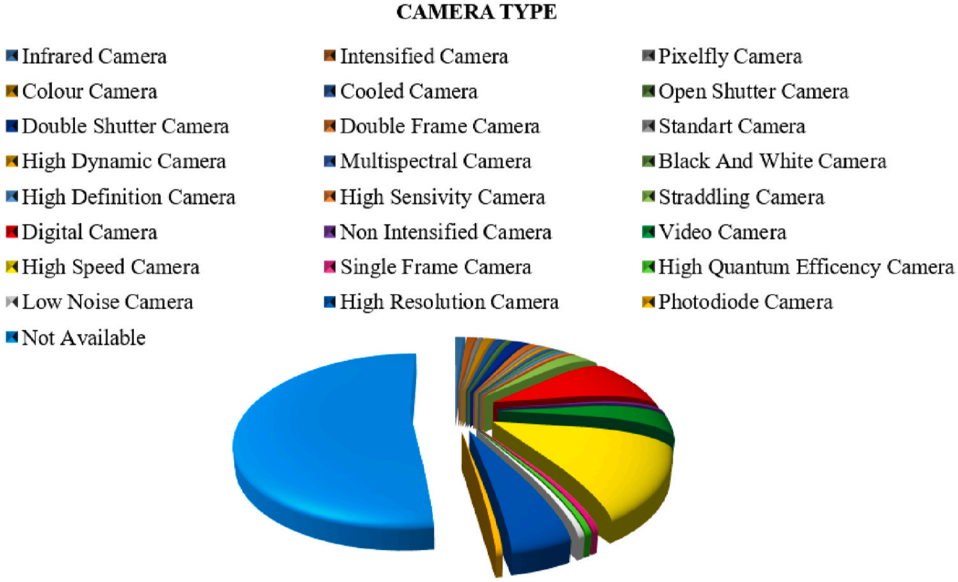

Fig. 2. Camera types.

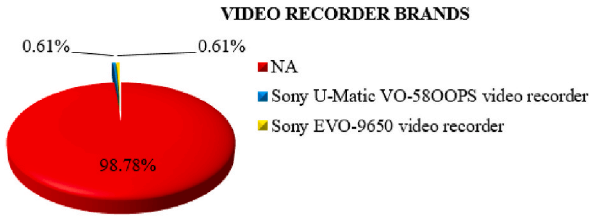

Fig. 3. Video recorder brands.

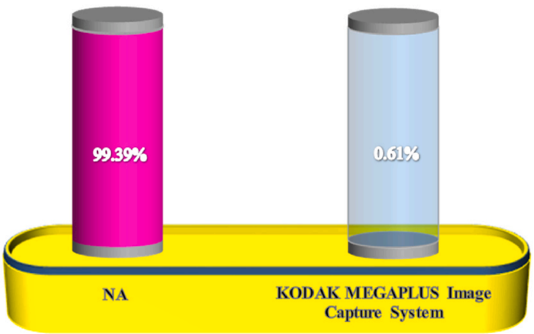

Fig. 4. Image capture system brands.

studies examined in the open literature, respectively. Instead of pixel counts and bit values, resolution values are preferred. In some studies, resolution values and bit values are the same. Pixel arrays and pixel sequences are not available in most of the PIV studies. Pixel values are generally used. Forliti et al. [41] used CCD array as 1320 × 1035 pixels. Sun and Huang [156] mentioned chip array as 1600 × 1600. The resolution, pixel, image sizes and sensor sizes values are available in approximately a total of 60–61% of PIV studies. It can be concluded from Fig. 9, the term of the resolution is used more than bit values, pixel sequences, pixel arrays, pixel counts. Resolution is one of the crucial parameters of particle image velocimetry applications [12].

In PIV applications, many efforts continue for high temporal and spatial resolutions [153]. Experimental data must have high resolution in time and space. So, there are various options for high resolutions [7]. For instance, plan, apochromatic or fluorite objectives have high numerical apertures are good for high-resolution images [7,153] Additionally, CCD cameras are one of the options in terms of high spatial resolution values compared to CMOS cameras [8].

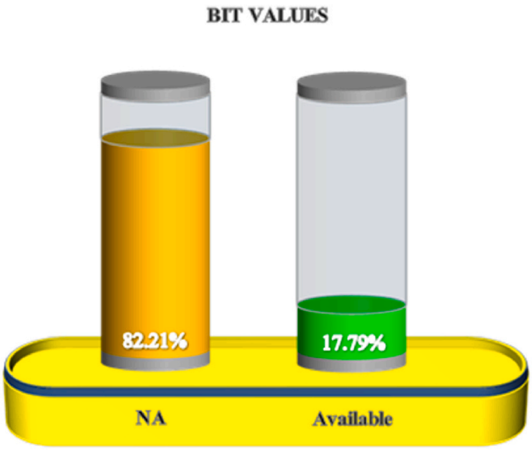

Fig. 5. Bit values.

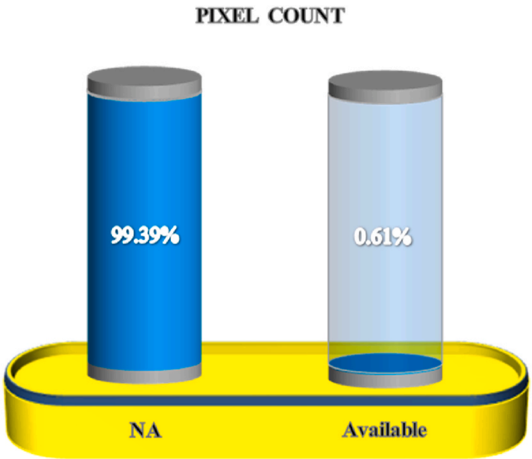

Fig. 6. Pixel counts.

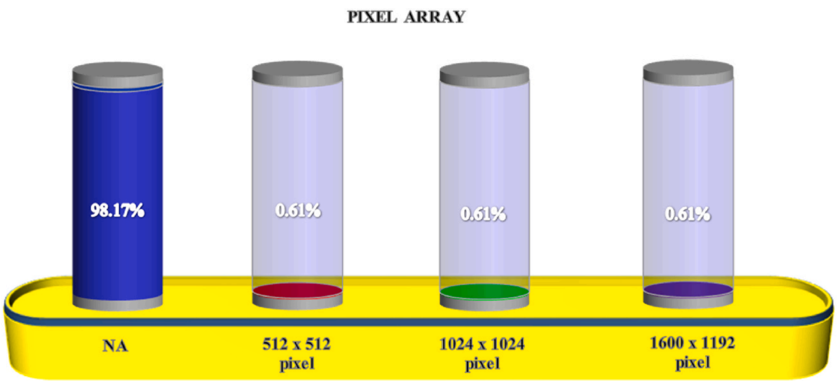

Fig. 7. Pixel array values.

As illustrated in Fig. 10, spatial resolution is mentioned in approximately 14–15% of PIV studies. High spatial resolutions are always desired in PIV applications. High spatial resolution values are found as mandatory for resolving large structures inflow [7]. In PIV experiments, CCD cameras are suitable in terms of high spatial resolution [8]. Also, smaller interrogation areas are preferred for higher spatial resolution [7]. Spatial resolution values are limited by present technological limitations. Hence, many innovations are

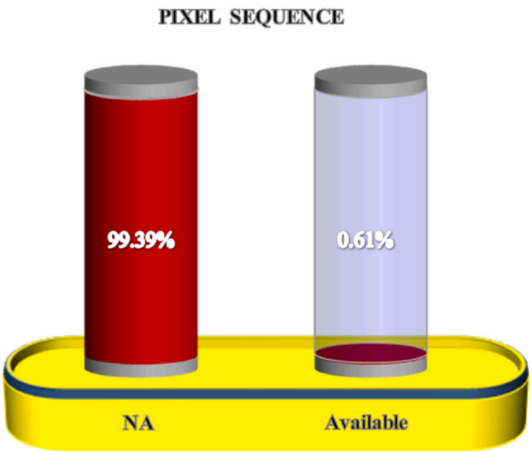

Fig. 8. Pixel sequences.

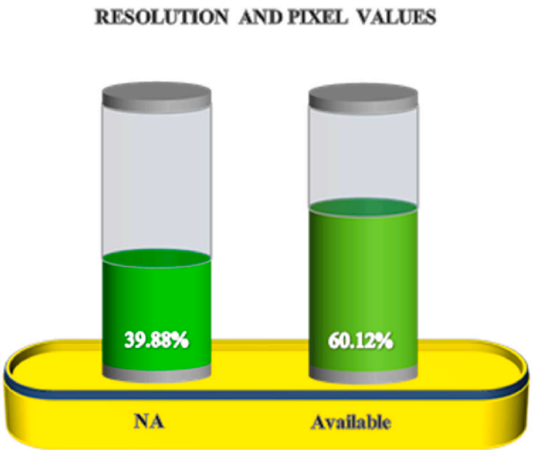

Fig. 9. Resolution and pixel values.

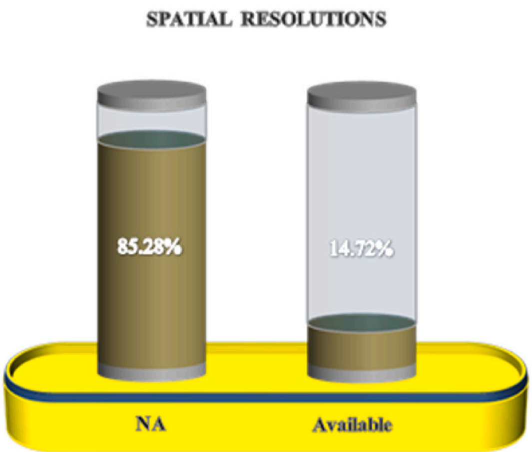

Fig. 10. Spatial resolutions values.

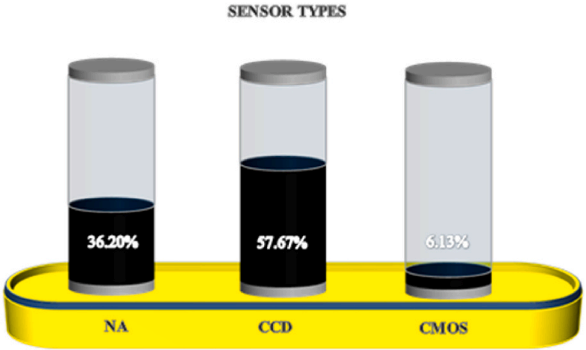

Fig. 11. Sensor types.

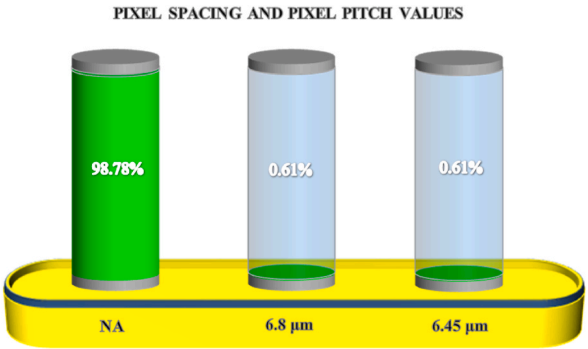

Fig. 12. Pixel spacing and pixel pitch values.

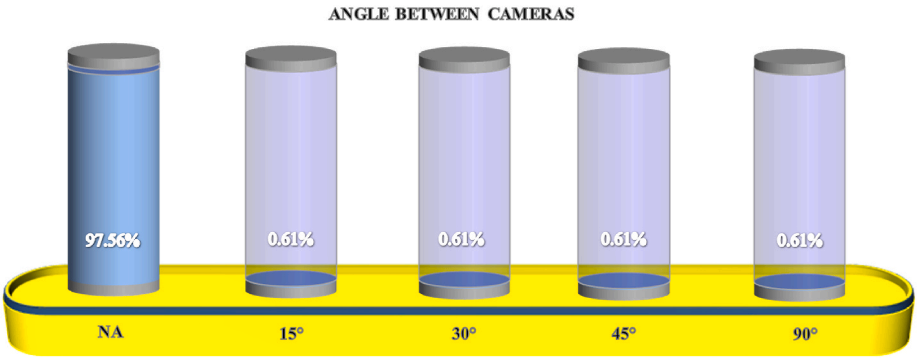

Fig. 13. Angle between cameras.

made for higher spatial resolutions [7,8]. Another camera features are sensor type, pixel spacing value and the angle between them.

Fig. 11 clearly indicates that the CCD sensor is preferred in nearly 57–58% of PIV studies examined in the open literature. The percent of the CMOS sensors is approximately 6–7%. CCD sensors have some superiorities in terms of efficiency, low noise, collection, transfer abilities, higher spatial resolution [8,229].

Compared to CCD sensors, CMOS sensors have some advantages [230]. CMOS sensors consume power lower than CCD sensors [230]. Readout rate is other benefit of CMOS sensors [230]. However, low spatial resolution is the major hindrance of CMOS sensors [8,231] Therefore, CMOS cameras can be used in small scale applications [8]. Consequently, CCD sensors are generally used in PIV studies [70].

According to Fig. 12, pixel spacing and pixel pitch values are available only in nearly total of 1–2% of PIV studies. Ragni et al. [87] mentioned the pixel pitch as 6.45 μm. Namely, pixel spacing and pixel pitch are not mentioned in most of PIV studies. Fig. 13 reveals that, in nearly 97–98% of the number of PIV studies examined in the open literature, the angles between cameras are not available. In most of PIV studies, single cameras are preferred. More than one camera means more cost. Each extra components bring additional costs [183]. Moreover, two dimensional and two component particle image velocimetry are widely used. 2D2C PIV applications use a single camera [12,183]. Consequently, single camera has the largest percent.

3.2. LENSES and LASERS

In PIV applications, using the proper lens and lens aperture is very crucial. Lens aperture has an inverse relationship with the depth of field. Larger apertures result in an insufficient depth of field [31]. Furthermore, small apertures may cause some problems. Generally, using f/4 or f/5.6 is satisfactory. In order to decrease distortions, high-quality lenses are good choices [31]. There are many lens types. Cylindrical lenses come first in terms of generation of the light sheet. With telescope lenses, the system can be more feasible [7]. Spherical lenses are good for experiments in the case of short focal lengths. Diverging lenses or negative focal length lenses are preferred with high power pulsed lasers due to the ionization [7]. In Table 3; lens brands, focal lengths and lens apertures can be seen. When Table 3 is examined in detail, there are several lens brands, focal lengths and apertures. Lasers are one of the important components in PIV. Lasers emit monochromatic light with high energy density and illuminate the tracer particles [17]. In PIV applications continuous wave (CW) lasers or, pulsed lasers are used. Generally, argon-ion lasers are preferred [17]. Argon-ion lasers can produce in the range of a few watts. Continuous-wave lasers create pulses by means of a chopper or reflection of the laser beam. In the chopped beam, a sheet forming module is crucial. However, in the swept beam sheet forming module isn't mandatory [17].

Another laser type is a pulsed laser. In PIV measurements the most preferred pulsed lasers are Neodymium Yttrium Aluminum Garnet (Nd: YAG) and Neodymium Doped Yttrium Lithium Fluoride (Nd: YLIF) respectively. The repetition rate of the pulsed lasers changes from 0.1 to 0.3 J/pulse. Compared to continuous-wave lasers, pulsed lasers have some advantages such as short duration, power storage and delivering, repetition rate [17].

In the main, higher flow velocity causes lower continuous wave laser energy based on the particle. But in pulsed lasers, the situation is the reverse. Although pulsed lasers are feasible for particle image velocimetry applications, argon-ion lasers are used in some laboratories due to the low-cost illumination system [17]. In addition, laser brands and laser types can be seen in Table 3.

As seen in Fig. 14, Nikon is the most preferred brand in PIV studies exist in the open literature. In nearly 13–14% of PIV studies, Nikon lenses are used. Nikkor lenses are taken into account with Nikor lenses. Lenses with sufficient focal lengths and apertures are very significant for particle image velocimetry applications [17]. By means of lenses, far fields can be viewed with no changes. There are many types of lenses such as cylindrical lenses, spherical lenses, oil immersion lenses, thermal lenses [7,17]. In Fig. 15, the focal length of lenses is mentioned in nearly 26% of PIV studies. As mentioned before focal lengths can be positive or negative. Negative focal lengths known as diverging lens are not used too much in PIV studies. As mentioned in Table 3, negative focal lengths have belonged to cylindrical lenses [7]. In general, positive focal lengths are used. In Fig. 16, lens apertures are mentioned in almost 20–21% of PIV studies. As mentioned in Gray and Greated [31], the parameter of lens and lens aperture are very important. Lens aperture should not be so small and large. Proper depth of focus can be acquired with a suitable lens aperture [17]. Sharp images can be obtained via proper lenses [17]. Increasing lens aperture makes the depth of field larger and causes lower resolution. Sometimes, low quality lenses can be useful [17,222]. Large particle images can be viable by using low quality lenses. The situation comes from spherical shape [7].

According to Fig. 17, laser brands are not mentioned in 68–69% of PIV studies. Dantec Dynamics lasers are used in nearly 9–10% of PIV studies examined in the open literature. Oxford lasers, DPGL-2W (Japan Laser Corporation), Shangai Dream Laser Technology have the same percent of nearly 1%. After the Dantec lasers, New Wave Lasers are utilized in almost 7–8% of PIV studies. In lasers, the delay time is an important parameter [232]. Time delay must not be too long or too short in the experiments [8,17].

As illustrated in Fig. 18, Nd: YAG lasers are commonly preferred. Some lasers have more than one feature. In nearly 55–56% of PIV studies, Nd: YAG lasers are used. Short duration and power storage are main superiorities of pulsed lasers [17]. Therefore, pulsed lasers are commonly preferred. After the Nd: YAG lasers, He–Ne and Argon-Ion lasers are in demand. He–Ne and Argon-ion lasers are used in 2.44% of PIV studies [17]. Double pulsed Nd: YAG lasers are preferred lasers in fish migration studies [8]. Double pulsed Nd:YAG lasers are suitable for emitting monochromatic lights with high energy. Double pulsed Nd: YAG lasers generally produce laser lights with 532 nm wavelength [8]. On the other hand; decreasing pulse separation time is one of the desired situation in particle image velocimetry applications [224]. The pulse separation time must be decreased as possible and can capture the motions properly [224,233]. In Table 3; main features of lasers such as maximum energy, laser energy, wavelengths and laser sheet thicknesses can be seen by year. As shown in Fig. 19, the maximum energy of lasers is available in nearly 6–7% of PIV studies examined in the open literature. Instead of maximum energy, nominal energy or normal energy is generally used in PIV studies. Maximum energy is not always required. Normal or nominal energy is found sufficient [7]. In some studies, energy values are given directly but in some studies, energy values are given with per pulse. Fig. 20 reveals that laser energies are available in approximately 45% of PIV studies. Normal energy concept is more favored than maximum energy. Like normal or nominal energy, energy values are given directly or pulse based. In, both energy values, generally ''mJ'' based energy values had dominance. Decreasing pulse separation time is one of the desired situations in particle image velocimetry applications. The pulse separation time must be short and can capture the motions properly [224,233].

According to Fig. 21, the wavelength of 532 nm was used in almost 40% of PIV studies. In some studies, more than one wavelength is used. In most of the PIV studies, continuous-wave lasers especially Nd: YAG lasers are used. Pulsed lasers especially Nd: YAG lasers have generally 532 nm wavelengths. Therefore, 532 nm of wavelength is commonly used [163].

Fig. 22 clearly indicates that laser sheet thicknesses are given in approximately 32% of PIV studies. Generally, 1–2 mm sheet thickness is used. Microscale thickness is used too. Thin light sheets can be feasible for illuminating and recording without chromatic aberrations [8]. Insufficient laser intensity, stiffness of the light sheet can cause some drawbacks [8].

High quality equipment or components are essential for obtaining accurate particle image velocimetry measurements. With the use of high quality components, several problems or errors can be prevented [234,235]. Less errors or uncertainties bring high degree of accurate experiment results. Time resolved particle image velocimetry can be realized with high speed cameras and high repetition lasers [234,235]. However, high quality components resulted in high initial cost. In spite of the high initial costs, high quality equipment should be followed [222].

Table 3
Brand of lenses, focal lengths, lens apertures, laser brands, laser types, the maximum energy of laser, laser energy, wavelength and laser sheet thickness.

Ref.	Lens brands	Lens focal length	Lens aperture mentioned in study	Laser Brand	Lasers types	Maximum energy of laser	Laser energy	Wavelength	Laser sheet thickness
[1]	N/A	N/A	N/A	N/A	N/A	N/A	N/A	N/A	N/A
[8]	N/A	N/A	N/A	N/A	N/A	N/A	N/A	N/A	N/A
[9]	N/A	N/A	N/A	N/A	N/A	N/A	N/A	N/A	N/A
[10]	Micro Nikon 60 mm F2.8D Nikon lenses	60 mm	f2.8D	N/A	Nd-YAG dual pulse laser	N/A	N/A	532 nm (Emission wavelength)	N/A
[11]	N/A	N/A	N/A	N/A	N/A	N/A	N/A	N/A	N/A
[12]	N/A	60 mm	N/A	N/A	Nd: YAG laser	N/A	200 mJ (Per pulse)	532 nm	About 1 mm
[13]	N/A	N/A	N/A	Beamtech PIV200	Dual head Nd: YAG laser	100 mJ (Maximum Energy Per Head)	N/A	527 nm	N/A
[14]	105 mm SIGMA lens at f# = 2.8	105 mm	−2.8	N/A	Solid-state frequency-doubled Nd: YAG laser	N/A	500 mJ (Nominal Energy)	532 nm	N/A
[15]	NIKON AF 85 mm/ F1.4 lens	85 mm	f/1.4	Kinder	Nd: YAG laser	N/A	N/A	532 nm	N/A
[16]	N/A	N/A	N/A	N/A	Double pulsed Nd: YAG laser	N/A	200 mJ	N/A	N/A
[22]	N/A	N/A	N/A	N/A	N/A	N/A	N/A	N/A	N/A
[23]	N/A	N/A	N/A	N/A	Double head Nd: YAG laser	N/A	N/A	532 nm	0.2 mm (expected sheet)
[24]	N/A	100 mm (Minus)	N/A	N/A	The frequency doubled Nd: YAG laser, a dye laser and a tuN/Able Ti: sapphire laser	N/A	10 mJ (Per Pulse) & 100 mJ (Per pulse)	532 nm & 650 nm & 780 nm	1 mm
[25]	N/A	N/A	N/A	N/A	Nd: YAG laser (Twin)	N/A	N/A	N/A	1 mm
[26]	N/A	N/A	N/A	N/A	He–Ne laser	N/A	5 mW	N/A	N/A
[27]	N/A	N/A	N/A	N/A	He–Ne laser	N/A	N/A	N/A	N/A
[28]	N/A	N/A	N/A	N/A	Double pulsed ruby laser and He–Ne laser beam	N/A	N/A	N/A	N/A
[29]	N/A	N/A	N/A	N/A	Double pulsed frequency doubled Nd: YAG laser	N/A	100 mJ/per pulse (Output energy)	512 nm	1 mm (Thickness) & 0.1 m (Width)
[30]	N/A	N/A	N/A	N/A	N/A	N/A	N/A	N/A	N/A
[31]	N/A	N/A	N/A	N/A	N/A	N/A	N/A	N/A	N/A
[32]	N/A	N/A	N/A	N/A	N/A	N/A	N/A	N/A	N/A
b[33]	N/A	N/A	N/A	N/A	N/A	N/A	N/A	N/A	N/A
[34]	N/A	8 mm	N/A	N/A	N/A	N/A	N/A	N/A	N/A
[35]	N/A	N/A	1.4 (Numerical Aperture)	N/A	N/A	N/A	N/A	N/A	2 mm
[36]	N/A	N/A	N/A	N/A	N/A	N/A	N/A	N/A	N/A
[37]	oil-immersion Nikon CFI Plan Apochromat 60× objective lens	N/A	1.4 (Numerical Aperture) and 1.23 (Effective numerical aperture)	New Wave, Inc	Two Nd: YAG lasers	N/A	Approximately 1 mJ (Light Energy)	532 nm	N/A
[38]	N/A	N/A	N/A	N/A	He–Ne laser	N/A	22 mW	N/A	N/A
[39]	N/A	N/A	N/A	Twin Continuum Surelite II	Twin Nd: YAG lasers	N/A	300 mJ (per pulse at 10 Hz)	532 nm	N/A
[40]	N/A	N/A	N/A	N/A	Double cavity pulsed Nd: YAG laser	N/A	150 mJ (Per Pulse)	N/A	0.8 mm

(*continued on next page*)

Table 3 (*continued*)

[41]	N/A	50 and 1000 mm respectively	5,6	Continuum Surelite I-10 lasers	N/A	N/A	200 mJ (Per Pulse)	532 nm	Approximately 0.8 mm
[42]	N/A	N/A	N/A	New Wave Nd:Yag Mini-Lase	Nd: YAG laser	50 mJ (Per Pulse)	N/A	N/A	10 mm
[43]	N/A	N/A	0.25 (Numerical Aperture)	N/A	“Blue” Ar-ion CW laser	N/A	40 mW	488 nm	N/A
[44]	Nikon 50 mm lens	2.9 mm (Entrance lens) & −3.7 mm (Cylindrical lens) & 50 mm (Nikkor)	close to 8–11	PIV200, Spectra Physics, Mountain View, Calif laser (for engine)	Frequency doubled Nd: YAG laser & Laser (for engine)	N/A	100 mJ (laser energy monitor) & approximately 2 × 50 mJ (inside engine cylinder) 200 mJ (Measurements in engine)	532 nm	0.5–1 mm (Width in engine cylinder) & 1–2 mm (Thickness for measurement volume)
[45]	N/A	N/A	N/A	N/A	N/A	N/A	N/A	N/A	N/A
[46]	N/A	N/A	N/A	N/A	Double pulsed Nd: YAG laser	300 mJ/7 nsec pulse	N/A	N/A	N/A
[47]	N/A	N/A	1.0 (NA)	N/A	N/A	N/A	N/A	N/A	N/A
[48]	N/A	50 mm	f/1,2	N/A	Double pulse Nd: YAG laser	N/A	25 mJ (At 10 ns)	532 nm	2 mm (deep)
[49]	N/A	N/A	N/A	New Wave MiniLase pulsed Nd:YAG lasers	A pair of pulsed Nd: YAG laser	N/A	N/A	532 nm	3 mm
[50]	N/A	N/A	N/A	N/A	Double pulse Nd: YAG laser	N/A	25 mJ	N/A	N/A
[51]	N/A	N/A	N/A	Quantel Inc	Double pulsed Nd: YAG laser	N/A	200 mJ/pulse	532 nm	About 1.5 mm
[52]	N/A	N/A	N/A	N/A	Long pulse laser	N/A	N/A	N/A	N/A
[53]	N/A	N/A	N/A	N/A	N/A	N/A	N/A	N/A	N/A
[54]	N/A	N/A	N/A	N/A	Nd: YAG laser	N/A	120 mJ	N/A	N/A
[55]	N/A	N/A	N/A	N/A	N/A	N/A	N/A	N/A	N/A
[56]	N/A	N/A	N/A	Continuum Surelite II (for PIV)	Frequency doubled Nd:YAG laser (for LIF) and twin Nd: YAG lasers (for PIV)	N/A	300 mJ	532 nm	About 1 mm (for PIV) & 1 mm (for LIF)
[57]	N/A	N/A	N/A	N/A	Nd: YAG laser	N/A	50 mJ	N/A	N/A
[58]	N/A	N/A	N/A	Model 2060A-64 from Spectra Physics Argon laser	Double Nd: YAG lasers (for SPIV) and argon laser (for LDA)	N/A	120 mJ (Per Pulse)	N/A	N/A
[59]	Zeiss Achroplan lens	N/A	0.4 (Numerical aperture)	N/A	Nd: YAG laser	N/A	N/A	532 nm	N/A
[60]	N/A	N/A	N/A	N/A	Blue, green and violet laser beams (for PDA)	N/A	N/A	488 nm, 514 nm, 476.5 nm	N/A
[61]	N/A	N/A	N/A	N/A	N/A	N/A	N/A	N/A	N/A
[62]	N/A	N/A	N/A	N/A	Dual pulse Nd: YAG laser	N/A	N/A	N/A	50 μm
[63]	N/A	N/A	N/A	TSI Y120-15	Double pulsed Nd: YAG	N/A	120 mJ (Per Pulse)	532 nm	2 mm
[64]	N/A	N/A	N/A	Spectra Physics model 171	Continuous wave argon ion laser	N/A	18 Watt (operating in the blue-green region of the spectrum	532 nm (at 5 Watt)	N/A
[65]	N/A	N/A	N/A	N/A	N/A	N/A	N/A	N/A	N/A

(*continued on next page*)

Table 3 (*continued*)

[66]	N/A	N/A	N/A	N/A	N/A	N/A	N/A	N/A	N/A
[67]	A telecentric lens (SILL Optics GmbH & Co. KG, Wendelstein, Germany)	N/A	N/A	(Photonics, Edinburgh, Scotland)	Double pulse Nd: YAG laser	N/A	30 mJ (Per Pulse)	532 nm	0.2 mm
[68]	N/A	N/A	N/A	N/A	Two nitrogen lasers	N/A	N/A	N/A	N/A
[69]	N/A	N/A	N/A	N/A	N/A	N/A	N/A	N/A	N/A
[70]	N/A	N/A	N/A	N/A	N/A	N/A	N/A	N/A	N/A
[71]	N/A	N/A	N/A	N/A	N/A	N/A	N/A	N/A	N/A
[72]	N/A	−25 mm (Cylindrical lens) and 250 mm (Spherical lens)	N/A	New Wave Research (model Mini-Laser—15)	Double cavities with Nd: YAG laser	N/A	12 mJ	N/A	50.9 μm (Thickness) and 17.5 mm (Height)
[73]	N/A	N/A	N/A	(SOLO-I-15 PIV New Wave Research, USA)	Two pulsed Nd: YAG lasers	N/A	2 × 15 mJ	532 nm	2.5 mm (Maximum)
[74]	N/A	N/A	N/A	N/A	N/A	N/A	N/A	N/A	Approximately 1 mm
[75]	N/A	N/A	N/A	N/A	N/A	N/A	N/A	N/A	N/A
[76]	AF micro Nikkor, 60 mm (for PIV)	60 mm (Nikkor)	N/A	New Wave (for PIV) and Spectra Physics (for LDV)	Pulsed dual head Nd:YAG laser (for PIV) and Argon-ion laser (for LDV)	N/A	5 Watt (LDV)	N/A	0.5 mm (for PIV)
[77]	Nikkor camera lens	−25 mm (Cylindrical lens) and +500 mm (Spherical lens)	f/1.2	Continuum Surelite II (for PIV and PLIF)	Three Nd:YAG lasers	N/A	35 mJ/pulse (PIV) & 60 MJ (UV laser)	1064 nm & 532 nm & 266 nm	620 μm & 120 μm
[78]	N/A	40 mm and 100 mm (double concave lenses) & 40 mm (rectangular lens)	N/A	N/A	N/A	N/A	5 mW	660 nm	N/A
[79]	N/A	N/A	N/A	N/A	N/A	N/A	N/A	N/A	N/A
[80]	N/A	N/A	N/A	N/A	N/A	N/A	N/A	532 nm	N/A
[81]	N/A	N/A	N/A	N/A	Double pulsed Nd: YAG laser	N/A	200 mJ	532 nm	Approximately 1 mm
[82]	N/A	N/A	N/A	N/A	N/A	N/A	N/A	N/A	N/A
[83]	N/A	N/A	N/A	N/A	N/A	N/A	N/A	N/A	About 1 mm
[84]	Zeiss EC Plan-NEOFLUAR 103/0.3 lens	N/A	0,3	Litron	Double pulsed Nd: YAG laser	N/A	N/A	532 nm	N/A
[85]	N/A	N/A	N/A	N/A	Nd: YAG laser	N/A	N/A	N/A	N/A
[86]	N/A	N/A	N/A	N/A	Q-switched Yb-doped double-clad (DC) fiber lasers (Design)	N/A	0.2 mJ & 0.15 mJ & 0.14 mJ & 4.8 mJ (Mentioned)	N/A	N/A
[87]	Carl Zeiss Jena objective (f = 120 mm)	120 mm	N/A	Big Sky CFR-PIV-200	Nd:YAG laser	N/A	200 mJ	532 nm	Approximately 1.5 mm
[88]	N/A	N/A	N/A	N/A	CW Blue laser	N/A	N/A	473 nm	N/A
[89]	N/A	N/A	N/A	N/A	Two frequency doubled Nd:YAG lasers	N/A	50 mW	532 nm	2 mm

(*continued on next page*)

Table 3 (*continued*)

[90]	N/A	N/A	N/A	Litron Nano L PIV	Double pulsed Nd: YAG laser	N/A	N/A	N/A	N/A
[91]	Makro-Planar T 9 2/100 objective lens (by Carl Zeiss AG)	N/A	N/A	Litron Nano S	Double-cavity frequency doubled Nd: YAG laser	N/A	N/A	532 nm	N/A
[92]	N/A	N/A	N/A	Dantec Dynamics New Wave Solo III 15 Hz Laser	N/A	N/A	N/A	N/A	N/A
[93]	N/A	200 mm	N/A	N/A	Dual-cavity Nd-YAG laser	N/A	N/A	1064 nm (Original) & 532 nm (Green)	N/A
[94]	N/A	N/A	N/A	NewWave Research	Double headed laser unit	N/A	50 mJ (Per Pulse)	N/A	N/A
[95]	NOVAlaser collimating lens	N/A	N/A	NOVAlasers ×75 Compact Portable 475 mW Laser	N/A	N/A	75 mW	532 nm	2 mm
[96]	N/A	135 mm	f/2D	N/A	Double pulsed Nd: YAG laser	N/A	120 mJ (Per Pulse)	532 nm	About 1 mm
[97]	N/A	N/A	N/A	N/A	Pulsed Nd: YAG laser	N/A	300 Watt	532 nm	N/A
[98]	N/A	N/A	N/A	N/A	N/A	N/A	N/A	N/A	N/A
[99]	10× objective lens (Plan Fluor 10, Nikon)	N/A	N/A	N/A	N/A	N/A	N/A	N/A	N/A
[100]	N/A	N/A	N/A	N/A	Diode laser	N/A	N/A	N/A	N/A
[101]	N/A	N/A	N/A	N/A	N/A	N/A	N/A	N/A	N/A
[102]	N/A	N/A	N/A	N/A	N/A	N/A	N/A	N/A	N/A
[103]	NIKON 18–55 mm lens	18–55 mm	N/A	N/A	N/A	N/A	N/A	N/A	N/A
[104]	N/A	35 mm (Camera)	5.6	N/A	Double pulsed Nd: YAG laser	200 mJ (Maximum Output Energy Per Pulse)	N/A	532 nm	About 4 mm
[105]	N/A	N/A	N/A	N/A	Double pulsed Nd: YAG laser	N/A	120 mJ	N/A	N/A
[106]	N/A	N/A	N/A	N/A	N/A	N/A	N/A	N/A	N/A
[107]	N/A	N/A	N/A	N/A	Nd: YAG laser	N/A	N/A	N/A	N/A
[108]	N/A	N/A	N/A	N/A	N/A	N/A	N/A	N/A	N/A
[109]	N/A	N/A	N/A	Litron LPY 703	Double pulsed Nd: YAG laser	N/A	50 mJ	532 nm	N/A
[110]	N/A	N/A	N/A	N/A	N/A	N/A	N/A	N/A	N/A
[111]	N/A	180 mm (camera)	5.6 (Diaphragm aperture)	Quantum Evergreen	Double pulsed Nd: YAG laser	200 mJ (Maximum Energy Per Pulse)	N/A	532 nm	3 mm
[112]	N/A	N/A	N/A	N/A	Double caivity Nd: YAG laser	N/A	120 mJ/pulse	N/A	N/A
[113]	N/A	N/A	N/A	N/A	Argon-ion contionus laser	N/A	N/A	N/A	N/A
[114]	Nikkor 50 mm F/2.8 lens	50 mm	f/2.8	Litron Nano T PIV	Nd: YAG pulsed laser	N/A	N/A	532 nm	N/A

(*continued on next page*)

Table 3 (*continued*)

[115]	A lens (100 mm focal length, 25 mm diameter, ThorLabs) and SLR camera lens (65 mm, F# = 11, Nikon)	100 mm & 65 mm	11	LRS-0532-TF, Laserglow Technologies	N/A	N/A	1.6 Watt	532 nm	N/A
[116]	N/A	N/A	N/A	N/A	Twin pulsed Nd: YAG lasers	N/A	300 mJ (at 10 Hz)	532 nm	1 mm (wide sheet)
[117]	N/A	N/A	N/A	N/A	Nd: YAG laser (for PIV)	N/A	N/A	N/A	N/A
[118]	Toyo Optics 12.5–75 mm, F1.8 lens (MAC Group, USA)	12.5–75 mm	f/1.8	N/A	N/A	N/A	N/A	N/A	N/A
[119]	N/A	N/A	N/A	N/A	Double pulsed Nd: YAG laser	N/A	120 mJ	522 nm	N/A
[120]	N/A	50 mm	2,8	N/A	Double cavity Nd: YAG laser	N/A	120 mJ (Per pulse)	532 nm	N/A
[121]	N/A	N/A	N/A	N/A	Nd: YAG laser	N/A	N/A	N/A	N/A
[122]	N/A	N/A	N/A	N/A	N/A	N/A	N/A	N/A	N/A
[123]	N/A	N/A	N/A	N/A	Double pulsed Nd: YAG laser	N/A	200 mJ (Per pulse)	532 nm	N/A
[124]	N/A	N/A	N/A	N/A	Two Nd: YAG lasers	N/A	50 mJ (Per pulse)	N/A	N/A
[125]	N/A	N/A	N/A	N/A	Double pulsed Nd: YAG laser	N/A	120 mJ	N/A	N/A
[126]	N/A	N/A	N/A	N/A	N/A	N/A	N/A	N/A	N/A
[127]	N/A	N/A	N/A	N/A	N/A	N/A	N/A	N/A	N/A
[128]	Nikon Nikkor 50 mm f/ 1.8 lenses	50 mm	f/1.8	N/A	Double pulsed Nd: YAG laser	N/A	200 mJ	532 nm	2 mm
[129]	NA	N/A	N/A	N/A	Nd: YAG laser	N/A	135 mJ (Pulse Energy)	532 nm	N/A
[130]	Spherical and cylindrical lenses & macro LAVISION lens	N/A	N/A	Litron Incorporation, DualPower 65–15 DANTEC laser	Nd: YAG laser	N/A	65 mJ (Pulse Energy)	532 nm	0.11 mm
[131]	Nikon Computer TV Lens 1.4/75 & cylindrical lens	75 mm & 5 mm (cylindrical lens)	1,4	Nano L200 - 15 PIV (Litron Lasers Ltd., Rugby, UK)	Nd: YLF laser	N/A	200 mJ	532 nm	Thinner than 1 mm
[132]	N/A	N/A	N/A	N/A	Double pulsed Nd: YAG laser	N/A	120 mJ	N/A	N/A
[133]	N/A	N/A	N/A	N/A	N/A	1200 mJ (Maximum pulse energy)	N/A	532–1064 nm	0.6 mm
[134]	N/A	N/A	N/A	Nano 50–100, Litron	Double-cavity Q-switched Nd: YAG laser	N/A	N/A	N/A	N/A
[135]	Nikon 50 mm lens	50 mm	N/A	N/A	Double pulsed Nd: YAG laser	N/A	1200 mJ (Per pulse)	532 nm	N/A
[136]	60 mm Nikkorr SLR lens	60 mm	f/16	Solo III-15, New Wave Research	Nd: YAG laser	N/A	50 mJ (Per Pulse)	N/A	Less than 1 mm
[137]	N/A	N/A	N/A	NAND L50-100 laser system	Pulsed laser	N/A	N/A	N/A	1 mm
[138]	N/A	N/A	N/A	N/A	Nd: YAG laser	N/A	120 mJ	N/A	N/A

(*continued on next page*)

Table 3 (*continued*)

[139]	SIGMA lens (105/2.8, EX DG Macro, Sigma Corporation of America, Ronkonkoma, NY, USA and camera lens	105 mm	f/2.8	NANO S35, Litron Lasers, Rugby, UK	Q- switched, pulsed Nd: YAG	N/A	120 mJ	532 nm	About 0.6 mm
[140]	N/A	N/A	N/A	N/A	N/A	N/A	N/A	N/A	N/A
[141]	N/A	N/A	N/A	N/A	Double pulsed Nd: YAG laser	N/A	120 mJ	532 nm	N/A
[142]	N/A	N/A	N/A	New Wave	Pulsed Nd: YAG laser	N/A	200 mJ	N/A	N/A
[143]	N/A	N/A	N/A	NewWave Research	Double pulsed Nd: YAG laser	N/A	200 mJ	532 nm	0.5 mm (Height)
[144]	Nikon AF Nikkor 50 mm f/1.8 lens & cylindrical lens	50 mm (Nikkor)	f/1.8	N/A	Nd: YAG laser	N/A	60 mJ (Per Pulse)	532 nm	N/A
[145]	N/A	0.5–2 m (Adjustable focus)	N/A	N/A	Pair of double cavity Nd: YAG lasers	N/A	100 mJ (Per Pulse)	532 nm	3 mm
[146]	N/A	N/A	N/A	LISTRON NANO L200-15 PIV	Double pulsed laser	N/A	N/A	N/A	N/A
[147]	The Nikon AF Nikkor 50 mm f/1.8 lens	50 mm	f/1.8	N/A	Nd:YAG laser	N/A	60 mJ (Per Pulse)	532 nm	N/A
[148]	N/A	N/A	N/A	Litron Nano PIV	Dual head Nd: YAG laser	N/A	N/A	532 nm	N/A
[149]	N/A	N/A	N/A	N/A	Green light laser	N/A	N/A	545 nm	2 mm
[150]	AF Nikkor 50 mm f/1.8D prime lens & Two cylindrical lenses (25 mm and 15 mm)	50 mm (Nikkor lens) & 25 mm, 15 mm (Two cylindrical lenses)	f/1.8D (Nikkor lens)	Litron Laser	Dual cavity Nd: YAG green laser	N/A	1200 mJ	532 nm	1 mm
[151]	N/A	60 mm	N/A	N/A	Double pulsed Nd: YAG laser	N/A	120 mJ (Nominal Output Energy)	532 nm	Almost 1 mm
[152]	SIGMA AF 105 mm f/2.8 EX DG MACRO lenses	105 mm	f/2.8	Photonix DM100-532	High-repetition pulsed Nd: YAG laser	N/A	100 Watt (Average Power)	532 nm	N/A
[153]	N/A	N/A	N/A	N/A	N/A	N/A	N/A	N/A	N/A
[154]	Nikon AF Micro 60 f/2.8D lenses	60 mm	f/2.8D	N/A	Double pulsed Nd: YAG laser	120 mJ	N/A	532 nm	2 mm
[155]	N/A	N/A	N/A	N/A	High power double pulsed Nd: YAG laser	N/A	400 mJ	532 nm	N/A
[156]	N/A	N/A	N/A	New Wave Minilase	Dual cavity dual pulse Nd: YAG laser	120 mJ	N/A	N/A	N/A
[157]	Nikon AF Mikro 60 mm f/2.8D lens	60 mm	f/2.8D	N/A	Double pulsed Nd: YAG laser	50 mJ	N/A	532 nm	1 mm
[158]	Nikon 105 mm macro lens	105 mm	N/A	N/A	Dual cavity Nd: YAG laser	N/A	135 mJ	N/A	About 1 mm
[159]	N/A	N/A	N/A	Dual Power 30-15	N/A	N/A	N/A	N/A	N/A
[160]	N/A	N/A	N/A	N/A	Double pulsed Nd: YAG laser	N/A	120 mJ	532 nm	2 mm

(*continued on next page*)

Table 3 (*continued*)

[161]	N/A	250 mm ve 50 mm	0.45 (Numerical Aperture for objective lens)	Shanghai Dream Laser Technology, Ltd, China (Micro PIV)	Nd: YAG laser (Micro PIV)	N/A	1 Watt (Mikro PIV) & 3 GeV (Stored energy in X-Ray PIV)	532 nm	N/A
[162]	N/A	N/A	N/A	New Wave Research Solo	Dual pulsed Nd: YAG laser	N/A	200 mJ	532 nm	N/A
[163]	N/A	N/A	N/A	DPGL-2W by Japan Laser Corp	Visualization laser	N/A	2 Watt	532 nm	1 mm
[164]	N/A	N/A	N/A	N/A	N/A	N/A	N/A	N/A	N/A
[165]	N/A	N/A	N/A	N/A	Pulsed Nd: YAG laser	N/A	100 mJ	N/A	About 1.5 mm
[166]	Particular lens (50 mm) and wide-angle Nikkor 28 mm F/2.8 D lens	50 mm and 28 mm	f/2.8D	Quantel EverGreen	Double pulsed Nd: YAG laser	N/A	145 mJ (Pulse Energy)	532 nm	N/A
[167]	N/A	N/A	N/A	N/A	N/A	N/A	N/A	N/A	N/A
[168]	N/A	N/A	N/A	Oxford Laser Firefly LED-laser	LED (Diode) laser	N/A	N/A	808 nm	N/A
[169]	N/A	N/A	N/A	N/A	N/A	N/A	N/A	N/A	N/A
[170]	Nikkor lens	60 mm	N/A	Litron LDY300	Nd:YLF laser	N/A	N/A	N/A	1 mm
[171]	AF Nikko 50 mm f/1.8D objective lens & A telephoto lens with a focal length of 25 mm	50 mm & 25 mm	f/1.8D	Nano L PIV	Double pulsed Nd: YAG laser	N/A	135 mJ	532 nm	Approximately 1–2 mm
[172]	N/A	N/A	N/A	Litron lasers Nd:Yag DuaPower Nano L200-15PIV laser unit	Dual power Nd: YAG laser	N/A	N/A	532 nm & 1064 nm	N/A
[173]	Two spherical and a cylindrical lenses & SLR lenses (Sigma)	60 mm (SLR)	f/16 (Aperture diameter)	New Wave Research, Solo PIV III	Nd: YAG laser	50 mJ	N/A	532 nm (Pulse width)	1 mm
[174]	N/A	N/A	N/A	N/A	Two Nd: YAG lasers	190 mJ (Per pulse)	N/A	N/A	N/A

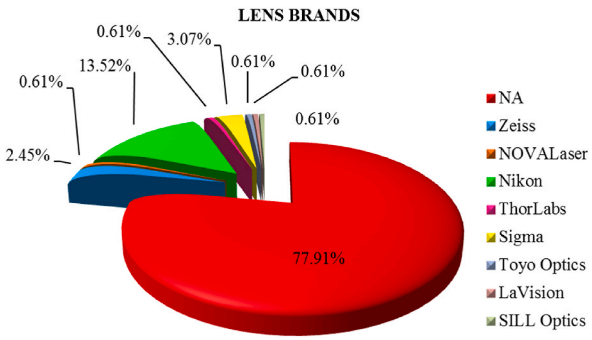

Fig. 14. Lens brands.

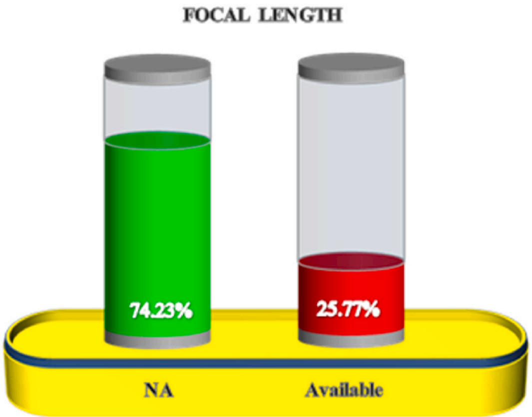

Fig. 15. Focal lengths.

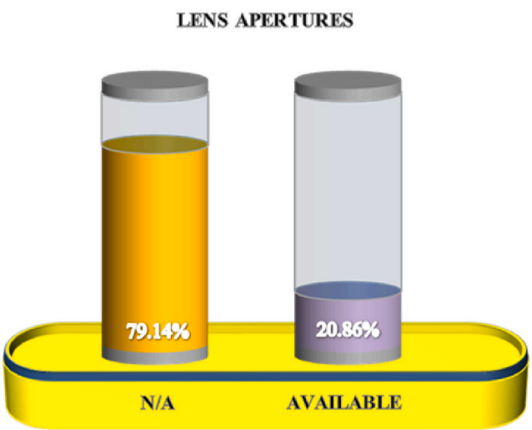

Fig. 16. Lens apertures.

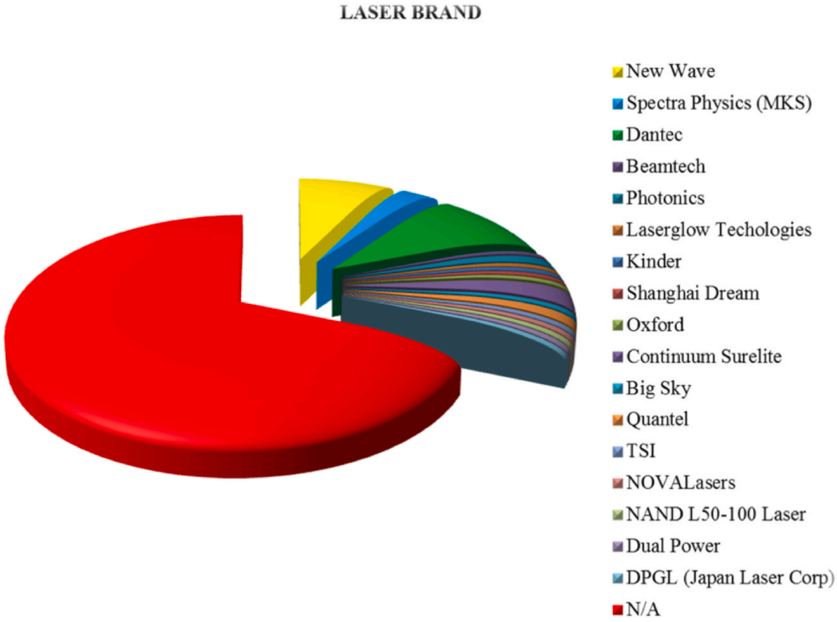

Fig. 17. Laser brands.

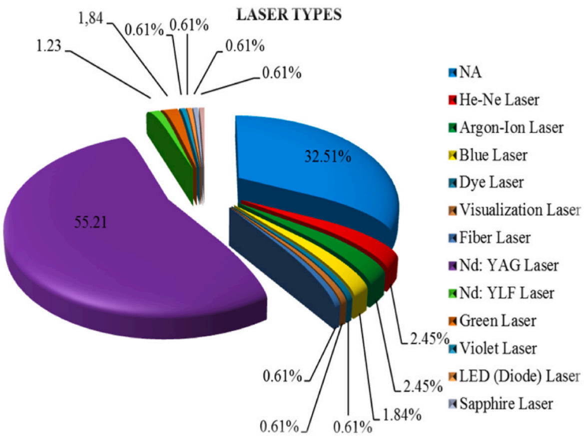

Fig. 18. Laser types.

3.3. TRACER and SEEDER

Choosing suitable seeding material is one of the significant topics for PIV measurements [7,33]. The seeding particles must be small and large enough to follow the flow and reflecting of the light. In liquid flows, two types of seeding particles are preferred [7,17]. Solid particles and gaseous bubbles are the main seeding particles. Different oils can be used too. Polystyrene, aluminum flakes, hollow glass spheres, granules for synthetic coatings are the most preferred seeding particles for liquid flows [7,17]. Solid particles must have narrow diameter distribution and good light scattering behavior such as hollow glass spheres and polyamide particles [17]. However, solid particles have some disadvantages. One of the drawbacks of solid particles is the tendency to sediment in eddies. Also, solid particles are hardly accessible in complex flow regions [236,237]. Moreover, filtering of expensive refractive index wastes much time [7,238].

Gaseous bubbles are other seeding particles used in PIV applications. With respect to the solid particles, gaseous bubbles do not contaminate the test fluid [238]. Bigger gaseous bubbles have a tendency to show poor following behaviors. The situation comes from the increased inertia at a larger radius [237,238]. In liquid flows, oxygen bubbles as a gas phase seeding particles are preferred [17]. In gas flows; polystyrene, Al_2O_3, TiO_2, glass micro-spheres, glass micro-balloons, granules for synthetic coating, dioctyphathalate, smoke, different oils, di-ethyl-hexyl-sebacate (DEHS) and helium-filled soap bubbles are the most preferred tracers [7,17,238]. In Table 4,

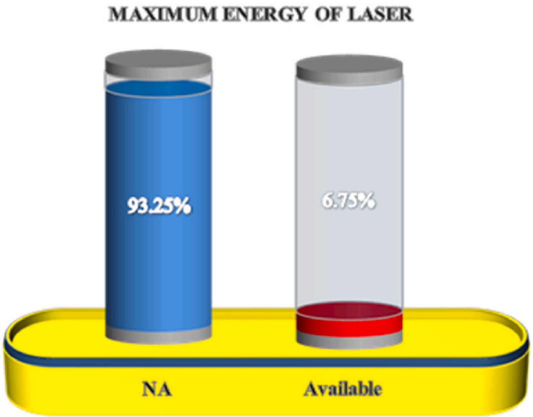

Fig. 19. Maximum energy of laser.

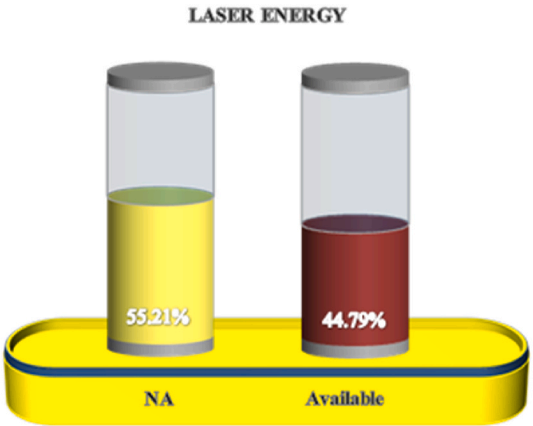

Fig. 20. Laser energy.

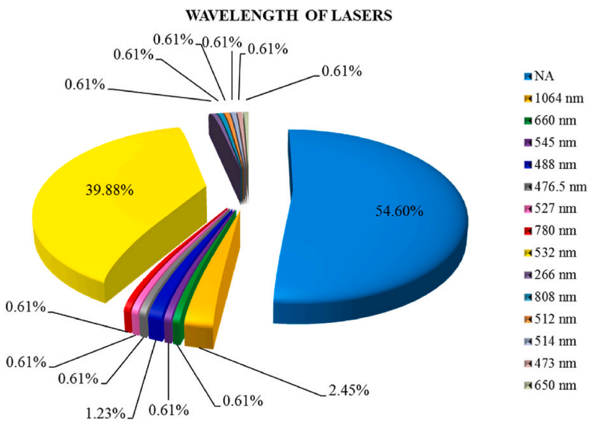

Fig. 21. Wavelength of lasers.

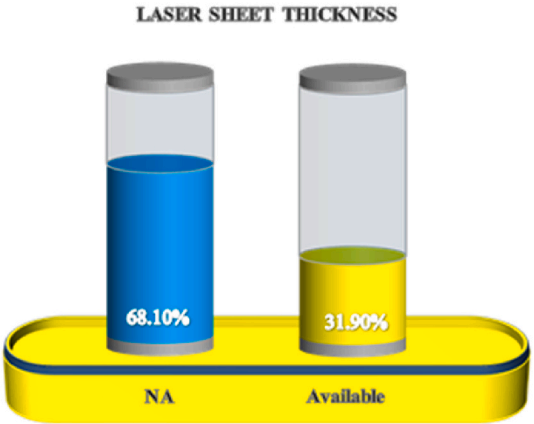

Fig. 22. Laser sheet thickness.

Table 4
Tracer-seeding particles, particle dimensions and seeders.

Ref.	Tracer/seeding particles mentioned/added/followed in the study	Particle dimensions	Seeders
[1]	N/A	N/A	N/A
[8]	N/A	N/A	N/A
[9]	N/A	N/A	N/A
[10]	Hollow silver coated particles	10 μm	N/A
[11]	N/A	N/A	N/A
[12]	Hollow glass sphere	12 μm	N/A
[13]	Hollow glass spheres	10 μm	N/A
[14]	TiO_2 particles	30 nm (Nominal diameter)	Particle generator (mentioned)
[15]	Hollow glass beads	6 μm (Approximately)	N/A
[16]	Spherical smoke droplets	1–2 μm (Mean particle size)	Smoke generator (Type: Rosco 1700)
[22]	N/A	N/A	N/A
[23]	Silver-coated hollow glass spheres	15 μm	N/A
[24]	Hollow glass balls	35 μm (approximately)	N/A
[25]	Spherical fog drops	1–2 μm (average diameter)	Rosco1600 fog generator
[26]	N/A	N/A	N/A
[27]	N/A	N/A	N/A
[28]	N/A	100 and 400 μm	N/A
[29]	Polystyrene micro spheres	0.5 μm	N/A
[30]	0.01% micro-encapsulated Liquid crystal particles	100 μm (Mean diameter)	N/A
[31]	N/A	N/A	N/A
[32]	N/A	N/A	N/A
[33]	N/A	N/A	N/A
[34]	Low concentrations of polypropylene beads (for flow tracing and simulation)	3 mm (for simulation)	N/A
[35]	Polystyrene particles tagged with fluorescent dye	300 nm	N/A
[36]	Thermochromic liquid crystals	N/A	N/A
[37]	Fluorescent polystyrene particles	200 nm	N/A
[38]	Plastic seed particles	100–200 μm	N/A
[39]	Hollow glass spheres	60 μm	N/A
[40]	Oil smoke	1 μm (approximately)	N/A
[41]	Olive oil droplets	N/A	Laskin nozzle aerosol generator
[42]	N/A	N/A	N/A
[43]	Fluorescent micro-spheres	500 nm	N/A
[44]	Oil droplets	1–2 μm	Aerosol Generator equipped with a set of Laskin nozzles
[45]	N/A	N/A	N/A
[46]	Lubricating oil (glycerin, SG-α 10G) (accepted)	N/A	Lubricating oil (glycerin, SG-α 10G) (atomizer)
[47]	N/A	5 μm (2–4 μm)	N/A
[48]	N/A	30 μm	N/A
[49]	Fluorescent tracer particles (rhodamin-B)	75 μm	N/A
[50]	Fluorescent polymer particle	10 μm	N/A
[51]	Hollow glass particles	8–12 μm	N/A
[52]	N/A	N/A	Injection seeder

(continued on next page)

Table 4 (*continued*)

Ref.	Tracer/seeding particles mentioned/added/followed in the study	Particle dimensions	Seeders
[53]	N/A	N/A	N/A
[54]	N/A	N/A	N/A
[55]	Polyamide tracer particles	50 µm (mean diameter)	N/A
[56]	Hollow glass spheres	8 µm	N/A
[57]	Hollow spherical glass spheres	10 µm (lower region) & 50 µm (upper region)	N/A
[58]	N/A	12 µm (mean diameter)	N/A
[59]	Polystyrene particles	1 µm	N/A
[60]	Magnesium oxide	5 µm (nominal diameter)	N/A
[61]	N/A	N/A	N/A
[62]	Water droplets and smoke particles	N/A	A water generator, a mist generator, a smoke generator
[63]	N/A	N/A	N/A
[64]	Polyamide particles	18 µm and 108 µm (Mean diameter)	N/A
[65]	Rhodamine-B dye particles	20–40 µm	N/A
[66]	PSP	20 µm (Approximately)	N/A
[67]	Small fluorescent tracer particles	5 µm (Average diameter)	N/A
[68]	N/A	N/A	N/A
[69]	N/A	N/A	N/A
[70]	Glass particles	1.5 mm and 2.5 mm	N/A
[71]	N/A	N/A	N/A
[72]	Nylon particles (TSI, pt-900845)	4 µm	N/A
[73]	Silvered glass microspheres	15 µm (average diameter)	N/A
[74]	N/A	N/A	N/A
[75]	N/A	N/A	N/A
[76]	Hollow glass silver particles	20 µm	N/A
[77]	Spherical hollow glass spheres (type 110P8 Potters Industries, U.K.)	11 µm (Mean diameter)	Cyclone aerosol seeder (CAS)
[78]	Mixture of vestowax H and titanium II oxide 1050 MG	50 µm (mean diameter)	N/A
[79]	N/A	N/A	N/A
[80]	Silver coated plastic particles	12 µm (Mean diameter)	N/A
[81]	Silver coated hollow glass balls	8–12 µm (diameter size distribution)	N/A
[82]	N/A	N/A	N/A
[83]	N/A	N/A	N/A
[84]	Fluorescent tracer particles (Micro PIV) & Fluorescent MF-RhB-2150 particles (Mesochannel)	10.20 µm ± 0.17 µm (micro spheres for meso scale experiments)	N/A
[85]	Silver coated particles	N/A	N/A
[86]	N/A	N/A	N/A
[87]	Degussa Aerosil R104, Degussa Aerosil R972, Kemira P170, Kemira P580, Kemira L830, Kemira 300, XRDI-S, DuPont R931 & TiO2 particles and SiO_2	12, 14, 16, 30, 50, 170, 240 and 550 nm (primary crystal size)	Two solid seeding generators (a custommade cyclone seeder and a fluidized bed from PIVTEC GmbH
[88]	Spherical nylon particles	1 µm	N/A
[89]	DIAION- HP21	0.11 mm (average grain size)	N/A
[90]	Hollow glass spheres	6 µm	N/A
[91]	Polystyrene Latex particles coated with a red fluorescent dye	1 µm	N/A
[92]	Atomized paraffin oil	N/A	N/A
[93]	Glass particles covered with the fluorescent dye Rhodamine-B	13 µm	N/A
[94]	Fluorescent seeding microparticles	10 µm (average diameter)	N/A
[95]	Household processed cornstarch (for air) and cultured green algal cells (young cultures for water)	Approximately 10–18 µm (Mostly 15 µm for air) & 9–19 µm (Approximately 12 µm for water)	N/A
[96]	Smoke particles	1 µm (mean diameter)	Particle generator (combustion)
[97]	Fluorescent melamine microsphere suspension powder	8 µm (average diameter)	N/A
[98]	Silver-coated hollow glass particles	14 µm	N/A
[99]	Fluorescent particles (Fluoresbrite Carboxylate Microspheres, #15700, Polysciences, Inc)	0.50 µm	N/A
[100]	Rhodamin particles & Silver coated particles	50 µm and 10 µm respectively	N/A
[101]	N/A	N/A	N/A
[102]	Fluorescent polystyrene-DVB particles (Kanomax, Japan)	30 µm (mean diameter)	N/A
[103]	Ground black pepper & Sawdust particles of cypress wood (for surface flow visualization)	N/A	N/A
[104]	Griltexs seeding particles	400 µm (mean diameter) (300 µm–500 µm)	N/A
[105]	Silver coated particles	10–20 µm	N/A
[106]	N/A	N/A	N/A
[107]	Al2O3 particle	400 nm	N/A
[108]	N/A	N/A	N/A
[109]	Air bubbles	0.2–0.7 mm (Size)	N/A

(*continued on next page*)

Table 4 (*continued*)

Ref.	Tracer/seeding particles mentioned/added/followed in the study	Particle dimensions	Seeders
[110]	Pulp fines	up to 250 µm (length)	N/A
[111]	Smoke particles of diethylene glycol and water	1 µm (median diameter)	Fog generator Safex
[112]	Silver coated glass spheres	10 µm (mean diameter approximately)	N/A
[113]	N/A	N/A	Seeding tubes and tracer generator
[114]	Al2O3 particles	1 µm (nominal diameter)	N/A
[115]	Hollow glass sphere particles	10 µm	N/A
[116]	N/A	10 µm	N/A
[117]	Incense particles (for PIV) & Helium-filled soap bubbles (for PTV)	1 µm (average diameter for PIV) & 2 mm (average diameter for PTV)	Commercial bubble generator by Sage Action inc
[118]	Glass beads (Preliminary tests) & Milk Powder	88 µm (modal diameter for glass beads) & 128 ± 7 µm (laser diffraction analysis)	N/A
[119]	Metallic-coated tracer particles of hollow plastic spheres	14 µm	N/A
[120]	TiO_2 particles	N/A	N/A
[121]	Silver coated particles	N/A	N/A
[122]	N/A	N/A	N/A
[123]	Hollow glass spherical particles	10 µm (mean diameter)	N/A
[124]	N/A	N/A	N/A
[125]	N/A	N/A	N/A
[126]	Rhodamine imprinted PMMA particles	20–50 µm	N/A
[127]	N/A	N/A	N/A
[128]	Hollow glass spheres	10 µm	N/A
[129]	Fog fluid	N/A	Fog generator
[130]	Polyamide Seeding Particles (PSP-5)	1–10 µm (average 5 µm)	N/A
[131]	Ligaments and drops of molten steel (accepted as particles) X3CrNiMo13-4 and X5CrNi18-10	N/A	N/A
[132]	Silver coated particles	10–20 µm	N/A
[133]	Polyamide tracing particle (PSP-50)	50 µm	N/A
[134]	Fog of DEHS liquid and sunflower seed oil	N/A	High volume liquid seeding generator (10F03, Dantec Dynamics)
[135]	Oil aerosol (Di-Ethyl-Hexyl-Sebacat (DEHS))	1 µm	PIVTEC seed generators
[136]	Glass beads	18 µm	N/A
[137]	Fine glass beads	40 µm (About)	N/A
[138]	Neutrally buoyant fluorescing particles	36–75 µm	N/A
[139]	Polyamide seeding particles (PSP-50)	50 µm (Mean diameter)	N/A
[140]	N/A	15 mm	N/A
[141]	N/A	N/A	N/A
[142]	Crystal balls	1–5 µm (Particle size)	N/A
[143]	Neutrally buoyant florescent particles	15 µm	N/A
[144]	Hollow glass spheres	20–60 µm	N/A
[145]	TSI seeding particles & polyamide particles	55 µm (Mean diameter) & 20–55 µm	N/A
[146]	Rhodamine B (powder)	10–20 µm (average diameter)	N/A
[147]	Hollow glass sphere	20–60 µm	N/A
[148]	Silver coated hollow glass spheres	10 µm	N/A
[149]	Fluorescent particles	10 µm (Mean diameter)	N/A
[150]	Fluorescent polymer particles (melamine resin based) coated with rhodamine B	20–50 µm	N/A
[151]	Round metal particles	10 µm	N/A
[152]	Polyamide particles	50 µm	N/A
[153]	N/A	N/A	N/A
[154]	Silver coated hollow glass spheres	10 µm	N/A
[155]	Fluorescent tracers (Duke scientific polymer microspheres redfluorescing for µPIV) & polystyrene particles (Sigma-Aldrich) with a concentration of 0.1% w/w (for GPV)	3 µm and 200 nm	N/A
[156]	Sand particles	285 µm (Mean size)	N/A
[157]	Polyamide particle tracers	30 µm (average diameter)	N/A
[158]	DEHS	1 µm (average diameter)	Laskin-nozzle-based seeding generator
[159]	Silvered glass microspheres	15 µm (average diameter)	N/A
[160]	Silver coated particles	10–20 µm	N/A
[161]	Silver-coated hollow glass particles (X-Ray PIV) & Polymer fluorescent particles (µPIV)	14 µm and 1 µm (average diameter for 1 µm) respectively	N/A
[162]	Glass hollow spheres	9–13 µm	N/A
[163]	Ethylene glycol (EG), talc consisting of magnesium hydroxide and silicate, and Copper powder (Cu)	4 µm, 5 µm and 5 µm (typical particle size) respectively	Hazer (Antari Z-300 II)
[164]	N/A	N/A	N/A
[165]	Silver coated spheres	10 µm	N/A
[166]	Silicon Oxide particles	N/A	N/A
[167]	Opaque and white glass particles	0.4–0.6 mm	N/A
[168]	Water seeding particles	1 µm (About)	TSI Six-Jet Atomizer 9306

(*continued on next page*)

Table 4 (*continued*)

Ref.	Tracer/seeding particles mentioned/added/followed in the study	Particle dimensions	Seeders
[169]	N/A	N/A	N/A
[170]	TiO_2 particles (CAS No. 13463-67-7)	0.17 μm (primary crystal size)	N/A
[171]	Smoke particles	N/A	A VZ09 – 0751 smoke generator
[172]	TiO_2 particles	10 μm	TiO_2 seeding dispenser
[173]	Silver coated glass beads	2 μm	N/A
[174]	Olive oil tracers	1 μm (approximately)	A Laskin nozzle atomizers

tracer particles and dimensions can be seen. When Table 4 is examined in detail, it can be noticed that there is a great amount of tracer particles with dimensions.

Suitable flow seeding and uniform seeding size are two the important phenomena for PIV measurements [33]. Uniform seeding size influences the accuracy of measurements. Namely, particle generators that produce proper seeding are mandatory. Consequently; seeders have an important role in PIV measurements [7]. In addition, in Table 4, seeder brands namely brand of seeding devices or generators were given by the year.

Fig. 23 illustrates that fluorescent dyed particles and silver-coated particles were used in almost 12% of PIV studies examined in the open literature. According to Table 4, more than one type of seeding particles is used in some PIV studies. Fluorescent dyed particles and silver-coated particles have some advantages such as scattering light and narrow diameter distribution [7,238]. Hence, fluorescent dyed particles and silver-coated particles are commonly used [17,237].

Tracer particles must have some certain properties. For instance, being neutrally in terms of chemically and electrically is desired. On the other hand, tracer particles should not be affected by electrical and Brownian motion. Particle density must be almost same with fluid density. Brownian motion can be measured in micron scale particle image velocimetry [222]. Very small particles than desired must not be used for particle image velocimetry applications. Consequently, choosing tracer particles order of light wavelength is reasonable [239].

Apart from the fluorescent dyed particles and silver-coated particles, hollow glass spheres and rhodamine dyed particles have noticeable usage in PIV studies. However, sand, incense, milk powder, cornstarch, algal cell, pulp fines, ground black pepper, molten steel have the lowest percent of nearly 1%. For instance, algal cells can be used in only biological applications. Compared to other fields, the percent of biological applications can be ignored. Like algal cells, molten steels or ligaments are not used too much. Casting has a negligible percentage among other fields. Furthermore, nylon is not suitable for using as tracer particles. Like metallic particles, nylon is sensitive to heat too much. In addition, nylon is difficult to find. Finally, Prasad et al. [26] mentioned 30 μm black carbo-spheres and Sugii et al. [47] mentioned red blood cell in their studies. Brandt and Merzkirch [28] investigated spray jet and water particles with 100–400 μm. Yamamoto et al. [63] utilized MgO as particle scatters. Güler et al. [69] investigated three different drift retardants in wind tunnel. Decker et al. [108] mentioned solid phase fluid catalytic cracking (FCC) catalyst particles with about 62 μm geometric diameter.

As illustrated in Fig. 24, particle dimensions are available in nearly 68–69% PIV studies. Dimensions of tracer particles changes from nanoscale to millimeter scale. In some studies, mean diameters, average diameters, sauter diameters, nominal diameters are given. In general, micro scale particles are in demand owing to macro PIV usage. Micron-scale particle image velocimetry is used less than macro-scale particle image velocimetry. In micro PIV applications, nanoscale particles are widely used. In nano particles, Brownian motion is also taken into account [222,239].

As shown in Fig. 25, only brands are taken into account. In about 91% of PIV studies, seeder brands are not available. Laskin seeders are used in almost 2.4% of PIV studies. Laskin generators are good choices for air flows [44]. With the rapid technological developments, seeders or generators with better features are used in PIV applications. Except for Laskin, PIVTEC, Safex, Sage Action, Dantec Dynamics, Hazer, TSI and VZ09-0751 are used in appoximately 1% of PIV studies. In nearly 91% of PIV studies exist in the open literature, seeder brands are not mentioned. Rosco and PIVTEC brands have the same percent. Kürekci and Ozcan [92] mentioned atomized paraffin oil for seeding flow. Namely, homogenously seeding is regarded as one of the important topic for particle image velocimetry. Proper seeding can be acquired via well suited tracer particles. Otherwise, inhomogeneous seeding may bring some problems. Namely, tracer particles are serious problem. Labeling fluid elements without tracer particles in particle image velocimetry applications may be viable [222]. If the situation is achieved, this will be very good for future. Without tracer particles, bias errors and contamination can be prevented [222,240,241]. In order to perform experiments accurately, seeding devices must supply seeding particles in time sufficiently. Inaccurate seeding affects data and decreases accuracy. Consequently, the experiment becomes meaningless for us [235].

3.4. COMPUTER and SYNCHRONIZER

The recording and evaluation of PIV images are one of the important steps for PIV measurements. Measurements in PIV usually result in numerous images that should be further processed. Recorded data can be easily stored in gigabytes. With the use of a computer, recording became easier. Therefore, using a computer is mandatory. Only a twenty or thirty years ago, processing and handling of particle image velocimetry images, which had megapixel sizes required a great amount of effort. In today, processing and

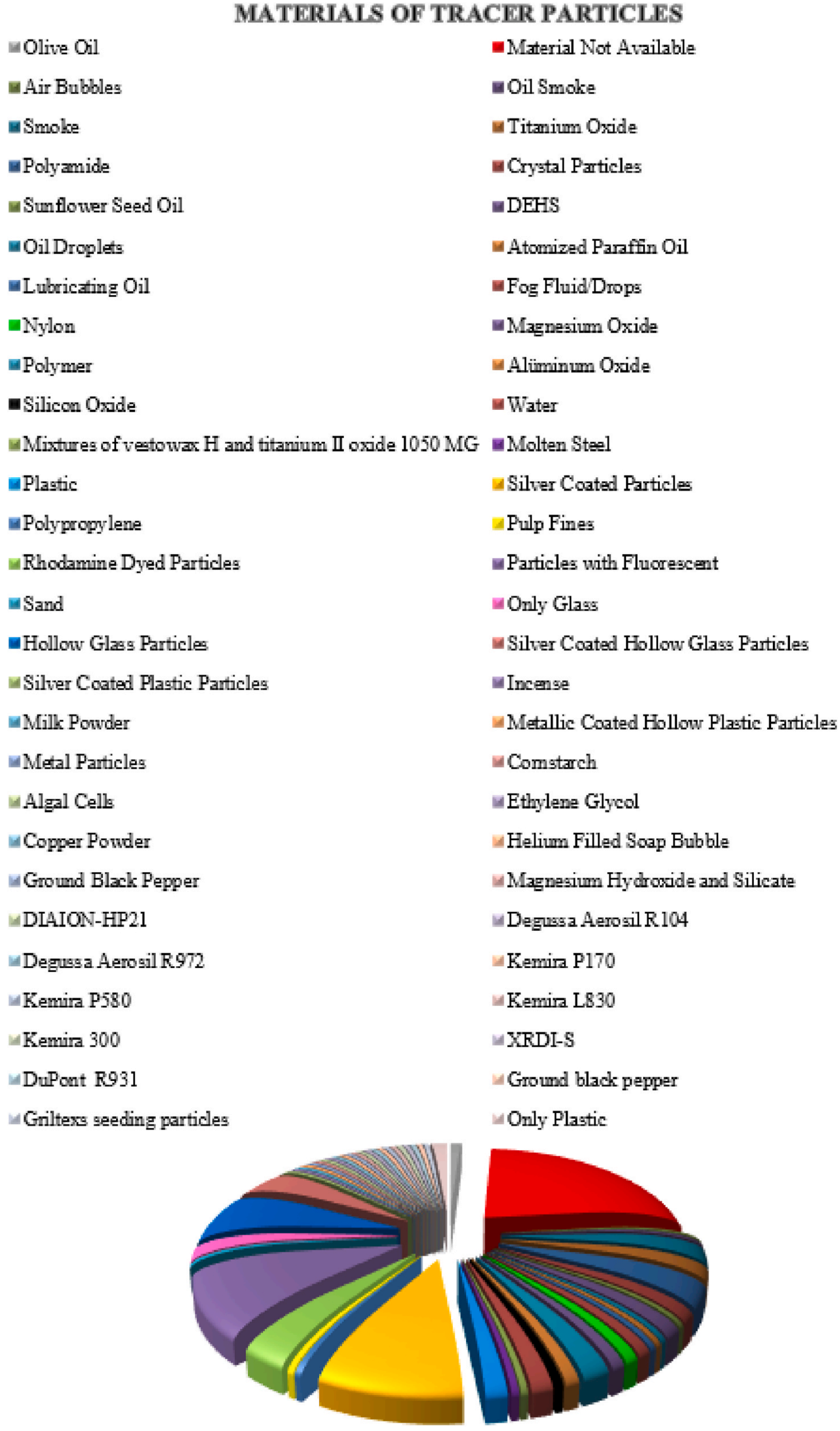

Fig. 23. Materials of tracer particles.

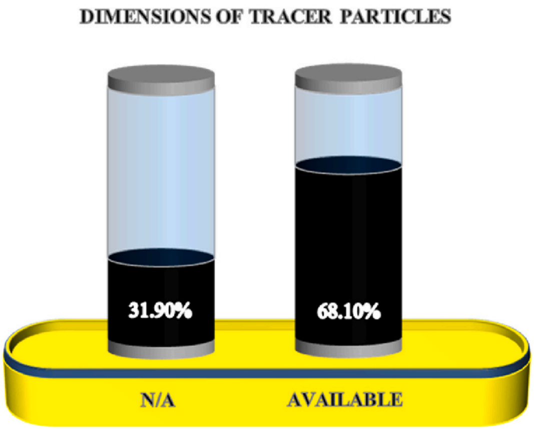

Fig. 24. Dimensions of tracer particles.

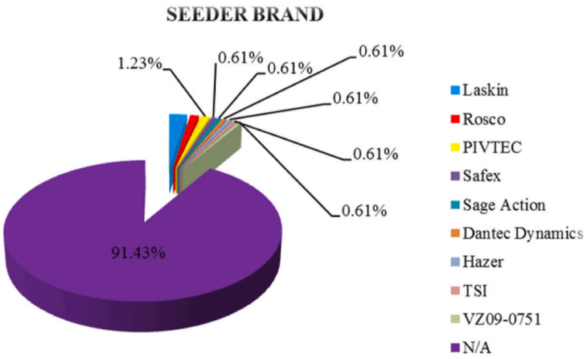

Fig. 25. Distribution of seeder brands in studies.

handling are very easy. Evaluation and processing can be carried out in seconds [7]. In Table 5, brands and essential features of computers are given. Brands and processor speeds are given with study by year.

In PIV systems, the synchronizer is also known as timer box is one of the components that make the trigger signal [7]. The component performs synchronization between the laser, camera, computer and other hardware and makes the components work coherently [1,233]. In addition, in Table 5, synchronizer brands directly mentioned in studies are given. According to Figs. 26 and 27, brands and essential features of computers are given in approximately 2–3% and 4–5% respectively in PIV studies. The percent of MicroVax, Dell, Casio, IBM PC/SX does not exceed 1% in PIV studies. It can be concluded from Figs. 26 and 27, computer brands and features are not required to mention too much. Computers are referred to as essential components of particle image velocimetry.

Without computers image processing, evaluation, post-processing, CFD, modeling cannot be conducted. In order to carry out pre-processing and post-processing, modeling related software is needed. Namely, computers are everywhere in our daily lives [156,242,243].

In the 1990s, computers didn't become common. So, PIV analyses were performed more difficult than today. Additionally, PIV analyses took a lot of time due to essential features of computers such as RAM, processor speed. In the 2000s, computers became more common. With technological developments, computers have high features. Processor speed and RAM are also important features. In today, workstations are widely in demand. Bryanston-Cross et al. [29] mentioned 8255 I/O card, Rosengarten et al. [38] used Scion LG3 capturecard, Triep et al. [67] mentioned countercard, Güler et al. [69] mentioned RS232, Olayiwola et al. [78] used NI-DAQ card, PCI 6602, Linux Cluster, Satake et al. [88] mentioned circuits, Sun and Huang [156] used data acquisition card and Ahmadi et al. [173] mentioned NI 9211 and 9263 data acquisition cards. Namely, percents of essential features for computers may change.

As illustrated in Fig. 28, TSI synchronizers are preferred in almost 4.3% of PIV studies. In nearly 88–89% of PIV studies, synchronizer brands are not mentioned directly. Directly given synchronizer brands are not too much. If PIV and software brands are taken into account, the percenatges will change. LPU, Alaser Pulse TM has the lowest percent. Lavision and Dantec has almost same percent.

Synchronizers or timer boxes are one of the most significant components of particle image velocimetry. The component conducts management of the system. Without synchronizers; lasers, cameras and other components do not work in time. Accurate results can not be obtained. Namely, the system becomes useless without synchronizers. Like other components, timer boxes developed with the technological steps [7].

Table 5
Brands and essential features of computers and synchronizer brands.

Ref.	Computer brands	Essential features of computers	Synchronizer/controlling unit brands mentioned/given directly in studies
[1]	N/A	N/A	N/A
[8]	N/A	N/A	N/A
[9]	N/A	N/A	N/A
[10]	N/A	N/A	Dantec Dynamics 80N77 timer box
[11]	N/A	Intel Core Duo CPU E8400@3.00 GHz with a RAM of 1.94 Go.	N/A
[12]	N/A	N/A	N/A
[13]	N/A	N/A	N/A
[14]	N/A	N/A	N/A
[15]	N/A	N/A	N/A
[16]	N/A	N/A	TSI610034 type synchronizer
[22]	N/A	N/A	N/A
[23]	N/A	N/A	N/A
[24]	N/A	N/A	N/A
[25]	N/A	N/A	N/A
[26]	MicroVax II Host Computer	Numerix 432 array processor	N/A
[27]	N/A	N/A	N/A
[28]	N/A	N/A	N/A
[29]	N/A	N/A	N/A
[30]	IBM PC/SX	N/A	N/A
[31]	N/A	N/A	N/A
[32]	N/A	N/A	N/A
[33]	N/A	N/A	N/A
[34]	N/A	133 MHz, Pentium personal computer	N/A
[35]	N/A	N/A	N/A
[36]	N/A	Pentium PC 133 Mhz running Linux OS	N/A
[37]	N/A	N/A	N/A
[38]	N/A	N/A	N/A
[39]	N/A	N/A	N/A
[40]	N/A	N/A	N/A
[41]	N/A	N/A	TSI Model 610 030 LaserPulse synchronizer
[42]	N/A	N/A	N/A
[43]	N/A	N/A	N/A
[44]	N/A	N/A	N/A
[45]	N/A	N/A	N/A
[46]	N/A	N/A	N/A
[47]	N/A	N/A	N/A
[48]	N/A	N/A	N/A
[49]	N/A	N/A	Dantec PIV 2100 processor
[50]	N/A	N/A	N/A
[51]	N/A	N/A	N/A
[52]	N/A	N/A	N/A
[53]	N/A	N/A	N/A
[54]	N/A	N/A	Model 610 032 synchronizer
[55]	N/A	Image processing PC (Intel Pentium III 700 MHz)	N/A
[56]	N/A	N/A	N/A
[57]	N/A	N/A	N/A
[58]	N/A	N/A	N/A
[59]	N/A	N/A	N/A
[60]	N/A	N/A	N/A
[61]	N/A	N/A	N/A
[62]	N/A	N/A	N/A
[63]	N/A	N/A	N/A
[64]	N/A	N/A	N/A
[65]	N/A	N/A	N/A
[66]	N/A	N/A	N/A
[67]	N/A	N/A	N/A
[68]	N/A	N/A	N/A
[69]	N/A	N/A	N/A
[70]	N/A	N/A	N/A
[71]	N/A	N/A	N/A
[72]	N/A	N/A	Synchronizer (TSI model 610 032)
[73]	N/A	N/A	N/A
[74]	N/A	N/A	N/A
[75]	N/A	N/A	N/A
[76]	N/A	N/A	N/A
[77]	N/A	N/A	N/A

(*continued on next page*)

Table 5 (*continued*)

Ref.	Computer brands	Essential features of computers	Synchronizer/controlling unit brands mentioned/given directly in studies
[78]	N/A	N/A	N/A
[79]	N/A	N/A	N/A
[80]	N/A	N/A	N/A
[81]	N/A	N/A	N/A
[82]	N/A	N/A	N/A
[83]	N/A	N/A	N/A
[84]	N/A	N/A	N/A
[85]	N/A	N/A	N/A
[86]	N/A	N/A	N/A
[87]	N/A	N/A	(Lavision PTU8)
[88]	N/A	N/A	N/A
[89]	N/A	N/A	N/A
[90]	N/A	N/A	N/A
[91]	N/A	N/A	N/A
[92]	N/A	N/A	DANTEC PIV 2100 processor
[93]	N/A	N/A	N/A
[94]	N/A	N/A	Lavision programmable timing unit
[95]	Casio Computer	N/A	N/A
[96]	N/A	N/A	N/A
[97]	N/A	N/A	N/A
[98]	N/A	N/A	N/A
[99]	N/A	N/A	N/A
[100]	N/A	N/A	N/A
[101]	N/A	N/A	N/A
[102]	N/A	N/A	N/A
[103]	N/A	N/A	N/A
[104]	N/A	N/A	N/A
[105]	N/A	N/A	N/A
[106]	N/A	N/A	N/A
[107]	N/A	N/A	N/A
[108]	N/A	N/A	N/A
[109]	N/A	N/A	N/A
[110]	N/A	N/A	N/A
[111]	N/A	N/A	N/A
[112]	N/A	N/A	N/A
[113]	N/A	N/A	N/A
[114]	N/A	N/A	N/A
[115]	N/A	N/A	N/A
[116]	N/A	N/A	N/A
[117]	N/A	N/A	N/A
[118]	N/A	N/A	N/A
[119]	N/A	N/A	N/A
[120]	N/A	N/A	BNC 575
[121]	N/A	Computer with 2.4 GHz processor speed and 4 GB RAM	N/A
[122]	N/A	N/A	N/A
[123]	N/A	N/A	N/A
[124]	N/A	N/A	N/A
[125]	N/A	N/A	N/A
[126]	N/A	N/A	N/A
[127]	N/A	N/A	N/A
[128]	N/A	N/A	N/A
[129]	N/A	Computer with Intel Xeon Quad Core processor	N/A
[130]	N/A	N/A	DANTEC, 80N77 synchronizer
[131]	N/A	N/A	N/A
[132]	N/A	N/A	N/A
[133]	N/A	N/A	N/A
[134]	N/A	N/A	N/A
[135]	N/A	N/A	N/A
[136]	N/A	N/A	N/A
[137]	N/A	N/A	Synchronizer LPU1000
[138]	N/A	N/A	N/A
[139]	N/A	N/A	N/A
[140]	N/A	N/A	N/A
[141]	N/A	N/A	N/A
[142]	N/A	N/A	Synchronizer (trigger) type 610 035
[143]	N/A	N/A	ALaserPulseTM computer controlled synchronizer
[144]	N/A	N/A	N/A
[145]	N/A	N/A	N/A

(*continued on next page*)

Table 5 (*continued*)

Ref.	Computer brands	Essential features of computers	Synchronizer/controlling unit brands mentioned/given directly in studies
[146]	N/A	N/A	N/A
[147]	N/A	N/A	N/A
[148]	N/A	N/A	Synchronizer (610 036, TSI Inc., USA)
[149]	N/A	N/A	N/A
[150]	N/A	Ten parallel processors using a 3.10 GHz Intel Xeon CPU E5-2687W v3 with 192.0 GB RAM	Laser Pulse Synchronizer (Model 610 035 TSI) and hall sensor
[151]	N/A	N/A	N/A
[152]	N/A	N/A	BNC 575
[153]	N/A	N/A	N/A
[154]	N/A	N/A	N/A
[155]	N/A	N/A	N/A
[156]	Dell Computer	N/A	N/A
[157]	N/A	N/A	N/A
[158]	N/A	N/A	N/A
[159]	N/A	N/A	N/A
[160]	N/A	N/A	N/A
[161]	N/A	N/A	N/A
[162]	N/A	N/A	N/A
[163]	N/A	N/A	N/A
[164]	N/A	N/A	N/A
[165]	N/A	N/A	N/A
[166]	N/A	N/A	N/A
[167]	N/A	N/A	N/A
[168]	N/A	N/A	N/A
[169]	N/A	N/A	N/A
[170]	N/A	N/A	LaVision high speed controller
[171]	N/A	N/A	N/A
[172]	N/A	N/A	N/A
[173]	N/A	N/A	Programmable timing unit (PTU9, LaVision, GmbH)
[174]	N/A	N/A	N/A

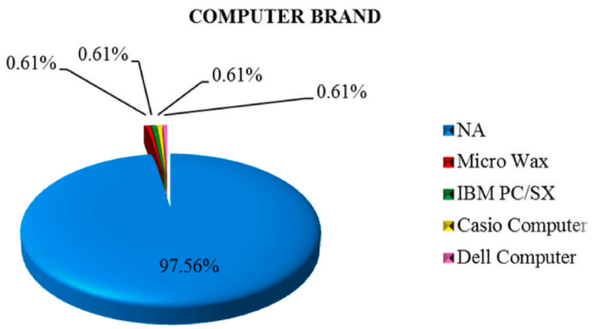

Fig. 26. Computer brands mentioned in PIV studies.

Apart from macro particle image velocimetry or micro particle image velocimetry, nano particle image velocimetry seems to be an interesting research topic [244,245]. Focusing on nano scale particle image velocimetry can be useful [246].

4. Conclusion

In this study; studies of particle image velocimetry exist in open literature from early of the 1990s to present is categorized and explained in detail in terms of its components. Main conclusions of this study are given in below:

With technological developments, recorder hardware develops. Video recorders are used in the early 1990s. Technology did not develop in the past as present. From the 1990s to present, instead of video recorders high-speed cameras become common. High-speed cameras allow recording a lot of images in less time. Especially, TSI and LaVision camera brands are preferred. However, some camera brands may not available now or may have changed their names or stopped producing cameras. Apart from the brands, spatial resolution is another important factor. Therefore, efforts are still continuing in making spatial resolutions greater. CCD cameras have dominance due to spatial resolutions. CMOS cameras have to be improved in terms of spatial resolution. Finally, single cameras show widely usage. Most of PIV studies are performed in two dimensional and two components. Two or three cameras are used but the usage is not as comparable as single camera's.

Pulsed lasers especially Nd: YAG lasers are considerably used. With technological developments, laser technology offers some

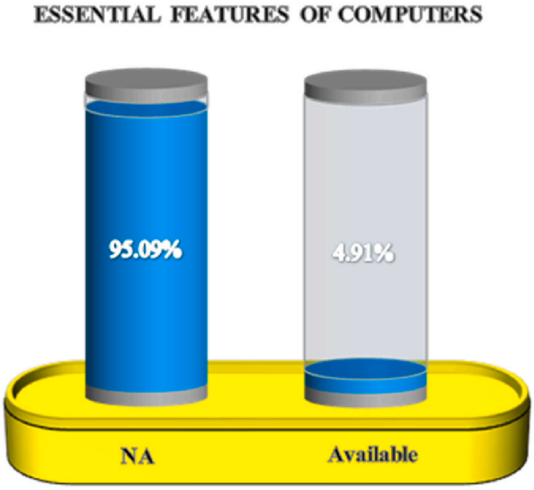

Fig. 27. Essential features of computers.

innovations. Instead of argon-ion and ruby lasers, Nd:YAG lasers become favored in PIV studies. Double pulsed Nd: YAG lasers first. Furthermore, laser sheet thickness change in range of 1–2 mm. Lasers are given with nominal energies instead of maximum energies. Dantec Dynamics lasers are preferred. Some laser brands may have changed their names or had a bankruptcy. Hence, brand percents may change.

Lenses are commonly used components in particle image velocimetry applications with technological developments. Generally, positive focal lengths were chosen. Usage of negative focal lengths in PIV studies can be ignored. Lens apertures strongly affect the depth of field. Apertures must be taken to a certain degree.

Tracer particles are one of the most important components of particle image velocimetry. With the technological developments, micron-scale particle image velocimetry allows the nanoscale particles usage. In macro PIV, micron-scale particles are seeded. In micro PIV, nanoscale particles are seeded. In PIV applications, silver-coated particles and dyed particles have a common usage. Silver-coated particles and dyed particles offer suitable scattering, tracking and dimension respectively. Nylon or metallic particles owing to the heat sensitivity are not used too much. Cells or living organisms are used in biological applications. Homogenous seeding is considered as significant matter. Labelling fluid elements without tracer particles will be very useful for future.

Seeders are components of particle image velocimetry, which supply seeding materials in the experiments. From past to present, seeders developed with technological innovations. So, better seeding and better results can be acquired in particle image velocimetry applications. Adequate and proper seeding is a very significant parameter in PIV. Therefore, seeders have a crucial role in terms of the accuracy of experimental results.

Computers are one of the fundamental components of particle image velocimetry. In the early 1990s, computers weren't used too much. From past to present, computers with high features become common. In the past, image processing and post-processing were harder than today because of computers features. In today, image processing and post-processing are easier with computers. In today, computers with high-speed processors are favored. Especially, workstations are in demand.

Synchronizers are one of the essential components of particle image velocimetry. With technological developments, synchronizers with better features can be used in particle image velocimetry studies. From past to present, TSI synchronizer brand becomes common. The synchronizers are used for making computer, camera and laser work coherently. With the better synchronizers, working of PIV systems becomes better.

High quality components must be acquired due to high level of accuracy and making lower errors. However, the cost should not be disregarded. Components with high quality show some benefits in terms of results, errors and uncertainities.

Robust and reasonable cost with 3D PIV sounds good. 3D micro PIV will be better for micro applications. If the essential improvements are done, particle image velocimetry may be used for all moving things in universe. Also; nano scale PIV may be a reasonable topic for researchers.

Peak locking is one of the hindrances of particle image velocimetry. Particle image diameters of 2 pixel may be a valid solution in order to prevent peak locking. However, particle image diameter larger than 3 pixel may not be reasonable.

Decreasing pulse separation time is not a negligible parameter. Short and efficient pulse separation time is generally wanted in particle image velocimetry applications. Therefore, pulse separation time should be regarded and adjusted sensitively in optimization or application of particle image velocimetry.

Based on examined studies, some suggestions and possible future scenarios are given in below:

- Pumps are significant devices for fluid transport and fluid mechanics. Unsteady flow in pumps should be investigated in three dimensional by using both tomographic PIV and CFD. User defined function (UDF) can be written for three dimensional CFD simulations.

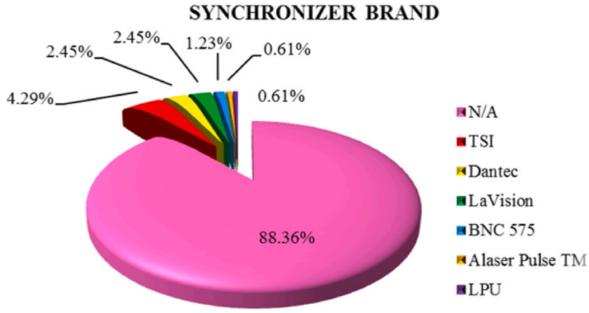

Fig. 28. Synchronizers in studies.

- Fuel cells with hydrogen will be involved in numerous areas in the future. In examined studies, fuel cells are not investigated too much. Instead of real fuel cells in operation, design of prototype channels is investigated. Examining of fuel cells while in operation with PIV is crucial for performance evaluation. In future, real fuel cells in operation should be investigated with PIV by using CO_2 bubbles.
- CFD is a reliable tool for PIV studies and it constitutes a good combination with PIV. Utilization of CFD will be increased in near future. Both CFD and PIV allow a good comparison and validation.
- Heat exchangers are irreplaceable devices for engineering. Based on examined studies, spiral or shell and tube heat exchangers are studied. Pillow plate heat exchangers (PPHE) are not studied with PIV. Pillow plate heat exchangers are used in dairy industry, condensers and coolers. Revealing flow structures of pillow plate heat exchangers with staggered arrangements with 2D PIV or 3D PIV may be an interesting and fruitful research for open literature.
- Typical two dimensional PIV is generally used in studies. However, PIV does not only consist of 2D PIV. Defocusing PIV, holographic PIV, tomographic PIV and particle shadow velocimetry are other types of PIV. In this paper, several PIV studies with different topics and goals are reviewed. We recommend future works performed with defocusing PIV, holographic PIV, tomographic PIV and particle shadow velocimetry.
- Biological applications are also explored in the paper. In general, main fluids are selected with similar viscosity to real blood. Although the use of real blood or cells may seem difficult, it brings a novelty for open literature. PIV should be used for this area.

Author contribution statement

All authors listed have significantly contributed to the development and the writing of this article.

Funding statement

This research did not receive any specific grant from funding agencies in the public, commercial, or not-for-profit sectors.

Data availability statement

No data was used for the research described in the article.

Declaration of interest's statement

The authors declare no conflict of interest.

References

[1] A.K. Prasad, Particle image velocimetry, Curr. Sci. 79 (2000) 51–60.
[2] A. Manz, N. Graber, H.M. Widmer, Miniaturized total chemical analysis systems: a novel concept for chemical sensing, Sensor. Actuator. B Chem. 1 (1–6) (1990) 244–248, https://doi.org/10.1016/0925-4005(90)80209-I.
[3] R.M. Guijt, E. Baltussen, G. van der Steen, R.B.M. Schasfoort, S. Schlautmann, H.A.H. Billiet, et al., New approaches for fabrication of microfluidic capillary electrophoresis devices with on-chip conductivity detection, Electrophoresis 22 (2) (2001) 235–241, https://doi.org/10.1002/1522-2683(200101)22:2<235:AID-ELPS235>3.0.CO;2-O.
[4] M.-P. Yang, Z. Huang, Y. Xie, H. You, Development of microchip electrophoresis and its applications in ion detection, Chin. J. Anal. Chem. 46 (5) (2018) 631–641, https://doi.org/10.1016/S1872-2040(18)61085-0.
[5] M. Raffel, J. Kompenhans, Theoretical and experimental aspects of image-shifting by means of a rotating mirror system for particle image velocimetry, Meas. Sci. Technol. 6 (6) (1995) 795–808, https://doi.org/10.1088/0957-0233/6/6/016.
[6] M. Raffel, C.E. Willert, J. Kompenhans, Particle Image Velocimetry, Springer Berlin Heidelberg, Berlin, Heidelberg, 1998.
[7] M. Raffel, S. Willert, W. Kähler, J. Kompenhans, Particle Image Velocimetry: a Practical Guide, Springer, 2018.
[8] S.M. Sayeed-Bin-Asad, T.S. Lundström, A.G. Andersson, J.G.I. Hellström, A review of particle image velocimetry for fish migration, WJM 6 (4) (2016) 131–149, https://doi.org/10.4236/wjm.2016.64011.
[9] I. Grant, Particle image velocimetry: a review, Proc. IME C J. Mech. Eng. Sci. 211 (1) (1997) 55–76, https://doi.org/10.1243/0954406971521665.

[10] N. Liu, W. Wang, Y. Wang, Z. Wang, J. Han, C. Wu, et al., Comparison of turbulent flow characteristics of liquid-liquid dispersed flow between CFD simulations and direct measurements with particle image velocimetry, Appl. Therm. Eng. 125 (2017) 1209–1217, https://doi.org/10.1016/j.applthermaleng.2017.07.106.
[11] A. Daigle, F. Bérubé, N. Bergeron, P. Matte, A methodology based on Particle image velocimetry for river ice velocity measurement, Cold Reg. Sci. Technol. 89 (2013) 36–47, https://doi.org/10.1016/j.coldregions.2013.01.006.
[12] P. Liu, N. Zheng, L. Rui, F. Shan, Z. Liu, W. Liu, PIV measurement of flow structures in a circular heat exchange tube with central slant rod inserts, Energy Proc. 142 (2017) 3793–3798, https://doi.org/10.1016/j.egypro.2017.12.278.
[13] H. Wang, S. Lee, Y.A. Hassan, Particle image velocimetry measurements of the flow in the converging region of two parallel jets, Nucl. Eng. Des. 306 (2016) 89–97, https://doi.org/10.1016/j.nucengdes.2015.09.032.
[14] F. Chen, H. Liu, Z. Yang, H. Hu, Tracking characteristics of tracer particles for PIV measurements in supersonic flows, Chin. J. Aeronaut. 30 (2) (2017) 577–585, https://doi.org/10.1016/j.cja.2016.12.033.
[15] X. Pan, L. Ding, P. Luo, H. Wu, Z. Zhou, Z. Zhang, LES and PIV investigation of turbulent characteristics in a vessel stirred by a novel long-short blades agitator, Chem. Eng. Sci. 176 (2018) 343–355, https://doi.org/10.1016/j.ces.2017.10.054.
[16] A. Li, C. Yang, T. Ren, X. Bao, E. Qin, R. Gao, PIV experiment and evaluation of air flow performance of swirl diffuser mounted on the floor, Energy Build. 156 (2017) 58–69, https://doi.org/10.1016/j.enbuild.2017.09.045.
[17] M. Jahanmiri, Particle Image Velocimetry: Fundamentals and its Applications, 2011.
[18] A. Etminan, Y.S. Muzychka, K. Pope, B. Nyantekyi-Kwakye, Flow visualization: state-of-the-art development of micro-particle image velocimetry, Meas. Sci. Technol. 33 (9) (2022), 92002, https://doi.org/10.1088/1361-6501/ac75b0.
[19] M. van Helvert, S. Engelhard, J. Voorneveld, M. van der Vee, J.G. Bosch, M. Versluis, et al., High-frame-rate contrast-enhanced ultrasound particle image velocimetry in patients with a stented superficial femoral artery: a feasibility study, Eur. Radiol. Exp. 6 (1) (2022), https://doi.org/10.1186/s41747-022-00278-w.
[20] S.J. Beresh, Time-resolved particle image velocimetry, Meas. Sci. Technol. 32 (10) (2021), 102003, https://doi.org/10.1088/1361-6501/ac08c5.
[21] A. Capone, F. Di Felice, F.A. Pereira, Particle Image Velocimetry measurements in a turbulent channel flow laden with elongated particles, J. Phys.: Conf. Ser. 2293 (1) (2022), 12005, https://doi.org/10.1088/1742-6596/2293/1/012005.
[22] R.J. Adrian, Twenty years of particle image velocimetry, Exp. Fluid 39 (2) (2005) 159–169, https://doi.org/10.1007/s00348-005-0991-7.
[23] M.S. Song, S.H. Park, E.S. Kim, Particle image velocimetry measurements of 2-dimensional velocity field around twisted tape, Fusion Eng. Des. 109–111 (2016) 596–601, https://doi.org/10.1016/j.fusengdes.2016.02.039.
[24] C. Tang, E. Li, H. Li, Particle image velocimetry based on wavelength division multiplexing, Opt Laser. Technol. 98 (2018) 318–325, https://doi.org/10.1016/j.optlastec.2017.08.013.
[25] J. Wen, Y. Li, A. Zhou, Y. Ma, PIV investigations of flow patterns in the entrance configuration of plate-fin heat exchanger, Chin. J. Chem. Eng. 14 (1) (2006) 15–23, https://doi.org/10.1016/S1004-9541(06)60032-3.
[26] A.K. Prasad, R.J. Adrian, C.C. Landreth, P.W. Offutt, Effect of resolution on the speed and accuracy of particle image velocimetry interrogation, Exp. Fluid 13 (2–3) (1992) 105–116, https://doi.org/10.1007/BF00218156.
[27] D. Rockwell, C. Magness, J. Towfighi, O. Akin, T. Corcoran, High image-density particle image velocimetry using laser scanning techniques, Exp. Fluid 14 (3) (1993) 181–192, https://doi.org/10.1007/BF00189509.
[28] A. Brandt, W. Merzkirch, Particle image velocimetry applied to a spray jet, Part. Part. Syst. Char. 11 (2) (1994) 156–158, https://doi.org/10.1002/ppsc.19940110208.
[29] P.J. Bryanston-Cross, T.R. Judge, C. Quan, G. Pugh, N. Corby, The application of digital particle image velocimetry (DPIV) to transonic flows, Prog. Aerosp. Sci. 31 (3) (1995) 273–290, https://doi.org/10.1016/0376-0421(94)00004-5.
[30] K. Jambunathan, X.Y. Ju, B.N. Dobbins, S. Ashforth-Frost, An improved cross correlation technique for particle image velocimetry, Exp. Fluid 6 (5) (1995) 507–514, https://doi.org/10.1088/0957-0233/6/5/012.
[31] C. Gray, C.A. Greated, Evolution of the partial image velocimetry measuring technique, Strain 31 (1) (1995) 3–8, https://doi.org/10.1111/j.1475-1305.1995.tb00948.x.
[32] R.J. Adrian, Dynamic ranges of velocity and spatial resolution of particle image velocimetry, Exp. Fluid 8 (12) (1997) 1393–1398, https://doi.org/10.1088/0957-0233/8/12/003.
[33] A. Melling, Tracer particles and seeding for particle image velocimetry, Exp. Fluid 8 (12) (1997) 1406–1416, https://doi.org/10.1088/0957-0233/8/12/005.
[34] R. Ettema, I. Fujita, M. Muste, A. Kruger, Particle-image velocimetry for whole-field measurement of ice velocities, Cold Reg. Sci. Technol. 26 (2) (1997) 97–112, https://doi.org/10.1016/S0165-232X(97)00011-6.
[35] J.G. Santiago, S.T. Wereley, C.D. Meinhart, D.J. Beebe, R.J. Adrian, A particle image velocimetry system for microfluidics, Exp. Fluid 25 (4) (1998) 316–319, https://doi.org/10.1007/s003480050235.
[36] G.M. Quénot, J. Pakleza, T.A. Kowalewski, Particle image velocimetry with optical flow, Exp. Fluid 25 (3) (1998) 177–189, https://doi.org/10.1007/s003480050222.
[37] C.D. Meinhart, S.T. Wereley, J.G. Santiago, PIV measurements of a microchannel flow, Exp. Fluid 27 (5) (1999) 414–419, https://doi.org/10.1007/s003480050366.
[38] G. Rosengarten, M. Behnia, G. Morrison, Some aspects concerning modelling the flow and heat transfer in horizontal mantle heat exchangers in solar water heaters, Int. J. Energy Res. 23 (11) (1999) 1007–1016, https://doi.org/10.1002/(SICI)1099-114X(199909)23:11<1007:AID-ER537>3.0.CO;2-1.
[39] L.M. Hopkins, J.T. Kelly, A.S. Wexler, A.K. Prasad, Particle image velocimetry measurements in complex geometries, Exp. Fluid 29 (1) (2000) 91–95, https://doi.org/10.1007/s003480050430.
[40] F. Scarano, M.L. Riethmuller, Advances in iterative multigrid PIV image processing, Exp. Fluid 29 (7) (2000) S051–S060, https://doi.org/10.1007/s003480070007.
[41] D.J. Forliti, P.J. Strykowski, K. Debatin, Bias and precision errors of digital particle image velocimetry, Exp. Fluid 28 (5) (2000) 436–447, https://doi.org/10.1007/s003480050403.
[42] K.V. Sharp, R.J. Adrian, PIV study of small-scale flow structure around a Rushton turbine, AIChE J. 47 (4) (2001) 766–778, https://doi.org/10.1002/aic.690470403.
[43] M. Kim, A. Beskok, K. Kihm, Electro-osmosis-driven micro-channel flows: a comparative study of microscopic particle image velocimetry measurements and numerical simulations, Exp. Fluid 33 (1) (2002) 170–180, https://doi.org/10.1007/s00348-002-0449-0.
[44] U. Dierksheide, P. Meyer, T. Hovestadt, W. Hentschel, Endoscopic 2D particle image velocimetry (PIV) flow field measurements in IC engines, Exp. Fluid 33 (6) (2002) 794–800, https://doi.org/10.1007/s00348-002-0499-3.
[45] N.G. Deen, J. Westerweel, E. Delnoij, Two-phase PIV in bubbly flows: status and trends, Chem. Eng. Technol. 25 (1) (2002) 97, https://doi.org/10.1002/1521-4125(200201)25:1<97:AID-CEAT97>3.0.CO;2-7.
[46] S.-H. Cho, I.-S. Lee, J.-H. Choi, Y.-S. Nam, PIV measurement and numerical analysis of a new refrigeration compartment of a refrigerator, Ann. N. Y. Acad. Sci. 972 (2002) 260–264, https://doi.org/10.1111/j.1749-6632.2002.tb04582.x.
[47] Y. Sugii, S. Nishio, K. Okamoto, Measurement of a velocity field in microvessels using a high resolution PIV technique, Ann. N. Y. Acad. Sci. 972 (2002) 331–336, https://doi.org/10.1111/j.1749-6632.2002.tb04592.x.
[48] J. Richard, A. Susset, J.-P. Vantelon, Velocity measurements by particle image velocimetry using a direct intercorrelation algorithm: application to the interaction between a water mist and a liquid pool fire, Ann. N. Y. Acad. Sci. 972 (2002) 229–234, https://doi.org/10.1111/j.1749-6632.2002.tb04577.x.
[49] N.G. Deen, T. Solberg, B.H. Hjertager, Flow generated by an aerated Rushton impeller: two-phase PIV experiments and numerical simulations, Can. J. Chem. Eng. 80 (4) (2002) 1–15, https://doi.org/10.1002/cjce.5450800406.
[50] H.M. Choi, T. Terauchi, H. Monji, G. Matsui, Visualization of bubble-fluid interaction by a moving object flow image analyzer system, Ann. N. Y. Acad. Sci. 972 (2002) 235–241, https://doi.org/10.1111/j.1749-6632.2002.tb04578.x.

[51] H. Hu, T. Saga, T. Kobayashi, N. Taniguchi, Simultaneous velocity and concentration measurements of a turbulent jet mixing flow, Ann. N. Y. Acad. Sci. 972 (2002) 254–259, https://doi.org/10.1111/j.1749-6632.2002.tb04581.x.

[52] R. Bömmels, T. Rösgen, Components for a planar three–component velocimeter using Doppler global velocimetry (DGV) and PIV, Proc. Appl. Math. Mech. 1 (1) (2002) 250, https://doi.org/10.1002/1617-7061(200203)1:1<250:AID-PAMM250>3.0.CO;2-R.

[53] D.J. White, W.A. Take, M.D. Bolton, Soil deformation measurement using particle image velocimetry (PIV) and photogrammetry, Geotechnique 53 (7) (2003) 619–631, https://doi.org/10.1680/geot.53.7.619.37383.

[54] W.Y. Fei, Y.D. Wang, X.Y. Song, Y.D. Yin, L.Y. Sun, Intensification of random packing via CFD simulation, PIV measurement and traditional experiments, J. Chem. Technol. Biotechnol. 78 (2–3) (2003) 142–145, https://doi.org/10.1002/jctb.715.

[55] D. Bröder, M. Sommerfeld, Combined PIV/PTV-Measurements for the analysis of bubble interactions and coalescence in a turbulent flow, Can. J. Chem. Eng. 81 (3–4) (2003) 756–763, https://doi.org/10.1002/cjce.5450810356.

[56] Q. Cao, A.L. Ventresca, K.R. Sreenivas, A.K. Prasad, Instability due to viscosity stratification downstream of a centerline injector, Can. J. Chem. Eng. 81 (5) (2003) 913–922, https://doi.org/10.1002/cjce.5450810501.

[57] F.R. Khan, C.D. Rielly, G.K. Hargrave, A multi-block approach to obtain angle-resolved PIV measurements of the mean flow and turbulence fields in a stirred vessel, Chem. Eng. Technol. 27 (3) (2004) 264–269, https://doi.org/10.1002/ceat.200401998.

[58] J. Kilander, A. Rasmuson, Hydrodynamics in a stirred square tank investigated using a 3-D PIV LES decomposition approach and LDA measurements, Chem. Eng. Technol. 27 (3) (2004) 270–274, https://doi.org/10.1002/ceat.200401983.

[59] M.R. Bown, J.M. MacInnes, R.W.K. Allen, Micro-PIV simulation and measurement in complex microchannel geometries, Exp. Fluid 16 (3) (2005) 619–626, https://doi.org/10.1088/0957-0233/16/3/002.

[60] W. Dezhong, W. Songping, S. Shan, L. Yingzheng, Experimental investigation of turbulent boundary layer flow with surfactant additives using PIV and PDA, Heat Trans. Asian Res. 34 (2) (2005) 99–107, https://doi.org/10.1002/htj.20047.

[61] J. Westerweel, F. Scarano, Universal outlier detection for PIV data, Exp. Fluid 39 (6) (2005) 1096–1100, https://doi.org/10.1007/s00348-005-0016-6.

[62] S.Y. Yoon, J.W. Ross, M.M. Mench, K.V. Sharp, Gas-phase particle image velocimetry (PIV) for application to the design of fuel cell reactant flow channels, J. Power Sources 160 (2) (2006) 1017–1025, https://doi.org/10.1016/j.jpowsour.2006.02.043.

[63] K. Yamamoto, S. Inoue, H. Yamashita, D. Shimokuri, S. Ishizuka, Y. Onuma, PIV measurement and turbulence scale in turbulent combustion, Heat Tran. Asian Res. 35 (7) (2006) 501–512, https://doi.org/10.1002/htj.20129.

[64] M.H. Al-Hajeri, A. Aroussi, K. Simmons, S.J. Pickering, CFD and PIV investigation of flow past a single hot gas filter, Chem. Eng. Technol. 29 (3) (2006) 348–354, https://doi.org/10.1002/ceat.200500048.

[65] M.K. Thet, C.-H. Wang, R.B.H. Tan, Experimental studies of hydrodynamics and regime transition in bubble columns, Can. J. Chem. Eng. 84 (1) (2006) 63–72, https://doi.org/10.1002/cjce.5450840110.

[66] Z.F. Xu, B.C. Khoo, K. Carpenter, Mass transfer across the turbulent gas–water interface, AIChE J. 52 (10) (2006) 3363–3374, https://doi.org/10.1002/aic.10972.

[67] M. Triep, C. Brücker, W. Schröder, T. Siess, Computational fluid dynamics and digital particle image velocimetry study of the flow through an optimized micro-axial blood pump, Artif. Organs 30 (5) (2006) 384–391, https://doi.org/10.1111/j.1525-1594.2006.00230.x.

[68] F.-W. Bach, K. Möhwald, T. Rothardt, J. Prehm, L. Engl, K. Hartz, et al., Particle image velocimetry in thermal spraying, Adv. Eng. Mater. 8 (7) (2006) 650–653.

[69] H. Güler, H. Zhu, E. Ozkan, R. Derksen, C. Krause, Sürüklenme Azaltıcı Katkıların Yüksek Çalışma basınçlarında Sürüklenme Potansiyellerinin Ve Püskürtme Karakteristiklerinin Rüzgar Tünelinde belirlenmesi, Tarım Makinaları Bilimi Dergisi 3 (2007) 73–80.

[70] W. Dijkhuizen, G.A. Bokkers, N.G. Deen, M.S. van Annaland, J.A.M. Kuipers, Extension of PIV for measuring granular temperature field in dense fluidized beds, AIChE J. 53 (1) (2007) 108–118, https://doi.org/10.1002/aic.11044.

[71] B. Wieneke, Volume self-calibration for 3D particle image velocimetry, Exp. Fluid 45 (4) (2008) 549–556, https://doi.org/10.1007/s00348-008-0521-5.

[72] R.J. Santos, E. Erkoç, M.M. Dias, A.M. Teixeira, J.C.B. Lopes, Hydrodynamics of the mixing chamber in RIM: PIV flow-field characterization, AIChE J. 54 (5) (2008) 1153–1163, https://doi.org/10.1002/aic.11472.

[73] N. Dietrich, S. Poncin, S. Pheulpin, H.Z. Li, Passage of a bubble through a liquid–liquid interface, AIChE J. 54 (3) (2008) 594–600, https://doi.org/10.1002/aic.11399.

[74] E. Andersen, S. Furbo, M. Hampel, W. Heidemann, H. Müller-Steinhagen, Investigations on stratification devices for hot water heat stores, Int. J. Energy Res. 32 (3) (2008) 255–263, https://doi.org/10.1002/er.1345.

[75] M. Rodriguez Pascual, F. Ravelet, R. Delfos, J.J. Derksen, G.J. Witkamp, Large eddy simulations and stereoscopic particle image velocimetry measurements in a scraped heat exchanger crystallizer geometry, Chem. Eng. Sci. 64 (9) (2009) 2127–2135, https://doi.org/10.1016/j.ces.2009.01.034.

[76] S.S. Deshpande, M.J. Sathe, J.B. Joshi, Evaluation of local turbulent energy dissipation rate using PIV in jet loop reactor, Ind. Eng. Chem. Res. 48 (10) (2009) 5046–5057, https://doi.org/10.1021/ie8007924.

[77] C.R. Müller, G. Hartung, J. Hult, J.S. Dennis, C.F. Kaminski, Laser diagnostic investigation of the bubble eruption patterns in the freeboard of fluidized beds: simultaneous acetone PLIF and stereoscopic PIV measurements, AIChE J. 55 (6) (2009) 1369–1382, https://doi.org/10.1002/aic.11802.

[78] B.O. Olayiwola, G. Schaldach, P. Walzel, Average crossflow velocity in laminar flow systems with periodic finned surfaces, Chem. Eng. Technol. 32 (10) (2009) 1605–1616, https://doi.org/10.1002/ceat.200800507.

[79] Körbahti B. Sesalti akış Etkisindeki delta Kanadin deneysel Olarak İncelenmesi. İstanbul Üniversitesi Mühendislik Bilimleri Dergisi;1:33–44.

[80] S. Yayla, C. Canpolat, B. Sahin, H. Akilli, Elmas kanat Modelinde Oluşan Girdap Çökmesine Sapma Açısının etkisi, J. Therm. Sci. Technol. (2010) 79–89.

[81] F. Guo, B. Chen, L. Guo, X. Zhang, Investigation of turbulent mixing layer flow in a vertical water channel by particle image velocimetry (PIV), Can. J. Chem. Eng. 88 (6) (2010) 919–928, https://doi.org/10.1002/cjce.20355.

[82] L. Ragnarsson, W. Song, Y. Ma, D. Sichen, Oxygen penetration in the Protection shroud in steel Casting, Steel Res. Int. 81 (11) (2010) 965–973, https://doi.org/10.1002/srin.201000088.

[83] J.R. Cooper, S.J. Tait, Examining the physical components of boundary shear stress for water-worked gravel deposits, Earth Surf. Process. Landforms 35 (10) (2010) 1240–1246, https://doi.org/10.1002/esp.2020.

[84] M. Nordlund, T.S. Lundström, An investigation of particle deposition mechanisms during impregnation of dual-scale fabrics with Micro Particle Image Velocimetry, Polym. Compos. 38 (3) (2009), https://doi.org/10.1002/pc.20910. NA-NA.

[85] A. Oner, M. Cobaner, S. Kırkgöz, Aköz, M. Sami, Yatay bir dairesel silindir etrafındaki akımda maksimum hızın yapay sinir ağları ile tahmini, Erciyes Üniversitesi Fen Bilimleri Enstitüsü Dergisi 26 (1) (2010) 63–70.

[86] D. Mgharaz, N. Rouchdi, A. Boulezhar, M. Brunel, Double-clad fiber laser design for particle image velocimetry and material science applications, Opt Laser. Eng. 49 (1) (2011) 1–7, https://doi.org/10.1016/j.optlaseng.2010.08.015.

[87] D. Ragni, F. Schrijer, B.W. van Oudheusden, F. Scarano, Particle tracer response across shocks measured by PIV, Exp. Fluid 50 (1) (2011) 53–64, https://doi.org/10.1007/s00348-010-0892-2.

[88] S-i Satake, G. Sorimachi, N. Masuda, T. Ito, Special-purpose computer for particle image velocimetry, Comput. Phys. Commun. 182 (5) (2011) 1178–1182, https://doi.org/10.1016/j.cpc.2011.01.022.

[89] M. Umeyama, S. Matsuki, Measurements of velocity and trajectory of water particle for internal waves in two density layers, Geophys. Res. Lett. 38 (3) (2011), https://doi.org/10.1029/2010GL046419 n/a-n/a.

[90] T.M. Green, E.M. Lindmark, T.S. Lundström, L.H. Gustavsson, Flow characterization of an attraction channel as entrance to fishways, River Res. Appl. 27 (10) (2011) 1290–1297, https://doi.org/10.1002/rra.1426.

[91] C.J. Kähler, S. Scharnowski, C. Cierpka, On the resolution limit of digital particle image velocimetry, Exp. Fluid 52 (6) (2012) 1629–1639, https://doi.org/10.1007/s00348-012-1280-x.

[92] A. Kürekci, O. Ozcan, An experimental and numerical study of laminar natural convection in a differentially-heated cubical enclosure, J. Heat Sci. Technol. 32 (1) (2012) 1–8.
[93] A. Figueredo-Cardero, E. Chico, L. Castilho, R de Andrade Medronho, Particle image velocimetry (PIV) study of rotating cylindrical filters for animal cell perfusion processes, Biotechnol. Prog. 28 (6) (2012) 1491–1498, https://doi.org/10.1002/btpr.1618.
[94] H. El-Gendy, M. Alcoutlabi, M. Jemmett, M. Deo, J. Magda, R. Venkatesan, et al., The propagation of pressure in a gelled waxy oil pipeline as studied by particle imaging velocimetry, AIChE J. 58 (1) (2012) 302–311, https://doi.org/10.1002/aic.12560.
[95] W.G. Ryerson, K. Schwenk, A simple, inexpensive system for digital particle image velocimetry (DPIV) in biomechanics, J. Exp. Zool. Ecol. Genet. Physiol. 317 (2) (2012) 127–140, https://doi.org/10.1002/jez.725.
[96] J.V. Simo Tala, S. Russeil, D. Bougeard, J.-L. Harion, Investigation of the flow characteristics in a multirow finned-tube heat exchanger model by means of PIV measurements, Exp. Therm. Fluid Sci. 50 (2013) 45–53, https://doi.org/10.1016/j.expthermflusci.2013.05.003.
[97] R. Atibeni, Z. Gao, Y. Bao, Effect of baffles on fluid flow field in stirred tank with floating particles by using PIV, Can. J. Chem. Eng. 91 (3) (2013) 570–578, https://doi.org/10.1002/cjce.21652.
[98] S.Y. Jung, H.W. Park, B.H. Kim, S.J. Lee, Time-resolved X-ray PIV technique for diagnosing opaque biofluid flow with insufficient X-ray fluxes, J. Synchrotron Radiat. 20 (Pt 3) (2013) 498–503, https://doi.org/10.1107/S0909049513001933.
[99] Y. Hayasaka, M. Nagai, N. Matsumoto, T. Kawashima, T. Shibata, Flow field analysis of Micromixer powered by Ciliary motion of vorticella, Trans. IEE Jpn. 132 (3) (2012) 58–63, https://doi.org/10.1541/ieejsmas.132.58.
[100] W. Weheliye, M. Yianneskis, A. Ducci, On the fluid dynamics of shaken bioreactors- flow characterization and transition, AIChE J. 59 (1) (2013) 334–344, https://doi.org/10.1002/aic.13943.
[101] T. Fujimura, M. Hotta, A novel method to investigate the relationship between facial movements and wrinkle formation using particle image velocimetry, Skin Res. Technol. 19 (1) (2013) e54–e59, https://doi.org/10.1111/j.1600-0846.2011.00607.x.
[102] M.M. Hoque, M.J. Sathe, J.B. Joshi, G.M. Evans, Analysis of turbulence energy spectrum by using particle image velocimetry, Procedia Eng. 90 (2014) 320–326, https://doi.org/10.1016/j.proeng.2014.11.856.
[103] M. Muste, A. Hauet, I. Fujita, C. Legout, H.-C. Ho, Capabilities of large-scale particle image velocimetry to characterize shallow free-surface flows, Adv. Water Resour. 70 (2014) 160–171, https://doi.org/10.1016/j.advwatres.2014.04.004.
[104] J. Keller, G. Möller, R.M. Boes, PIV measurements of air-core intake vortices, Flow Meas. Instrum. 40 (2014) 74–81, https://doi.org/10.1016/j.flowmeasinst.2014.08.004.
[105] M.A. Akar, M. Kücük, Silindir arkasındaki daimi olmayan akış yapısının pasif yöntemle kontrolü, Pamukkale Üniversitesi Mühendislik Bilimleri Dergisi 20 (2014) 123–128.
[106] N.G. Soydan, S. Aköz, O. Şimşek, S. Kırkgöz, Tabana Oturan Yatay Bir Boru Etrafindaki Türbülansli Akimin Deneysel Ve Sayisal Analizi. 8, Kıyı Mühendisliği Sempozyumu, 2014, pp. 999–1010.
[107] Y.-P. Liu, P.-Y. Wang, X.-L. Zhao, Z.-H. Du, Study on the flow structure and its effects on the interaction and formation of cryogenic taylor bubbles by PIV technique and POD analysis, Can. J. Chem. Eng. 92 (2) (2014) 374–389, https://doi.org/10.1002/cjce.21810.
[108] R.K. Decker, M.C. Betto, D. Noriler, H.F. Meier, Comparison between numerical results and PIV experimental data for gas-solid flow in ducts, Can. J. Chem. Eng. 92 (6) (2014) 1113–1120, https://doi.org/10.1002/cjce.21952.
[109] S.K. Pawar, R.H.M. Abrahams, N.G. Deen, J.T. Padding, G.-J. van der Gulik, A. Jongsma, et al., An experimental study of dynamic jet behaviour in a scaled cold flow spray dryer model using PIV, Can. J. Chem. Eng. 92 (12) (2014) 2013–2020, https://doi.org/10.1002/cjce.22065.
[110] H.J. Salem, M.D. Martinez, R.W. Gooding, J.A. Olson, Experimental study of a time-varying turbulent cross-flow near a two-dimensional rough wall with narrow apertures, Can. J. Chem. Eng. 92 (11) (2014) 1965–1974, https://doi.org/10.1002/cjce.22058.
[111] V. del Campo, D. Ragni, D. Micallef, B. Akay, F.J. Diez, C. Simão Ferreira, 3D load estimation on a horizontal axis wind turbine using SPIV, Wind Energy 17 (11) (2014) 1645–1657, https://doi.org/10.1002/we.1658.
[112] F. Karakaş, O. Paça, C. Köse, O. Son, B. Zaloğlu, Fenercioğlu, et al., Çirpan kanatta kanat profilinin etkisi, J. Aeronaut. Space Technol. 7 (2) (2014) 1240, https://doi.org/10.7603/s40690-014-0015-z.
[113] W. Hongwei, H. Zhan, G. Jian, X. Hongliang, The optical flow method research of particle image velocimetry, Procedia Eng. 99 (2015) 918–924, https://doi.org/10.1016/j.proeng.2014.12.622.
[114] A. Sergis, Y. Hardalupas, T.R. Barrett, Isothermal velocity measurements in two HyperVapotron geometries using Particle Image Velocimetry (PIV), Exp. Therm. Fluid Sci. 61 (2015) 48–58, https://doi.org/10.1016/j.expthermflusci.2014.10.003.
[115] A. Vali, D.S. Nobes, L.W. Kostiuk, Characterization of flow field within the liquid phase of a small pool fire using particle image velocimetry technique, Exp. Therm. Fluid Sci. 75 (2016) 228–234, https://doi.org/10.1016/j.expthermflusci.2016.02.012.
[116] E. Keramaris, Similarities and differences between hot-film anemometry and particle image velocimetry in open channels, Procedia Eng. 162 (2016) 388–395, https://doi.org/10.1016/j.proeng.2016.11.079.
[117] S. Fu, P.H. Biwole, C. Mathis, Numerical and experimental comparison of 3D particle tracking velocimetry (PTV) and particle image velocimetry (PIV) accuracy for indoor airflow study, Build. Environ. 100 (2016) 40–49, https://doi.org/10.1016/j.buildenv.2016.02.002.
[118] P. Mühlich, W. Case, J. Hörmansperger, M. Beyrer, E.J. Windhab, Particle image velocimetry (PIV) in food powders during vacuum-steam-vacuum (VSV) treatment, Powder Technol. 299 (2016) 1–8, https://doi.org/10.1016/j.powtec.2016.04.041.
[119] N.A. Ozturk, C. Ozalp, C. Canpolat, B. Sahin, PIV measurements of flow through normal triangular cylinder arrays in the passage of a model plate-tube heat exchanger, Int. J. Heat Fluid Flow 61 (2016) 531–544, https://doi.org/10.1016/j.ijheatfluidflow.2016.06.013.
[120] O.T. Tunçer, S.K. Kahraman, B.K. Kaynaroğlu, Girdap Vanesinden Geçen Akişin Piv Yöntemi İle İncelenmesi, Gazi Üniversitesi Mühendislik-Mimarlık Fakültesi Dergisi 31 (4) (2016), https://doi.org/10.17341/gazimmfd.278439.
[121] A.A. Oner, Geçirimsiz bir taban Yakınındaki başlıklı bir boru Hattı etrafındaki Akımın deneysel ve Sayısal Olarak İncelenmesi, Electron. J. Constr. Technol. 12 (1) (2016) 40–54.
[122] B. Ruonan, C. Liekai, W. Xingkui, L. Danxun, Comparison of ADV and PIV measurements in open channel flows, Procedia Eng. 154 (2016) 995–1001, https://doi.org/10.1016/j.proeng.2016.07.588.
[123] S. Im, H.T. Kim, B.W. Rhee, H.J. Sung, PIV measurements of the flow patterns in a CANDU-6 model, Ann. Nucl. Energy 98 (2016) 1–11, https://doi.org/10.1016/j.anucene.2016.07.012.
[124] Y. Oguma, N. Fujisawa, Sound source measurement of a semi-circular cylinder in a uniform flow by particle image velocimetry, JFCMV 4 (4) (2016) 162–170, https://doi.org/10.4236/jfcmv.2016.44014.
[125] B. Oğuz, M.A. Akar, E. Pınar, H. Akıllı, B. Şahin, Control of flow structure in the wake region of circular cylinder with meshy wire in deep water, Pamukkale J. Eng. Sci. 22 (4) (2016) 280–284, https://doi.org/10.5505/pajes.2016.41033.
[126] T. Ziegenhein, D. Lucas, On sampling bias in multiphase flows: particle image velocimetry in bubbly flows, Flow Meas. Instrum. 48 (2016) 36–41, https://doi.org/10.1016/j.flowmeasinst.2016.02.003.
[127] E. Fleischhauer, F. Azimi, P. Tkacik, R. Keanini, B. Mullany, Application of particle image velocimetry (PIV) to vibrational finishing, J. Mater. Process. Technol. 229 (2016) 322–328, https://doi.org/10.1016/j.jmatprotec.2015.09.017.
[128] L. Cristofano, M. Nobili, G.P. Romano, G. Caruso, Investigation on bathtub vortex flow field by Particle Image Velocimetry, Exp. Therm. Fluid Sci. 74 (2016) 130–142, https://doi.org/10.1016/j.expthermflusci.2015.12.005.
[129] M. Dogan, Atilla Igci, Abir, Visualization of the flow with PIV in rectangular channels, Electron. Lett. Sci. Eng. 12 (3) (2016) 1–10.
[130] G. Boutin, M. Wei, Y. Fan, L. Luo, Experimental measurement of flow distribution in a parallel mini-channel fluidic network using PIV technique, Asia Pac. J. Chem. Eng. 11 (4) (2016) 630–641, https://doi.org/10.1002/apj.2013.
[131] C. Kirmse, H. Chaves, Measurements of the velocity of drops in a melt atomization process using particle image velocimetry, Steel Res. Int. 87 (10) (2016) 1295–1301, https://doi.org/10.1002/srin.201500360.

[132] M.A. Atar, O. Baş, M. Küçük, Altıgen delikli Silindirin Geçirgenlik Oranının silindir arkasındaki akış bölgesine etkisi, Çukurova Üniversitesi Mühendislik-Mimarlık Fakültesi Dergisi 31 (ÖS2) (2016) 79–86, https://doi.org/10.21605/cukurovaummfd.315876.
[133] J. Gong, C-y Guo, T-c Wu, D-g Zhao, Particle image velocimetry measurement of velocity distribution at inlet duct of waterjet self-propelled ship model, J. Hydrodyn. 29 (5) (2017) 879–893, https://doi.org/10.1016/S1001-6058(16)60800-4.
[134] G. Hu, K.T. Tse, Z.S. Chen, K.C.S. Kwok, Particle Image Velocimetry measurement of flow around an inclined square cylinder, J. Wind Eng. Ind. Aerod. 168 (2017) 134–140, https://doi.org/10.1016/j.jweia.2017.06.001.
[135] K. Kurec, J. Piechna, K. Gumowski, Investigations on unsteady flow within a stationary passage of a pressure wave exchanger, by means of PIV measurements and CFD calculations, Appl. Therm. Eng. 112 (2017) 610–620, https://doi.org/10.1016/j.applthermaleng.2016.10.142.
[136] R. Shokri, S. Ghaemi, D.S. Nobes, R.S. Sanders, Investigation of particle-laden turbulent pipe flow at high-Reynolds-number using particle image/tracking velocimetry (PIV/PTV), Int. J. Multiphas. Flow 89 (2017) 136–149, https://doi.org/10.1016/j.ijmultiphaseflow.2016.06.023.
[137] J. Wen, H. Yang, S. Wang, X. Gu, PIV experimental investigation on shell-side flow patterns of shell and tube heat exchanger with different helical baffles, Int. J. Heat Mass Transfer 104 (2017) 247–259, https://doi.org/10.1016/j.ijheatmasstransfer.2016.08.048.
[138] T. Mitchell Ferguson, I. Penesis, G. Macfarlane, A. Fleming, A PIV investigation of OWC operation in regular, polychromatic and irregular waves, Renew. Energy 103 (2017) 143–155, https://doi.org/10.1016/j.renene.2016.11.019.
[139] M. Ismail, F. Kabinejadian, Y.N. Nguyen, E. Tay Lik Wui, S. Kim, H.L. Leo, Hemodynamic assessment of extra-cardiac tricuspid valves using particle image velocimetry, Med. Eng. Phys. 50 (2017) 1–11, https://doi.org/10.1016/j.medengphy.2017.08.003.
[140] A. Patalano, C.M. García, A. Rodríguez, Rectification of image velocity results (RIVeR): a simple and user-friendly toolbox for large scale water surface particle image velocimetry (PIV) and particle tracking velocimetry (PTV), Comput. Geosci. 109 (2017) 323–330, https://doi.org/10.1016/j.cageo.2017.07.009.
[141] C. Gürlek, Experimental investigation of the channel flow equipped with rectangular obstacles by means of PIV method, Cumhuriyet Sci. J. 38 (2) (2017) 293, https://doi.org/10.17776/cumuscij.295476.
[142] Y. Jiang, H. Li, Q. Xiang, C. Chen, Comparison of PIV experiment and numerical simulation on the velocity distribution of intermediate pressure jets with different nozzle parameters, Irrigat. Drain. 66 (4) (2017) 510–519, https://doi.org/10.1002/ird.2133.
[143] J.M.D. Thomas, A. Chakraborty, R.E. Berson, M. Shakeri, M.K. Sharp, Validation of a CFD model of an orbiting culture dish with PIV and analytical solutions, AIChE J. 63 (9) (2017) 4233–4242, https://doi.org/10.1002/aic.15762.
[144] Y. Zhang, M. Yang, D. Ni, N. Zhang, B. Gao, Particle image velocimetry measurement of complex flow structures in the diffuser and spherical casing of a reactor coolant pump, Nucl. Eng. Technol. 50 (3) (2018) 368–378, https://doi.org/10.1016/j.net.2017.12.012.
[145] R. Goyal, B.K. Gandhi, M.J. Cervantes, PIV measurements in Francis turbine – a review and application to transient operations, Renew. Sustain. Energy Rev. 81 (2018) 2976–2991, https://doi.org/10.1016/j.rser.2017.06.108.
[146] X. Xie, C. Le Men, N. Dietrich, P. Schmitz, L. Fillaudeau, Local hydrodynamic investigation by PIV and CFD within a Dynamic filtration unit under laminar flow, Sep. Purif. Technol. 198 (2018) 38–51, https://doi.org/10.1016/j.seppur.2017.04.009.
[147] N. Zhang, B. Gao, Z. Li, D. Ni, Q. Jiang, Unsteady flow structure and its evolution in a low specific speed centrifugal pump measured by PIV, Exp. Therm. Fluid Sci. 97 (2018) 133–144, https://doi.org/10.1016/j.expthermflusci.2018.04.013.
[148] C.J.U. Espinoza, M.J.H. Simmons, F. Alberini, O. Mihailova, D. Rothman, A.J. Kowalski, Flow studies in an in-line Silverson 150/250 high shear mixer using PIV, Chem. Eng. Res. Des. 132 (2018) 989–1004, https://doi.org/10.1016/j.cherd.2018.01.028.
[149] A.H. Haidari, S.G.J. Heijman, W.G.J. van der Meer, Effect of spacer configuration on hydraulic conditions using PIV, Sep. Purif. Technol. 199 (2018) 9–19, https://doi.org/10.1016/j.seppur.2018.01.022.
[150] M. Cortada-Garcia, W.H. Weheliye, V. Dore, L. Mazzei, P. Angeli, Computational fluid dynamic studies of mixers for highly viscous shear thinning fluids and PIV validation, Chem. Eng. Sci. 179 (2018) 133–149, https://doi.org/10.1016/j.ces.2018.01.010.
[151] S. Yayla, S. Teksin, Flow measurement around a cylindrical body by attaching flexible plate: a PIV approach, Flow Meas. Instrum. 62 (2018) 56–65, https://doi.org/10.1016/j.flowmeasinst.2018.05.003.
[152] S.V. Alekseenko, S.S. Abdurakipov, M.Y. Hrebtov, M.P. Tokarev, V.M. Dulin, D.M. Markovich, Coherent structures in the near-field of swirling turbulent jets: a tomographic PIV study, Int. J. Heat Fluid Flow 70 (2018) 363–379, https://doi.org/10.1016/j.ijheatfluidflow.2017.12.009.
[153] F. Chen, H. Liu, Particle image velocimetry for combustion measurements: applications and developments, Chin. J. Aeronaut. 31 (7) (2018) 1407–1427, https://doi.org/10.1016/j.cja.2018.05.010.
[154] T. Durhasan, E. Pinar, G.M. Ozkan, M.M. Aksoy, H. Akilli, B. Sahin, PIV measurement downstream of perforated cylinder in deep water, Eur. J. Mech. B Fluid 72 (2018) 225–234, https://doi.org/10.1016/j.euromechflu.2018.06.001.
[155] M. Riccomi, F. Alberini, E. Brunazzi, D. Vigolo, Ghost Particle Velocimetry as an alternative to μPIV for micro/milli-fluidic devices, Chem. Eng. Res. Des. 133 (2018) 183–194, https://doi.org/10.1016/j.cherd.2018.03.005.
[156] W. Sun, N. Huang, A study on velocity of aeolian sand particles over leeward slope by particle image velocimetry, Geomorphology 317 (2018) 157–169, https://doi.org/10.1016/j.geomorph.2018.05.024.
[157] K. Liu, J. Deng, F. Ye, Visualization of flow structures in a rotary type energy recovery device by PIV experiments, Desalination 433 (2018) 33–40, https://doi.org/10.1016/j.desal.2018.01.022.
[158] R. You, H. Li, H. Wu, Z. Tao, PIV flow measurements for a rotating square smooth channel heated by basically uniform heat flux, Int. J. Heat Mass Transfer 119 (2018) 236–246, https://doi.org/10.1016/j.ijheatmasstransfer.2017.11.073.
[159] Y. Hu, J. Wu, S. Poncin, Z. Cao, Z. Li, H.Z. Li, Flow field investigation of high solid anaerobic digestion by Particle Image Velocimetry (PIV), Sci. Total Environ. 626 (2018) 592–602, https://doi.org/10.1016/j.scitotenv.2018.01.111.
[160] H. Akıllı, M.A. Akar, O. Baş, B. Oğuz, E. Pınar, B. Şahin, The effect of the splitter plates on flow characteristics that are vertically placed to the flow between side by side cylinders in shallow water, Pamukkale J. Eng. Sci. 24 (4) (2018) 582–585, https://doi.org/10.5505/pajes.2017.43007.
[161] H. Park, S.Y. Jung, J.H. Park, J.H. Kim, S.J. Lee, Enhancement of measurement accuracy of X-ray PIV in comparison with the micro-PIV technique, J. Synchrotron Radiat. 25 (Pt 2) (2018) 552–559, https://doi.org/10.1107/S1600577517017398.
[162] C. Wang, Y. Xu, Y. Wu, Z. An, PIV investigation of the flow features of double and single 45° up-pumping pitched blade turbines in a square tank, Can. J. Chem. Eng. 96 (3) (2018) 788–799, https://doi.org/10.1002/cjce.22952.
[163] H. Miyashita, Y. Ehara, T. Thunoda, J. Enomoto, T. Inui, PIV analysis of particle behavior in Electrostatic Precipitator, IEE J. Trans. FM 136 (12) (2016) 797–803, https://doi.org/10.1541/ieejfms.136.797.
[164] S.E. Yalcin, E.Y. Yakin, M.C. Kushan, T.H. Karakoc, Jet Motorlarinda Uygulanan Efüzyon film Soğutma Akiş Karakteristiklerinin PIV Yöntemiyle İncelenmesi, Sustain. Aviation Res. Soc. 3 (2) (2018) 55–62.
[165] S. Doğan, M. Özgören, A. Okbaz, B. Şahin, H. Akıllı, Serbest yüzey ve bir küre art izi arasındaki etkileşimlerin araştırılması, Gazi Üniversitesi Mühendislik-Mimarlık Fakültesi Dergisi (2018) 1123–1134, https://doi.org/10.17341/gazimmfd.453552.
[166] E.L. Loboda, I.S. Anufriev, M.V. Agafontsev, E.P. Kopyev, E.Y. Shadrin, V.V. Reyno, et al., Evaluating characteristics of turbulent flames by using IR thermography and PIV, Infrared Phys. Technol. 92 (2018) 240–243, https://doi.org/10.1016/j.infrared.2018.06.006.
[167] M. Banaei, R. Dellaert, N.G. Deen, J.A.M. Kuipers, M. van Sint Annaland, Borescopic particle image velocimetry in bubbling gas–solid fluidized beds, Particuology 43 (2019) 66–75, https://doi.org/10.1016/j.partic.2018.01.012.
[168] K. Vaagsaether, A.V. Gaathaug, D. Bjerketvedt, PIV-measurements of reactant flow in hydrogen-air explosions, Int. J. Hydrogen Energy 44 (17) (2019) 8799–8806, https://doi.org/10.1016/j.ijhydene.2018.10.025.
[169] R.G. González-Acuña, A. Dávila, J.C. Gutiérrez-Vega, Optical flow of non-integer order in particle image velocimetry techniques, Signal Process. 155 (2019) 317–322, https://doi.org/10.1016/j.sigpro.2018.10.006.
[170] A.J. Head, M. Novara, M. Gallo, F. Schrijer, P. Colonna, Feasibility of particle image velocimetry for low-speed unconventional vapor flows, Exp. Therm. Fluid Sci. 102 (2019) 589–594, https://doi.org/10.1016/j.expthermflusci.2018.10.028.

[171] Q. Wu, C-a Zhu, L. Liu, J. Liu, Z. Luo, Two-dimensional flow visualization and velocity measurement in natural convection near indoor heated surfaces using a thermal image velocimetry method, Appl. Therm. Eng. 146 (2019) 556–568, https://doi.org/10.1016/j.applthermaleng.2018.10.023.
[172] J. Kluska, K. Ronewicz, D. Kardaś, Thermal characteristics of single wood particle pyrolysis using particle image velocimetry, Int. J. Therm. Sci. 135 (2019) 276–284, https://doi.org/10.1016/j.ijthermalsci.2018.09.020.
[173] F. Ahmadi, M. Ebrahimian, R.S. Sanders, S. Ghaemi, Particle image and tracking velocimetry of solid-liquid turbulence in a horizontal channel flow, Int. J. Multiphase Flow 112 (2019) 83–99, https://doi.org/10.1016/j.ijmultiphaseflow.2018.12.007.
[174] R. Bardera, M.A. Barcala-Montejano, A.A. Rodríguez-Sevillano, M. León-Calero, Conical vortices investigation and mitigation over the ski-jump ramp of an aircraft carrier by PIV, Ocean Eng. 173 (2019) 672–676, https://doi.org/10.1016/j.oceaneng.2019.01.032.
[175] N. Yilmaz, R.E. Lucero, A.B. Donaldson, W. Gill, Flow characterization of diffusion flame oscillations using particle image velocimetry, Exp. Fluid 46 (4) (2009) 737–746, https://doi.org/10.1007/s00348-008-0605-2.
[176] N. Yilmaz, A.B. Donaldson, W. Gill, R.E. Lucero, Imaging of flame behavior in flickering methane/air diffusion flames, J. Vis. 12 (1) (2009) 47–55, https://doi.org/10.1007/BF03181942.
[177] C. Di Cristo, Particle imaging velocimetry and its applications in hydraulics: a state-of-the-art review, in: P. Rowinski (Ed.), Experimental Methods in Hydraulic Research, Springer Berlin Heidelberg, Berlin, Heidelberg, 2011, pp. 49–66.
[178] Q. Gao, H. Wang, G. Shen, Review on development of volumetric particle image velocimetry, Chin. Sci. Bull. 58 (36) (2013) 4541–4556, https://doi.org/10.1007/s11434-013-6081-y.
[179] G.E. Elsinga, F. Scarano, B. Wieneke, B.W. van Oudheusden, Tomographic particle image velocimetry, Exp. Fluid 41 (6) (2006) 933–947, https://doi.org/10.1007/s00348-006-0212-z.
[180] H. Tu, F. Wang, H. Wang, Q. Gao, R. Wei, Experimental study on wake flows of a live fish with time-resolved tomographic PIV and pressure reconstruction, Exp. Fluid 63 (1) (2022) 943, https://doi.org/10.1007/s00348-021-03378-2.
[181] E. Baum, B. Peterson, C. Surmann, D. Michaelis, B. Böhm, A. Dreizler, Investigation of the 3D flow field in an IC engine using tomographic PIV, Proc. Combust. Inst. 34 (2) (2013) 2903–2910, https://doi.org/10.1016/j.proci.2012.06.123.
[182] D. Ragni, D. Fiscaletti, W.J. Baars, Jet noise predictions by time marching of single-snapshot tomographic PIV fields, Exp. Fluid 63 (5) (2022) 44, https://doi.org/10.1007/s00348-022-03436-3.
[183] Y. Song, R. Xu, Y. Song, Y. Long, J. Yin, D. Wang, Hydrodynamics characteristics of non-uniform inflow in reactor coolant pump based on time-resolved tomographic particle image velocimetry, Phys. Fluids 34 (12) (2022), 125132, https://doi.org/10.1063/5.0130228.
[184] Y. Zhao, X. Ma, C. Zhang, H. Wang, Y. Zhang, 3D real-time volumetric particle tracking velocimetry – a promising tool for studies of airflow around high-rise buildings, Build. Environ. 178 (10) (2020), 106930, https://doi.org/10.1016/j.buildenv.2020.106930.
[185] H.G. Maas, A. Gruen, D. Papantoniou, Particle tracking velocimetry in three-dimensional flows, Exp. Fluid 15 (2) (1993) 133–146, https://doi.org/10.1007/BF00190953.
[186] H.-G. Maas, T. Putze, P. Westfeld, Recent developments in 3D-PTV and Tomo-PIV, in: E.H. Hirschel, W. Schröder, K. Fujii, W. Haase, B. Leer, M.A. Leschziner, et al. (Eds.), Imaging Measurement Methods for Flow Analysis, Springer Berlin Heidelberg, Berlin, Heidelberg, 2009, pp. 53–62.
[187] M.A. Mitrotta F, J. Sodja, A. Sciacchitano, On the combined flow and structural measurements via robotic volumetric PTV, Meas. Sci. Technol. 33 (4) (2022), 45201, https://doi.org/10.1088/1361-6501/ac41dd.
[188] A. Booysen, P. Das, S. Ghaemi, Large-scale 3D-PTV measurement of Ahmed-body wake in crossflow, Exp. Therm. Fluid Sci. 132 (1) (2022), 110562, https://doi.org/10.1016/j.expthermflusci.2021.110562.
[189] S.Y. Yoon, K.C. Kim, 3D particle position and 3D velocity field measurement in a microvolume via the defocusing concept, Meas. Sci. Technol. 17 (11) (2006) 2897–2905, https://doi.org/10.1088/0957-0233/17/11/006.
[190] L. Kajitani, D. Dabiri, A full three-dimensional characterization of defocusing digital particle image velocimetry, Exp. Fluid 16 (3) (2005) 790–804, https://doi.org/10.1088/0957-0233/16/3/022.
[191] Y. Kuwano, M. Tanaka, Y. Kazoe, Motion of submicrometer particles in micrometer-size channel measured by defocusing nano-particle image velocimetry, J. Appl. Phys. 131 (10) (2022), 104701, https://doi.org/10.1063/5.0080473.
[192] B. Pan, K. Qian, H. Xie, A. Asundi, Two-dimensional digital image correlation for in-plane displacement and strain measurement: a review, Opt Laser. Eng. 20 (6) (2009), 62001, https://doi.org/10.1088/0957-0233/20/6/062001.
[193] M.A. Sutton, J.-J. Orteu, H.W. Schreier, Image Correlation for Shape, Motion and Deformation Measurements: Basic Concepts, Theory and Applications, Springer, New York N.Y., 2009.
[194] B. Pan, Recent progress in digital image correlation, Exp. Mech. 51 (7) (2011) 1223–1235, https://doi.org/10.1007/s11340-010-9418-3.
[195] G. Gao, W. Yao, K. Xia, Z. Li, Investigation of the rate dependence of fracture propagation in rocks using digital image correlation (DIC) method, Eng. Fract. Mech. 138 (1) (2015) 146–155, https://doi.org/10.1016/j.engfracmech.2015.02.021.
[196] Y. Cheng, Z. Song, T. Yang, J. Han, B. Wang, Z. Zhang, Investigating the aging damage evolution characteristics of layered hard sandstone using digital image correlation, Construct. Build. Mater. 353 (1) (2022), 128838, https://doi.org/10.1016/j.conbuildmat.2022.128838.
[197] I. Grant, X. Pan, An investigation of the performance of multi layer, neural networks applied to the analysis of PIV images, Exp. Fluid 19 (3) (1995) 159–166, https://doi.org/10.1007/BF00189704.
[198] Y. Gim, D.K. Jang, D.K. Sohn, H. Kim, H.S. Ko, Three-dimensional particle tracking velocimetry using shallow neural network for real-time analysis, Exp. Fluid 61 (2) (2020) 73, https://doi.org/10.1007/s00348-019-2861-8.
[199] F. Pereira, H. Stüer, E.C. Graff, M. Gharib, Two-frame 3D particle tracking, Meas. Sci. Technol. 17 (7) (2006) 1680–1692, https://doi.org/10.1088/0957-0233/17/7/006.
[200] C. Yu, H. Luo, X. Bi, Y. Fan, M. He, An effective convolutional neural network for liquid phase extraction in two-phase flow PIV experiment of an object entering water, Ocean Eng. 237 (6) (2021), 109502, https://doi.org/10.1016/j.oceaneng.2021.109502.
[201] G. Hasanuzzaman, H. Eivazi, S. Merbold, C. Egbers, R. Vinuesa, Enhancement of PIV measurements via physics-informed neural networks, Meas. Sci. Technol. (2022), https://doi.org/10.1088/1361-6501/aca9eb.
[202] Estevadeordal J, Gogineni S, Kimmel R, Hayes J. Schlieren imaging in Hypersonic plasmas. In: 42nd AIAA Aerospace Sciences Meeting and Exhibit. Reston, Virigina: American Institute of Aeronautics and Astronautics; 01052004.
[203] Estevadeordal J, Goss L. PIV with LED: particle shadow velocimetry (PSV) technique. In: 43rd AIAA Aerospace Sciences Meeting and Exhibit. Reston, Virigina: American Institute of Aeronautics and Astronautics; 01102005.
[204] A.A. Aguirre-Pablo, K.R. Langley, S.T. Thoroddsen, High-speed time-resolved tomographic particle shadow velocimetry using smartphones, Appl. Sci. 10 (20) (2020) 7094, https://doi.org/10.3390/app10207094.
[205] G. Wu, B. Masia, A. Jarabo, Y. Zhang, L. Wang, Q. Dai, et al., Light field image processing: an Overview, IEEE J. Sel. Top. Signal Process. 11 (7) (2017) 926–954, https://doi.org/10.1109/JSTSP.2017.2747126.
[206] H. Zhu, Q. Wang, J. Yu, Light field imaging: models, calibrations, reconstructions, and applications, Front. Inf. Technol. Electron. Eng. 18 (9) (2017) 1236–1249, https://doi.org/10.1631/FITEE.1601727.
[207] I. Viola, M. Rerabek, T. Ebrahimi, Comparison and evaluation of light field image coding approaches, IEEE J. Sel. Top. Signal Process. 11 (7) (2017) 1092–1106, https://doi.org/10.1109/JSTSP.2017.2740167.
[208] Z. Liang, Y. Wang, L. Wang, J. Yang, S. Zhou, Light field image Super-resolution with transformers, IEEE Signal Process. Lett. 29 (2022) 563–567, https://doi.org/10.1109/LSP.2022.3146798.
[209] P. Hariharan, Optical Holography: Principles, Techniques, and Applications/P. Hariharan, second ed., Cambridge University Press, Cambridge, 1996.
[210] R.J. Collier, C.B. Burckhardt, LH-c Lin, Optical Holography, Academic Press, New York, London, 1971 [ie 1977].
[211] N.T. Shaked, B. Katz, J. Rosen, Review of three-dimensional holographic imaging by multiple-viewpoint-projection based methods, Appl. Opt. 48 (34) (2009) H120, https://doi.org/10.1364/AO.48.00H120.

[212] H.J. Caulfield, Handbook of Optical Holography, Elsevier Science, Saint Louis, 2014.
[213] Y. Frauel, T.J. Naughton, O. Matoba, E. Tajahuerce, B. Javidi, Three-dimensional imaging and processing using computational holographic imaging, Proc. IEEE 94 (3) (2006) 636–653, https://doi.org/10.1109/JPROC.2006.870704.
[214] K.D. Hinsch, Holographic particle image velocimetry, Meas. Sci. Technol. 13 (7) (2002) R61–R72, https://doi.org/10.1088/0957-0233/13/7/201.
[215] A. Ahmed, B. Sun, V.J. Cadarso, J. Soria, Using differential phase for 3D localization of tracer particles in digital inline holographic microscopy PIV/PTV (DIHM-PIV/PTV), ISPIV21 1 (1) (2021), https://doi.org/10.18409/ispiv.v1i1.145.
[216] J. Klappstein, T. Vaudrey, C. Rabe, A. Wedel, R. Klette, Moving object Segmentation using optical flow and depth information, in: T. Wada, F. Huang, S. Lin (Eds.), Advances in Image and Video Technology, Springer Berlin Heidelberg, Berlin, Heidelberg, 2009, pp. 611–623.
[217] K. Kale, S. Pawar, P. Dhulekar, Moving object tracking using optical flow and motion vector estimation, in: 2015 4th International Conference on Reliability, Infocom Technologies and Optimization (ICRITO) (Trends and Future Directions), IEEE, 2015 - 2015, pp. 1–6.
[218] M. Chaple, S.S. Paygude, Vehicle detection and tracking from video frame sequence, Int. J. Sci. Eng. Res. 4 (3) (2013) 1–7.
[219] D.K. Singh, D.S. Kushwaha, Tracking movements of Humans in a real-time Surveillance Scene, in: M. Pant, K. Deep, J.C. Bansal, A. Nagar, K.N. Das (Eds.), Proceedings of Fifth International Conference on Soft Computing for Problem Solving, Springer Singapore, Singapore, 2016, pp. 491–500.
[220] A. Agarwal, S. Gupta, D.K. Singh, Review of optical flow technique for moving object detection, in: 2016 2nd International Conference on Contemporary Computing and Informatics (IC3I), IEEE, 2016, pp. 409–413.
[221] A. Ammar, H.B. Fredj, C. Souani, Accurate Realtime motion estimation using optical flow on an Embedded system, Electronics 10 (17) (2021) 2164, https://doi.org/10.3390/electronics10172164.
[222] S. Scharnowski, C.J. Kähler, Particle image velocimetry - classical operating rules from today's perspective, Opt Laser. Eng. 135 (2020), 106185, https://doi.org/10.1016/j.optlaseng.2020.106185.
[223] F.-C. Li, K. Hishida, Chapter 3 particle image velocimetry techniques and its applications in multiphase systems, in: Characterization of Flow, Particles and Interfaces, Elsevier, 2009, pp. 87–147.
[224] F. Vergine, L. Maddalena, Stereoscopic particle image velocimetry measurements of supersonic, turbulent, and interacting streamwise vortices: challenges and application, Prog. Aero. Sci. 66 (2014) 1–16, https://doi.org/10.1016/j.paerosci.2013.12.001.
[225] D. Michaelis, D.R. Neal, B. Wieneke, Peak-locking reduction for particle image velocimetry, Meas. Sci. Technol. 27 (10) (2016), 104005, https://doi.org/10.1088/0957-0233/27/10/104005.
[226] A. Kislaya, A. Sciacchitano, Peak-locking error reduction by birefringent optical diffusers, Meas. Sci. Technol. 29 (2) (2018), 25202, https://doi.org/10.1088/1361-6501/aa97f7.
[227] M. Stanislas, K. Okamoto, C.J. Kähler, J. Westerweel, Main results of the second international PIV Challenge, Exp. Fluid 39 (2) (2005) 170–191, https://doi.org/10.1007/s00348-005-0951-2.
[228] Törnblom O. Introduction Course in Particle Image Velocimetry.
[229] P. Magnan, Detection of visible photons in CCD and CMOS: a comparative view, Nucl. Instrum. Methods Phys. Res. Sect. A Accel. Spectrom. Detect. Assoc. Equip. 504 (1–3) (2003) 199–212, https://doi.org/10.1016/S0168-9002(03)00792-7.
[230] H. Helmers, M. Schellenberg, CMOS vs. CCD sensors in speckle interferometry, Opt. Laser. Technol. 35 (8) (2003) 587–595, https://doi.org/10.1016/S0030-3992(03)00078-1.
[231] R. Hain, C.J. Kähler, C. Tropea, Comparison of CCD, CMOS and intensified cameras, Exp. Fluid 42 (3) (2007) 403–411, https://doi.org/10.1007/s00348-006-0247-1.
[232] D.P. Hart, PIV error correction, Exp. Fluid 29 (1) (2000) 13–22, https://doi.org/10.1007/s003480050421.
[233] R.J. Adrian, J. Westerweel, Particle Image Velocimetry, Cambridge University Press, Cambridge, New York, 2011, p. 2011.
[234] R. Hain, C.J. Kähler, Fundamentals of multiframe particle image velocimetry (PIV), Exp. Fluid 42 (4) (2007) 575–587, https://doi.org/10.1007/s00348-007-0266-6.
[235] A. Sciacchitano, F. Scarano, B. Wieneke, Multi-frame pyramid correlation for time-resolved PIV, Exp. Fluid 53 (4) (2012) 1087–1105, https://doi.org/10.1007/s00348-012-1345-x.
[236] T. Soodt, D. Pott, M. Klaas, W. Schröder, Analysis of basic flow regimes in a human airway model by stereo-scanning PIV, Exp. Fluid 54 (6) (2013) 1301, https://doi.org/10.1007/s00348-013-1562-y.
[237] T. van Overbrüggen, F. Schröder, M. Klaas, W. Schröder, A particle-image velocimetry tracer generating technique for liquid flows, Meas. Sci. Technol. 25 (8) (2014), 87001, https://doi.org/10.1088/0957-0233/25/8/087001.
[238] S. Große, W. Schröder, M. Klaas, A. Klöckner, J. Roggenkamp, Time resolved analysis of steady and oscillating flow in the upper human airways, Exp. Fluid 42 (6) (2007) 955–970, https://doi.org/10.1007/s00348-007-0318-y.
[239] M. Born, E. Wolf, in: A.B. Bhatia, et al. (Eds.), Principles of Optics: Electromagnetic Theory of Propagation, Interference and Diffraction of Light/Max Born and Emil Wolf with Contributions, seventh ed., Cambridge University Press, Cambridge, 2000.
[240] D.R. Jonassen, G.S. Settles, M.D. Tronosky, Schlieren "PIV" for turbulent flows, Opt. Laser. Eng. 44 (3–4) (2006) 190–207, https://doi.org/10.1016/j.optlaseng.2005.04.004.
[241] M. Raffel, R. Hernandez-Rivera, B. Heine, A. Schröder, K. Mulleners, Density tagging velocimetry, Exp. Fluid 51 (2) (2011) 573–578, https://doi.org/10.1007/s00348-011-1058-6.
[242] N. Yilmaz, R. Nelson, Cavity dynamics of smooth sphere and golf ball at low Froude numbers, part 1: high-speed imaging and quantitative measurements, J. Vis. 18 (2) (2015) 335–342, https://doi.org/10.1007/s12650-014-0234-1.
[243] N. Yilmaz, R. Nelson, Cavity dynamics of smooth sphere and golf ball at low Froude numbers, part 2: PIV analysis, J. Vis. 18 (4) (2015) 679–686, https://doi.org/10.1007/s12650-014-0262-x.
[244] H.F. Li, M. Yoda, Multilayer nano-particle image velocimetry (MnPIV) in microscale Poiseuille flows, Meas. Sci. Technol. 19 (7) (2008), 75402, https://doi.org/10.1088/0957-0233/19/7/075402.
[245] H. Li, R. Sadr, M. Yoda, Multilayer nano-particle image velocimetry, Exp. Fluid 41 (2) (2006) 185–194, https://doi.org/10.1007/s00348-006-0155-4.
[246] Y.U. Min, K.C. Kim, Hybrid micro-/nano-particle image velocimetry for 3D3C multi-scale velocity field measurement in microfluidics, Meas. Sci. Technol. 22 (6) (2011), 64001, https://doi.org/10.1088/0957-0233/22/6/064001.

Update

Heliyon

Volume 9, Issue 4, April 2023, Page

DOI: https://doi.org/10.1016/j.heliyon.2023.e15254

Heliyon 9 (2023) e15254

Contents lists available at ScienceDirect

Heliyon

journal homepage: www.cell.com/heliyon

Corrigendum

Corrigendum to "Past and current components-based detailing of particle image velocimetry: A comprehensive review" [Heliyon 9 (3), March 2023, Article e14404]

Daniel Rohacs [a], Onur Yasar [b], Utku Kale [a,c,*], Selcuk Ekici [d], Enver Yalcin [b], Adnan Midilli [e], T. Hikmet Karakoc [f,g]

[a] *Department of Aeronautics and Naval Architecture, Faculty of Transportation Engineering and Vehicle Engineering, Budapest University of Technology and Economics, HU-1111, Budapest, Hungary*
[b] *Department of Mechanical Engineering, Balıkesir University, TR-10145, Balıkesir, Turkey*
[c] *Aviation Academy, Amsterdam University of Applied Sciences, Amsterdam, Netherlands*
[d] *Department of Aviation, Iğdır University, TR-76000, Iğdır, Turkey*
[e] *Faculty of Mechanical Engineering, Department of Mechanical Engineering, Yıldız Technical University, TR-34349, İstanbul, Turkey*
[f] *Faculty of Aeronautics and Astronautics, Eskişehir Technical University, TR-26000, Eskişehir, Turkey*
[g] *Information Technology Research and Application Center, Istanbul Ticaret University, Istanbul, Turkey*

In the original published version of this article, the affiliations for the authors were listed incorrectly. This has now been corrected. The corrected affiliations for the authors can be found below. The authors apologize for the errors. Both the HTML and PDF versions of the article have been updated to correct the errors.

DOI of original article: https://doi.org/10.1016/j.heliyon.2023.e14404.

* Corresponding author. Department of Aeronautics and Naval Architecture, Faculty of Transportation Engineering and Vehicle Engineering, Budapest University of Technology and Economics, HU-1111, Budapest, Hungary.

E-mail address: kale.utku@kjk.bme.hu (U. Kale).

https://doi.org/10.1016/j.heliyon.2023.e15254
Received 31 March 2023; Accepted 31 March 2023
Available online 6 April 2023